

Comparison of first Saint Mary's University Open-Path Fourier Transform Infrared (OP-FTIR) spectrometer measurement results with National Air Pollution Surveillance (NAPS) air quality measurements in Halifax

By
Julia Purcell

A Thesis Submitted to
Saint Mary's University, Halifax, Nova Scotia
in Partial Fulfillment of the Requirements for
the Degree of B.Sc. Honours Environmental Science

September, 2016, Halifax, Nova Scotia

© Julia Purcell, 2016

Supervisor: Dr. Aldona Wiacek

Reader: Frances Di Cesare

Date: September 15, 2016

Comparison of first Saint Mary's University Open-Path Fourier Transform Infrared (OP-FTIR) spectrometer measurement results with National Air Pollution Surveillance (NAPS) air quality measurements in Halifax

By
Julia Purcell

A Thesis Submitted to
Saint Mary's University, Halifax, Nova Scotia
in Partial Fulfillment of the Requirements for
the Degree of B.Sc. Honours Environmental Science

September, 2016, Halifax, Nova Scotia

© Julia Purcell, 2016

Supervisor: Dr. Aldona Wiacek

Reader: Frances Di Cesare

Date: September 15, 2016

Comparison of first Saint Mary's University Open-Path Fourier Transform Infrared (OP-FTIR) spectrometer measurement results with National Air Pollution Surveillance (NAPS) air quality measurements in Halifax

By Julia Purcell

Abstract

The atmosphere is very complex and it involves many chemical and physical processes that affect the air people breathe. This is why it is important to characterize the air in the atmosphere in order to determine what people are exposed to every day. Carbon monoxide (CO), a toxic air pollutant emitted primarily as a result of incomplete combustion and oxidation of hydrocarbons, was measured in Halifax, Nova Scotia using an Open-Path Fourier Transform Infrared (OP-FTIR) spectrometer and compared to National Air Pollution Surveillance (NAPS) CO measurements as a verification step in the characterization of this new instrument.

Measured NAPS data was compared to OP-FTIR spectrometer results for three different measurement campaigns: Robie Street (at Inglis for 2 hours), Rice Building (at SMU for ~1 week), and Lake Major (in Dartmouth for ~1 week). For each campaign, spectra were recorded and a concentration of CO was retrieved for each spectrum (one per minute) by the program MALT. The retrieved CO concentrations were plotted in a time series for each campaign and compared to NAPS CO concentration measurements obtained on Barrington Street at the same time.

Data quality of the OP-FTIR spectrometer was assessed in detail, with the majority of spectral fit residuals and their RMS values below 0.01 (1%), indicating a reasonable fit between the measured spectra and the fitted spectra simulated by MALT. The technique's accuracy was previously conservatively estimated to be no worse than 10%; however, for all three campaigns, there was a clear systematic bias of up to 0.35 ppm (a factor of ~3) between the OP-FTIR spectrometer and NAPS measurements, along with unexplained enhancements in CO concentration at times and locations with minimal vehicle activity.

Further studies are suggested in order to fully explain the reason for the systematic bias and unusual enhancements in CO concentration observed.

September 15, 2016

Table of Contents

Acknowledgments.....	3
List of Tables	5
List of Figures	6
1 Introduction	11
1.1. Air Pollution – Key Players	11
1.1.1. The Planetary Boundary Layer and Chemical Reaction Initiation.....	11
1.1.2. HOx Family	14
1.1.3. NOx Family	17
1.1.4. Carbon Monoxide.....	19
1.1.5. Sulfur Dioxide	23
1.1.6. Ground-Level Ozone	24
1.1.7. Particulate Matter.....	28
1.2. Air Pollution – Halifax Context	30
1.2.1. Regulated Compounds.....	30
1.2.2. National Air Pollution Surveillance (NAPS) Data.....	37
1.2.3. Other Sources of Air Quality Measurements.....	48
2 Experimental Methods and Materials	50
2.1. Molecular Spectroscopy.....	50
2.2. Open-Path Fourier Transform Infrared (OP-FTIR) Spectrometer	54
2.3. Concentration Retrieval	70
2.3.1. MALT	70
2.3.2. Retrieval Parameters.....	72
2.3.3. MATLAB.....	75
2.4. National Air Pollution Surveillance (NAPS) Measuring Station and Equipment	78
2.5. Campaigns.....	80
2.5.1. Robie Street Campaign.....	80
2.5.2. Rice Campaign.....	82
2.5.3. Lake Major Campaign.....	86
3 Results and Discussion	88
3.1. Comparison of MALT CO Concentration Retrievals and NAPS Data.....	88

3.1.1.	Robie Street.....	88
3.1.2.	Rice.....	99
3.1.3.	Lake Major.....	114
3.2.	Comparison of Robie Street, Rice, and Lake Major OP-FTIR Spectrometer CO Concentration Data.....	126
4	Conclusions, Limitations, and Future Work.....	128
5	Appendices.....	133
5.1.	Sample MALT Parameter Input File	133
5.2.	MATLAB Code: Robie Street Campaign Individual Spectra and Time Series	135
5.3.	MATLAB Code: Rice Campaign Individual Spectra and Time Series	140
5.4.	MATLAB Code: Rice Campaign Combined Time Series.....	145
5.5.	MATLAB Code: Lake Major Campaign Individual Spectra and Time Series	148
5.6.	MATLAB Code: Lake Major Campaign Combined Time Series.....	153
5.7.	MATLAB Code: Generation of Maximum Residual Time Series.....	156
6	Bibliography	167

Acknowledgments

I would like to start by thanking my supervisor, Dr. Aldona Wiacek, for all of her help, support, and inspiration throughout this long and challenging process. Thank you for allowing me the chance to apply my skills and explore a subject that is very complex, yet very interesting to me. I appreciate everything you have done and the time you have set aside in your busy schedule to help me through this. You have truly made this process an enjoyable and valuable experience.

I would also like to thank Dr. Li Li and Keane Tobin from the TRSL group at Saint Mary's University (SMU) and Frances Di Cesare from Nova Scotia Environment for their help throughout this process. The effort and time you put into assisting me with data acquisition, running complex codes, analysis, etc., is very much appreciated.

Additionally, I would like to thank Colin Waddell from Halifax Water and Facilities Management at SMU for their logistical support, as well as Dr. Cristian Suteanu (SMU Environmental Science Department) and Dave Lane (SMU Astronomy and Physics Department) for their efforts to outfit SMU with a full weather station, and its maintenance.

Next, I would like to acknowledge National Science and Engineering Research Council (NSERC) and SMU for providing funding to allow me to pursue something I am passionate about, as well as Canada Foundation for Innovation (CFI) and Nova Scotia Research and Innovation Trust (NSRIT) for funding the project equipment.

Last, but certainly not least, I would like to thank my parents, my grandparents, my brother, and my partner, Coady, for their constant support, patience, and encouragement. I love you all very much and would not have been able to get through this without you. Thank you for everything you do.

List of Tables

Table 1 Estimated present-day sources of NO _x in the troposphere in units of teragrams (Tg) of nitrogen per year. (Jacob, 1999)	18
Table 2 Estimated present-day global budget of CO sources and sinks in teragrams (Tg) of CO per year. (Jacob, 1999).....	22
Table 3 Summary of ambient air quality criteria for the six air contaminants regulated in Nova Scotia. (NSE, AQB, 2009)	32
Table 4 The Air Quality Management Framework and associated threshold values. (NSE, AQB, 2015)	35
Table 5 Nova Scotia air zone management levels and CAAQS achievement results for air zone monitoring (2012-2014 average). (NSE, AQB, 2015)	36
Table 6 Summary of MALT parameters used for simulation of calculated spectra and the retrieval of CO concentration.	74
Table 7 Specifications of the Teledyne API Model 300 CO Analyzer. (Teledyne API, 2006).....	79

List of Figures

Figure 1 The planetary boundary layer shown in relation to the rest of the troposphere and Earth's surface. Source: [Untitled image of the troposphere and its planetary boundary layer] .	12
Figure 2 The chemistry of OH and HO ₂ in the troposphere, including their sinks and sources by chemical reaction or wet deposition. Species over the arrows are consumed, while many intermediate steps and products are not shown. Circles indicate radicals and boxes indicate more stable compounds. (Holloway & Wayne, 2010)	16
Figure 3 Mechanism for O ₃ -NO _x -HO _x -CO chemistry in the troposphere. The numbers follow the reaction numbers in this thesis. (Jacob, 1999)	21
Figure 4 Chemical model calculation of simulated O ₃ concentrations in the United States showing the two distinct regimes of O ₃ production: NO _x -limited (top left) and hydrocarbon-limited (bottom right). The thick line represents the boundary between the two regimes. Concentration of O ₃ are in units of ppbv. (Jacob, 1999).....	26
Figure 5 A new map of Nova Scotia's Ambient Air Quality Monitoring Network for 2016. Included is a list of pollutants monitored, monitoring equipment, organizations involved, and air pollutants measured at a particular site. The locations marked in blue represent sites operated by NSE and locations marked in grey represent sites operated by ECCC. (F. Di Cesare, personal communication, May 11, 2016).	31
Figure 6 A map of Nova Scotia's four Air Zones with yellow dots indicating the location of ambient air monitoring station sites. (NSE, AQB, 2015).....	34
Figure 7 Diurnal variation of O ₃ and NO ₂ concentrations in ppb for the city of Halifax based on data from 2006. (NSE, AQB, 2009).....	39
Figure 8 Annual 1-hour averages of NAPS O ₃ concentrations measured on Barrington Street in Halifax for years 2004 to 2014. January 1 st is day 1 and December 31 st is day 365 (x-axis).	40
Figure 9 Annual maximum 1-hour average PM _{2.5} concentrations from 2000 to 2007 for multiple stations in Nova Scotia. BAM and TEOM refer to two PM _{2.5} aerosol sampling instruments. (NSE, AQB, 2009)	41
Figure 10 Annual maximum 24-hour average TSP concentration for years 2000 to 2004 in Halifax and Sydney, Nova Scotia. (NSE, AQB, 2009)	42
Figure 11 Annual average TSP concentration for years 2000 to 2004 in Halifax and Sydney, Nova Scotia. (NSE, AQB, 2009)	43
Figure 12 Annual maximum 1-hour average CO concentrations for years 2000 to 2007 for Halifax and Sydney, Nova Scotia. There is no data for Halifax in years 2000 and 2007 or for Sydney in years 2005 and 2007 due to insufficient data. (NSE, AQB, 2009).....	43
Figure 13 Annual maximum 8-hour average CO concentrations for years 2000 to 2007 for Halifax and Sydney, Nova Scotia. There is no data for Halifax in years 2000 and 2007 or for Sydney in years 2005 and 2007 due to insufficient data. (NSE, AQB, 2009).....	44

Figure 14 Annual maximum 1-hour average NAPS CO concentrations measured on Barrington Street in Halifax for years 2004 to 2015.	44
Figure 15 One-hour averages of NAPS CO concentrations measured on Barrington Street in Halifax for years 2004 to 2014. January 1 st is day 1 and December 31 st is day 365 (x-axis).	45
Figure 16 Diurnal variation of NO ₂ concentrations at the Dartmouth, Halifax, and Sable Island monitoring stations based on data from 2007. (NSE, AQB, 2009)	46
Figure 17 Annual maximum 1-hour average concentrations of O ₃ , SO ₂ , NO, NO ₂ , NO _x , and PM _{2.5} measured on Barrington Street in Halifax from 2004 to 2015.	47
Figure 18 The electromagnetic spectrum in terms of frequency (top axis) and wavelength (bottom axis). [Untitled image of the electromagnetic spectrum]	50
Figure 19 Symmetry and fundamental vibrations of the carbon dioxide molecule. (a) Symmetric stretching, (b) antisymmetric stretching, and (c) bending mode. (Banwell & McCash, 1994).....	52
Figure 20 A simplified diagram showing the components of the OPS by Bruker. The red and yellow arrows represent the return-light path through the system, originating from the spectrometer. (Bruker Corporation, 2015).....	54
Figure 21 A classic Michelson interferometer. (Griffiths & de Haseth, 2007).....	55
Figure 22 (a) Interferogram of a monochromatic radiation source of wavelength λ . (b) Interferogram of a broadband infrared source. The y-axis represents voltage because this is the unit in which the detector produces an electrical response. (Smith, 1996).....	57
Figure 23 Configuration of the OPS used for this honours thesis work. (Russwurm & Childers, 2002)	59
Figure 24 (a) The OP-FTIR spectrometer on its tripod and pan-tilt head. (b) The telescope of the OP-FTIR spectrometer with its primary and secondary mirrors.	60
Figure 25 The retroreflector array on a tripod.	61
Figure 26 Setup for alignment of the spectrometer and telescope with the retroreflector on the other side of the open path. A camera points at the movable mirror in-line with the MIR beam axis. (Bruker Corporation, 2015).....	62
Figure 27 (a) The outline of the secondary mirror and its four suspension legs, (b) the magnified scene in the secondary mirror at the front of the telescope, (c) the retroreflector, with its lid down, at a distance away from the spectrometer as observed by the camera through the telescope, and (d) the rest of the scene in the view of the camera, not magnified. (Bruker Corporation, 2015).....	63
Figure 28 The whole recorded absorption spectrum as calculated from the interferogram. The x-axis is in wavenumbers and the y-axis represents the intensity of radiation after traversing the open path twice. Three regions of the spectrum are labelled with strong-absorbing gases, H ₂ O and CO ₂ , that cause intensity to be zero. The inset is a zoomed region of the intensity around 2500 cm ⁻¹ . (Bruker Corporation, 2015).....	65

Figure 29 A fit between a retrieved spectrum (pink) and a measured spectrum (blue) with the residual plot (orange). The residual has been offset from zero to appear next to the calculated and measured spectrum. (Bruker Corporation, 2015)	76
Figure 30 A residual plot (the difference between a measured spectrum and a retrieved spectrum) (red) along with its corresponding single calculated RMS value (blue). (Bruker Corporation, 2015).....	77
Figure 31 Location of the retroreflector and the spectrometer on Robie Street.....	80
Figure 32 (a) Graduate student Keane Tobin standing beside the retroreflector. Photo taken by Dr. Aldona Wiacek. (b) Honours thesis candidate, myself, setting up the OP-FTIR spectrometer. Photo taken by Dr. Aldona Wiacek.	81
Figure 33 Location of the retroreflector and the spectrometer on Saint Mary’s campus.	82
Figure 34 (a) View of the spectrometer from the top of the Rice Building on Saint Mary’s campus where the retroreflector is located. (b) Slightly zoomed view of the retroreflector from the fourth floor of the Science Building on Saint Mary’s campus where the spectrometer is located. (c) View of the window in room S425 that the spectrometer was pointing out of towards the retroreflector on the Rice Building. Photos taken by Dr. Aldona Wiacek.	83
Figure 35 Comparison of three different measured spectra to illustrate the effect of fog on the intensity of the returning beam.....	84
Figure 36 Effects of fog on retrieved CO concentrations. The data in red represents the non-foggy data and the data in blue represents the foggy data.....	85
Figure 37 (a) Aerial view of the location of the spectrometer and the retroreflector during the Lake Major campaign. (b) View of the retroreflector from the spectrometer. Photo taken by Dr. Aldona Wiacek. (c) Dr. Aldona Wiacek standing beside the OP-FTIR spectrometer setup at Lake Major. Photo taken by Dr. Li Li.....	86
Figure 38 Retrieved transmittance spectrum corresponding to data collected at 12:59pm on May 15 th , 2015 for the Robie Street campaign. The temperature, pressure, and relative humidity at this time was 22.6°C, 1020.8 mbar, and 45%, respectively. Top panel: Measured and fitted spectra, also showing the contribution of the target gas (CO) and interfering gases. Bottom panel: The residual plot obtained by taking the difference (measured – fitted spectrum). Absorptions mismatches greater than 1% are identified as H ₂ O and CO ₂	88
Figure 39 Top panel: Zoomed view of the CO ₂ absorption line (2075-2080 cm ⁻¹). Bottom panel: Zoomed view of the corresponding residual values.	89
Figure 40 Maximum residual values for the full CO spectral window (blue line) and the CO ₂ spectral microwindow (red dots) corresponding to the location of the systematic CO ₂ feature in Figure 38 for the Robie Street campaign.	90
Figure 41 Contribution of: (a) H ₂ O, (b) CO, (c) CO ₂ , and (d) N ₂ O to absorption in the air across the open path and the overall measured absorption spectrum as fitted by MALT.....	92
Figure 42 Time series of retrieved CO concentrations by MALT for the Robie Street campaign. The shaded region represents 10% uncertainty of OP-FTIR spectrometer data. A time series of RMS for each spectrum is included.....	94

Figure 43 Comparison between OP-FTIR spectrometer retrieved CO concentrations on Robie Street and NAPS measured CO concentrations on Barrington Street. The shaded region represents 10% uncertainty on OP-FTIR spectrometer data. The NAPS measurement error is 10% and not shown. One representative 10% error bar is shown on the NAPS time series. 95

Figure 44 Wind speed/gust and wind direction measured at a weather station on Francklyn Street compared to the CO concentration time series. Wind direction represents the direction wind is coming from..... 97

Figure 45 Aerial view of Halifax, including the location of the NAPS station on Barrington Street, the OP-FTIR spectrometer on Robie Street, and the weather station on Francklyn Street. The predominant wind direction is shown in red..... 98

Figure 46 Retrieved transmittance spectrum of results corresponding to data collected at 4:11pm on August 13th, 2015 for the Rice campaign. The temperature, pressure, and relative humidity at this time was 22.6°C, 1005.3 mbar, and 93%, respectively. Top panel: Measured and fitted spectra, also showing the contribution of the target gas (CO) and interfering gases. Bottom panel: The residual plot obtained by taking the difference (measured – fitted spectrum). 100

Figure 47 Maximum residual values for the full CO spectral window and the CO₂ spectral microwindow corresponding to the location of the systematic CO₂ feature for the Rice campaign. Circled residuals are those that do not correspond to the systematic CO₂ feature..... 101

Figure 48 Time series of retrieved CO concentrations by MALT with an error of 10% for the Rice campaign. A time series of RMS for each spectrum is included. Circled enhancements in CO concentration in the top panel may correspond to rush hour traffic. Circled RMS values in the bottom panel are those above 0.01 (1%). Arrows point to enhancements detailed in Figure 51. 103

Figure 49 Zoomed-in CO concentration time series measured by the OP-FTIR spectrometer (top panel) and corresponding RMS values (bottom panel). Black circles represent events that may be related to rush hour traffic and black arrows point to unexplained overnight events. 105

Figure 50 Aerial view of Saint Mary’s University campus marking the location of the smoke stacks..... 106

Figure 51 (a) Portion of the Rice campaign time series zoomed to real CO concentration enhancement at ~7:30pm on August 13th with corresponding RMS values. (b) Portion of the Rice campaign time series zoomed to spurious CO concentration enhancement at ~7:30am on August 15th with corresponding RMS values. 107

Figure 52 Comparison between OP-FTIR spectrometer retrieved CO concentrations on the Saint Mary’s University campus and NAPS measured CO concentrations on Barrington Street. OP-FTIR spectrometer error bars of 10% were excluded as they are too small to be seen at this scale. Circled NAPS data are discussed in detail (see text)..... 109

Figure 53 Aerial view of Halifax, including the location of the NAPS station on Barrington Street and the OP-FTIR spectrometer and the weather station on Saint Mary’s University campus.... 110

Figure 54 Wind speed/gust and wind direction measured at a weather station on Saint Mary’s University campus compared to the CO concentration time series comparison between NAPS

data and retrieved OP-FTIR spectrometer CO concentrations for the Rice campaign. Wind direction represents the direction wind is coming from.	111
Figure 55 Zoomed time series showing measured CO concentrations (by NAPS and the OP-FTIR spectrometer), wind direction, and wind speed/gust for the two prolonged NAPS events on August 19 th and 20 th (circled in the top panel).	112
Figure 56 Zoomed time series showing measured CO concentrations (by NAPS and the OP-FTIR spectrometer), wind direction, and wind speed/gust for the three NAPS events on August 15 th and 16 th (circled in the top panel).	114
Figure 57 Retrieved transmittance spectrum corresponding to data collected at 5:43pm on September 4 th , 2015 for the Lake Major campaign. The temperature, pressure, and relative humidity at this time was 21.3°C, 1014.5 mbar, and 66%, respectively. Top panel: Measured and fitted spectra, also showing the contribution of the target gas (CO) and interfering gases. Bottom panel: The residual plot obtained by taking the difference (measured – fitted spectrum).	115
Figure 58 Maximum residual values for the full CO spectral window and the CO ₂ spectral microwindow corresponding to the location of the systematic CO ₂ feature for the Lake Major campaign. See text for discussion of boxed regions.	116
Figure 59 Time series of Lake Major RMS values and recorded temperature. Boxed RMS values show no correlation with temperature.	117
Figure 60 Time series of retrieved CO concentrations by MALT with an error of 10% for the Lake Major campaign. A time series of RMS for each spectrum is included. Circled RMS values are fog-not temperature-related.	119
Figure 61 Comparison between OP-FTIR spectrometer retrieved CO concentrations at Lake Major and NAPS measured CO concentrations on Barrington Street. OP-FTIR spectrometer error bars of 10% were excluded as they are too small to be seen at this scale. Circled regions point to overlap in the two datasets.	120
Figure 62 Aerial view of Halifax and Dartmouth, including the location of the NAPS station on Barrington Street and the OP-FTIR spectrometer and the weather station at Lake Major, which are separated by approximately 11 kilometers.	122
Figure 63 Wind speed and wind direction measured by Nova Scotia Environment at Lake Major compared to the CO concentration time series comparison between NAPS data and retrieved OP-FTIR spectrometer CO concentrations for the Lake Major campaign. Wind direction represents the direction wind is coming from.	123
Figure 64 Zoomed-in plot of wind speed and wind direction measured by Nova Scotia Environment at Lake Major, on September 8 th , compared to the CO concentration time series comparison between NAPS data and retrieved OP-FTIR spectrometer CO concentrations for the Lake Major campaign. Wind direction represents the direction wind is coming from.	124
Figure 65 Time series of CO concentration from the Robie Street campaign (blue), the Rice campaign (red), and the Lake Major campaign (green) with an error of 10%.	126

1 Introduction

1.1. Air Pollution – Key Players

1.1.1. *The Planetary Boundary Layer and Chemical Reaction Initiation*

The troposphere is the portion of the atmosphere closest to the Earth's surface, and it is defined as a region in which temperature decreases with increasing altitude (Jacobson, 2012). The planetary boundary layer (PBL) is the lower portion of the troposphere that extends from the Earth's surface up to between 500 and 3000 meters above the Earth's surface (Jacobson, 2012). It is subject to frictional processes and direct influence by other physical and chemical processes that occur at the Earth's surface (Jacobson, 2012). The PBL is of great interest because it is the portion of the atmosphere that people live in and in which air pollution forms (Jacobson, 2012). Therefore, understanding the air chemistry in this layer is important. Figure 1 illustrates the PBL as a small portion of the troposphere that fluctuates in height above the ground depending on the geographic location, and also depending on the time of day due to solar radiation effects on vertical mixing and convection. The remainder of the troposphere is called the free troposphere, and away from human activity is called the background troposphere.

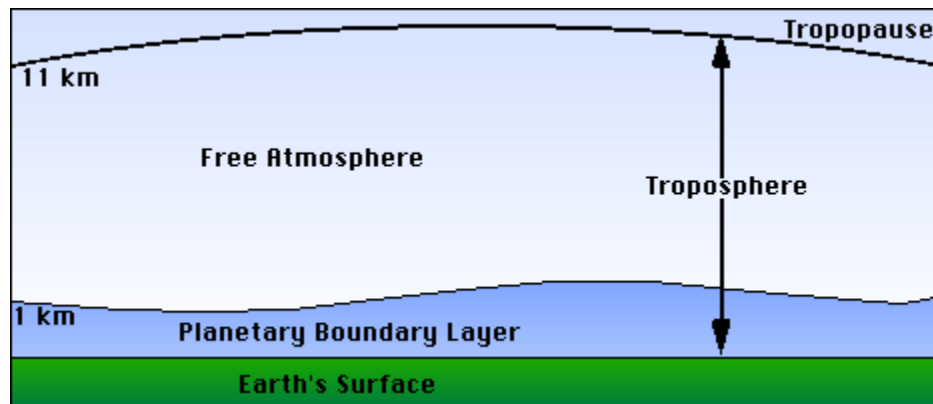


Figure 1 The planetary boundary layer shown in relation to the rest of the troposphere and Earth's surface. Source: [Untitled image of the troposphere and its planetary boundary layer]

The PBL is different from the free troposphere in that the temperature in the PBL responds to changes in ground temperatures within an hour, which is much faster than the response in the free troposphere (Jacobson, 2012). The variation in the height of the PBL is indicative of the temperature variation of the Earth's surface at a certain location (M. N. Patil, S. D. Patil, Waghmare, & Dharmaraj, 2013). A PBL reaching 500 meters above the Earth's surface is characteristic of relatively cooler land, meaning there is less buoyant air and convection. A PBL reaching 3000 meters above the Earth's surface is driven by hotter land and stronger vertical mixing, allowing the PBL to extend to this height. These are some of the physical processes that occur in the PBL. Other physical processes, important for this honours thesis work, are the horizontal transport of pollutants (advection) and dilution.

Atmospheric chemistry on its own is a very complex subject, dedicated to understanding air pollutant concentrations. Gases in the atmosphere are at low concentrations, which allows one to relate the pressure, temperature, and density of a gas by the ideal gas law. The ideal gas law is written as: $PV = nRT$, where P is the

pressure of a gas, V is the volume of a gas, n is the number of gas moles, R is the universal gas constant, and T is the temperature of a gas (Jacobson, 2012). Due to low gas concentrations, collisions between molecules are relatively infrequent, yet chemical reactions occur continuously in the atmosphere (Jacob, 1999). Most chemical reaction chains include an initiation step, which allows different gases to react more often with one another than they would through colliding by chance (Jacob, 1999). One type of chemical reaction initiation involves an incident solar photon being absorbed by a gas molecule and breaking the chemical bond in that molecule (Jacob, 1999). This type of reaction is called photolysis. The breakdown of ozone (O₃) by photolysis is quite common and is described by the following gas phase chemical reaction:



where $h\nu$ is the incident photon of energy $h\nu$ (Planck's constant h multiplied by photon frequency ν), $O^*(^1D)$ is the excited oxygen atom radical, and O_2 is an oxygen molecule (Holloway & Wayne, 2010). Once $O^*(^1D)$ has been created, one outcome may be that it reacts with water vapour to produce the hydroxyl radical (OH) (Holloway & Wayne, 2010):



Radicals are electrically neutral chemical species with an unpaired electron in the outer valence shell, making them more reactive with other chemical species that can fill their valence shell (Jacob, 1999). Radicals are another type of initiator for chemical reaction chains, allowing them to occur more frequently. Radicals form through

photolysis or reaction involving other radicals, producing a species in an excited state (Jacob, 1999).

As a result of Reactions (1.1) and (1.2), radicals $O^*(^1D)$ and OH are produced by photolysis and chemical reaction, respectively, and remain in the atmosphere for only a short period of time until they react with other molecules; however, they are quickly replenished and maintain trace concentrations of parts per trillion volume (pptv). Having said this, it is interesting that the most important oxidant species in the troposphere exists at such low concentrations.

1.1.2. HOx Family

The HOx family is a major oxidant family of hydrogen oxide radicals, consisting of hydrogen (H), the hydroxyl radical (OH), and the hydroperoxy radical (HO_2) (Jacob, 1999). These compounds are not directly emitted by human activities and they belong to the same family because they cycle rapidly between one another (Jacob, 1999).



An oxidant, also known as an oxidizing agent, is a chemical species that provides another species with an oxygen atom to make it progressively more stable (Jacobson, 2012). OH is a major oxidizing agent in the troposphere with a sufficient amount of it being produced by reactions (1.1) to (1.2), to allow for oxidation of species such as carbon monoxide (CO) and methane (CH_4) to carbon dioxide (CO_2) and CO, respectively (Jacob, 1999). The importance of OH as an oxidant and a radical will become more clear in the next few sections as it helps keep pollutants in the atmosphere at stable concentrations.

The major sink of OH are those reactions where OH is consumed in order to oxidize another chemical species. For example, OH is consumed in oxidizing nitrogen dioxide (NO₂) to nitric acid (HNO₃), as shown in Reaction (1.4) (Holloway & Wayne, 2010).



Due to its high solubility, HNO₃ can then be efficiently scavenged by precipitation and deposited on the Earth's surface as acid rain (Jacob, 1999), or by adsorption to water films on solid surfaces (dry deposition).

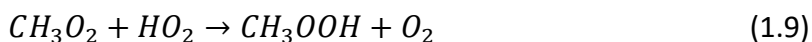
Global mean concentrations of OH are difficult to determine because they are so variable due to its short lifetime in the atmosphere as a radical species and the difficulty of detection (Jacob, 1999). Typical concentrations of OH in the troposphere are believed to be less than 0.1 parts per trillion (ppt) (Finlayson-Pitts & Pitts, 2000).

HO₂ is another member of the HO_x family. Again, it is not emitted into the atmosphere, but sources of HO₂ include any reactions that produce the hydrogen atom (H) or the formyl radical (HCO), such as daytime formaldehyde (CH₂O) photolysis (Finlayson-Pitts & Pitts, 2000):



Reaction (1.5) is formaldehyde photolysis producing H and HCO, which can lead to Reactions (1.6) and (1.7), where M represents any compound that acts as a stabilizing body. The major sinks of HO₂ involve the formation and subsequent loss of highly soluble hydrogen peroxide (H₂O₂) and less soluble (longer lived) methyl hydroperoxide

(CH₃OOH) (Whalley et al., 2010). HO₂ can either react with another HO₂ molecule and produce H₂O₂ or it can react with the methylperoxy radical (CH₃O₂) to produce CH₃OOH (Jacob, 1999).



However, if H₂O₂ is not removed from the troposphere, it can either photolyze to produce OH or react with OH and cycle back to HO₂ (Jacob, 1999). If CH₃OOH is not removed from the troposphere, it can react to form (HCHO), which can photolyze and again cycle back to HO₂. Another way HO₂ can be removed from the troposphere is direct wet deposition by cloud droplets (Holloway & Wayne, 2010).

The cycling of OH and HO₂ in the troposphere is very complex and is well illustrated in Figure 2.

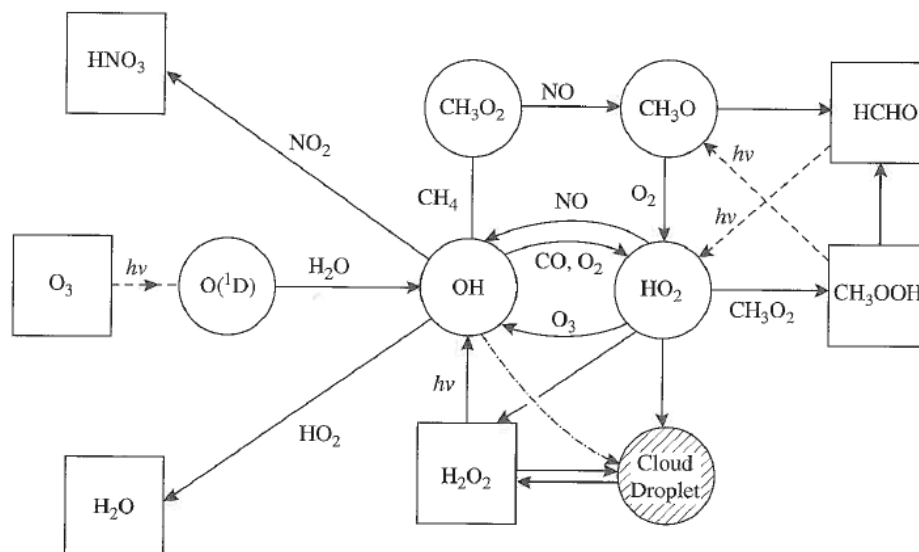


Figure 2 The chemistry of OH and HO₂ in the troposphere, including their sinks and sources by chemical reaction or wet deposition. Species over the arrows are consumed, while many intermediate steps and products are not shown. Circles indicate radicals and boxes indicate more stable compounds. (Holloway & Wayne, 2010)

Global mean concentrations of HO₂ are within the range of 4-8 ppt, whereas, typical peak concentrations of HO₂ in polluted areas are of the order of ~40 ppt (Finlayson-Pitts & Pitts, 2000). While important, HO_x cannot be measured by the OP-FTIR technique.

1.1.3. NO_x Family

The NO_x family refers to nitrogen oxides, consisting of nitric oxide (NO) and nitrogen dioxide (NO₂).



NO is a colourless gas and NO₂ is a toxic, brown gas at standard temperature and pressure in the atmosphere and both are radical species (Jacobson, 2012). Fossil fuel combustion accounts for approximately half of the global source of NO_x, where NO_x is mainly emitted as NO (Jacob, 1999). Biomass burning then follows at approximately 26%. Even though this is true, there is rapid cycling (in minutes) between NO and NO₂ in the troposphere (a net “null cycle”) by Reactions (1.11), (1.12), and others involving HO_x (Jacob, 1999). Because of this it is most convenient to consider the budget of the NO_x family as a whole (Jacob, 1999).



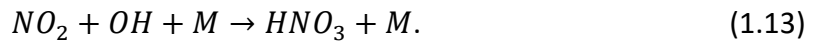
Other minor sources of emissions are from microorganisms in soils and plants during denitrification and chemical reaction between nitrogen gas and oxygen gas at high temperatures, i.e., lightening (Jacobson, 2012). A summary of estimated present-day

sources of tropospheric NO_x is found in Table 1, with fossil fuel combustion emissions making up the largest fraction (~46%).

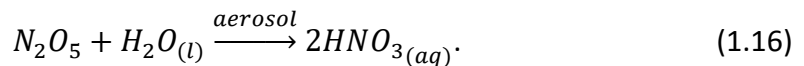
Table 1 Estimated present-day sources of NO_x in the troposphere in units of teragrams (Tg) of nitrogen per year. (Jacob, 1999)

Source	Tg N yr ⁻¹	% of Total Output
Fossil fuel combustion	21	~46%
Biomass burning	12	~26%
Soils	6	~13%
Lightning	3	~6.5%
NH ₃ oxidation	3	~6.5%
Aircraft	0.5	~1%
Transport from stratosphere	0.1	<1%

The main sink of NO_x, during the daytime, is oxidation to gaseous HNO₃ by OH (Jacob, 1999):



At nighttime, NO_x is present exclusively as NO₂ due to Reaction (1.11), and the main sink of NO_x is a series of chemical reactions to dinitrogen pentoxide (N₂O₅), which is then able to react with water in the presence of aerosols to form aqueous HNO₃ (Jacob, 1999):



While N₂O₅ acts as a reservoir for NO_x, able to release it again, aqueous HNO₃ is efficiently scavenged by precipitation and deposited on the Earth's surface as acid rain

(Jacob, 1999), removing NO_x permanently. The lifetime of NO_x as a family against these loss processes is approximately one day.

Typical sea-level concentrations of NO in the background troposphere (pristine conditions) is 5 pptv, at which it has no harmful human health effects, however, in urban regions NO concentrations can reach up to 100 parts per billion volume (ppbv) (Jacobson, 2012). Typical sea-level concentrations of NO₂ in the background troposphere can be from 10 to 50 pptv, and in urban regions NO₂ concentrations can be from 50 to 250 ppbv (Jacobson, 2012). Halifax-specific concentrations are discussed in Section 1.2. These species are accessible to OP-FTIR spectrometer measurements under certain favourable conditions, i.e., low H₂O concentrations and longer path lengths.

1.1.4. Carbon Monoxide

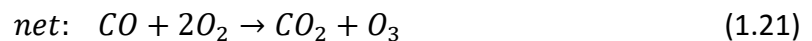
Carbon monoxide (CO) is a colourless, odourless, and tasteless gas and the most abundantly emitted anthropogenic gas, after water and CO₂ (Jacobson, 2012). Human exposure to high concentrations of CO for long periods of time (on the timescale of hours, or even less when concentrations are even higher) can result in death, and the reason it is so deadly is because it displaces oxygen and binds to hemoglobin (Martin et al., 2002). Acute CO poisoning has caused about 500 unintentional deaths in the United States between 1999 and 2004; many relating to CO buildup from leaking indoor combustion heaters in areas with low ventilation as it is undetectable by sight, scent, or taste (Jacobson, 2012). Chronic exposure effects are primarily found to be

neuropsychological in nature, such as changes in memory, sleep, vision, and balance problems (Townsend & Maynard, 2002).

The major sources of CO emissions into the atmosphere are incomplete fossil fuel and biofuel combustion and oxidation of methane (CH₄) by OH (Holloway & Wayne 2010). On the other hand, the major sink of CO is tropospheric oxidation to CO₂ by OH, as shown in Reaction (1.17):



The full CO oxidation mechanism, showing also the HOx and NOx catalysis, proceeds by Reactions (1.18) to (1.20), where Reaction (1.21) is the net reaction (Jacob, 1999):



HOx and NOx families contribute to these sub steps, but are unaffected (conserved).

These reactions are visually summarized in Figure 3.

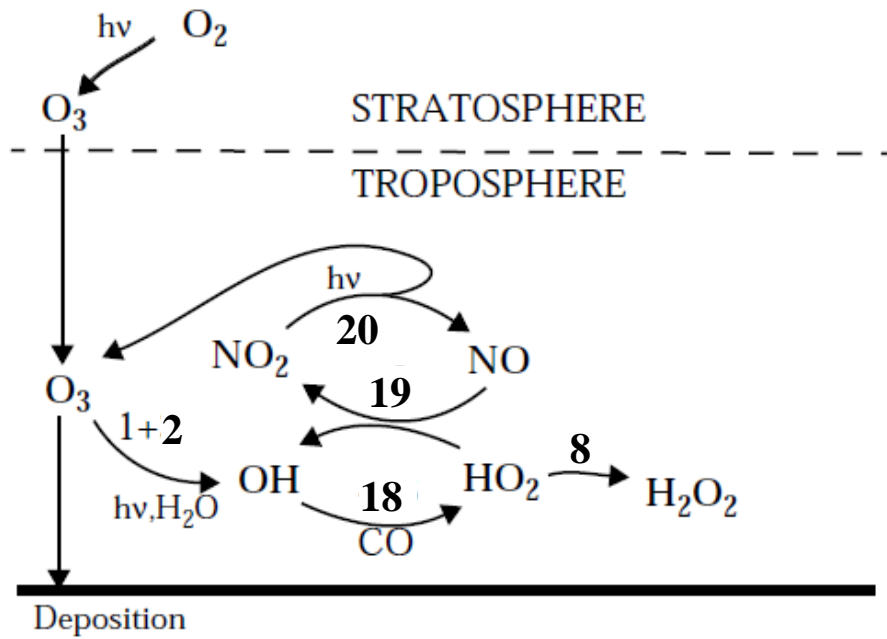


Figure 3 Mechanism for O_3 -NO $_x$ -HO $_x$ -CO chemistry in the troposphere. The numbers follow the reaction numbers in this thesis. (Jacob, 1999)

Although the removal of CO from the atmosphere prevents the accumulation of human emissions, it does result in the production of CO₂, which is a major greenhouse gas and the largest driver of climate change. The production of one O₃ molecule (Reaction (1.20)) is harmful to human health and more important for air quality. Table 2 summarizes the estimated present-day global budget of CO sources and sinks.

Table 2 Estimated present-day global budget of CO sources and sinks in teragrams (Tg) of CO per year. (Jacob, 1999)

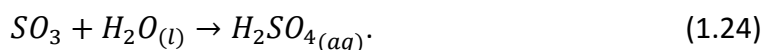
	Range of estimates (Tg CO yr-1)	% of Total Output/Input
SOURCES	1800-2700	
Fossil fuel combustion / industry	300-550	~ 16.7% - 20.4%
Biomass burning	300-700	~ 16.7% - 25.9%
Vegetation	60-160	~ 3.3% - 5.9%
Oceans	20-200	~ 1.1% - 7.4%
Oxidation of methane	400-1000	~ 22.2% - 37%
Oxidation of other hydrocarbons	200-600	~ 11.1% - 22.2%
SINKS	2100-3000	
Tropospheric oxidation by OH	1400-2600	~ 66.7% - 86.7%
Stratosphere	~100	~ 3.3% - 4.8%
Soil uptake	250-640	~ 11.9% - 21.3%

One may think the largest source of CO emissions is fossil fuel combustion or biomass burning, but the largest and most variable source of CO emissions comes from the oxidation of methane, as summarized in Table 2. The largest sink of CO is tropospheric oxidation by OH. Note also the large uncertainty of sinks and sources, but the overall larger magnitude of sinks, implying atmospheric CO depletion.

In the background troposphere, concentrations of CO can be from 50 to 150 ppbv, but in large urban regions CO concentrations are typically 2 to 10 ppmv (Jacobson, 2012). On freeways and in traffic tunnels, concentrations of CO may exceed 100 ppmv because of the high density of fast-moving vehicles (Jacobson, 2012). Halifax-specific concentrations are discussed in Section 1.2. CO is easily accessible to OP-FTIR spectrometer measurements.

1.1.5. Sulfur Dioxide

Sulfur dioxide (SO₂) is a colourless gas whose scent some people associate with rotten eggs at concentrations above 0.5 ppmv (Jacobson, 2012). Sources of SO₂ emissions include vehicles and volcanoes (Jacobson, 2012). Additionally, SO₂ makes up ~95% of the sulfur compounds resulting from the burning of fossil fuels (Kellogg, Cadle, Allen, Lazrus, & Martell, 1972). For the year 2000, estimated global SO₂ emissions from volcanoes and wildfires were 33.3 Tg, while estimated global SO₂ emissions from anthropogenic sources was 108.7 Tg, out of a total global estimate of 142 Tg (Dentener et al., 2006). SO₂ can also be produced by chemical reactions in the atmosphere from biologically produced hydrogen sulfide (H₂S), but the contribution is minor in the grand scheme of things (Kellogg et al., 1972). The major sink of SO₂ is by chemical reaction to produce sulfuric acid (H₂SO₄) (Jacobson, 2012). Reactions (1.22) through (1.24) show the multiple steps in achieving this, where HOSO₂ is the hydroxysulfonyl radical and SO₃ is sulfur trioxide (Finlayson-Pitts & Pitts, 2000):



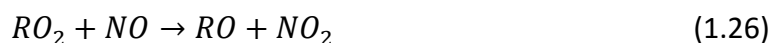
Once again, OH is the oxidant that starts the reaction chain leading to the removal of SO₂ from the atmosphere. Once formed by Reaction (1.23), SO₃ quickly forms aqueous H₂SO₄, and is scavenged by precipitation for deposition on the Earth's surface as acid rain, similar to HNO₃.

In the background troposphere, SO₂ concentrations can be from 10 pptv to 1 ppbv, but in urban regions, SO₂ concentrations can be from 1 to 30 ppbv (Finlayson-Pitts & Pitts, 2000). Halifax-specific concentrations are discussed in Section 1.2. SO₂ is also measurable by the OP-FTIR technique under certain favourable conditions, i.e., low H₂O concentrations and longer path lengths.

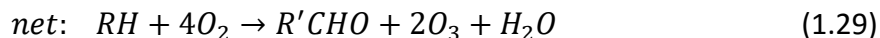
1.1.6. Ground-Level Ozone

One may think that ozone (O₃) in the atmosphere is beneficial because it absorbs ultraviolet radiation from the sun. This is true for O₃ in the stratosphere, but O₃ in the troposphere, otherwise known as ground-level ozone (GLO), is toxic to humans and vegetation because it oxidizes biological tissue (Jacob, 1999). Along with particulate matter (PM), GLO is a principal component of smog (Houtman, Karr, & Interlandi, 2013).

What is important to note about O₃ is that it is a secondary air pollutant, meaning it is only produced by chemical reaction, and not emitted by human activities directly. It is produced in the troposphere from the oxidation of CO and hydrocarbons by OH in the presence of NO_x (Jacob, 1999). As previously mentioned, Reaction (1.21) is the net reaction of O₃ production by the oxidation of CO (Jacob, 1999). Reactions (1.25) through (1.28) represent the steps in O₃ production by the oxidation of hydrocarbons, where Reaction (1.29) is the net reaction (Jacob, 1999).



R represents an organic group, therefore, RH is the simplified notation for a hydrocarbon, RO₂ is an organic peroxy radical, and RO is an organic oxy radical (Jacob, 1999). Methane is the simplest hydrocarbon and may be represented by RH, where R = CH₃ and RO₂ = CH₃O₂. After it is produced, RO (CH₃O) will typically react with oxygen to produce a carbonyl compound (R'CHO) and HO₂ (Jacob, 1999). R' represents an organic group that is altered to a different form; in the case of methane, R' = H and R'CHO = HCHO, also known as formaldehyde.



NO₂ produced in Reactions (1.26) and (1.28) will always rapidly photolyze to NO plus an oxygen atom because it is unstable during the day, which then combines with O₂ to produce O₃, which is why the net Reaction (1.29) for methane oxidation includes two O₃ molecules produced. R'CHO can then either photolyze, ending the reaction chain, or it can react with OH to continue the chain propagation (Jacob, 1999). In the case of formaldehyde, it forms CHO either by photolysis or reaction with OH, where CHO will oxidize to CO in a reaction with O₂. Formaldehyde can also oxidize directly to CO via photolysis, and CO ultimately oxidizes to CO₂ (Jacob, 1999). The complete oxidation chain of CH₄ to CO₂ generates 5O₃ and 2OH in a NO_x rich environment (Jacob, 1999). Without NO_x, no O₃ is produced and two HO_x are consumed, which is why NO_x is crucial to keeping up the oxidative power of the atmosphere (Jacob, 1999).

In general, both NO_x and hydrocarbons need to be present to produce O₃, however, the dependence of O₃ production on NO_x and hydrocarbons depends on whether one is in the so-called NO_x-limited regime or the hydrocarbon-limited regime (Jacob, 1999). Figure 4 illustrates the results of a chemical model calculation where O₃ concentrations were simulated and plotted as a function of NO_x and hydrocarbons.

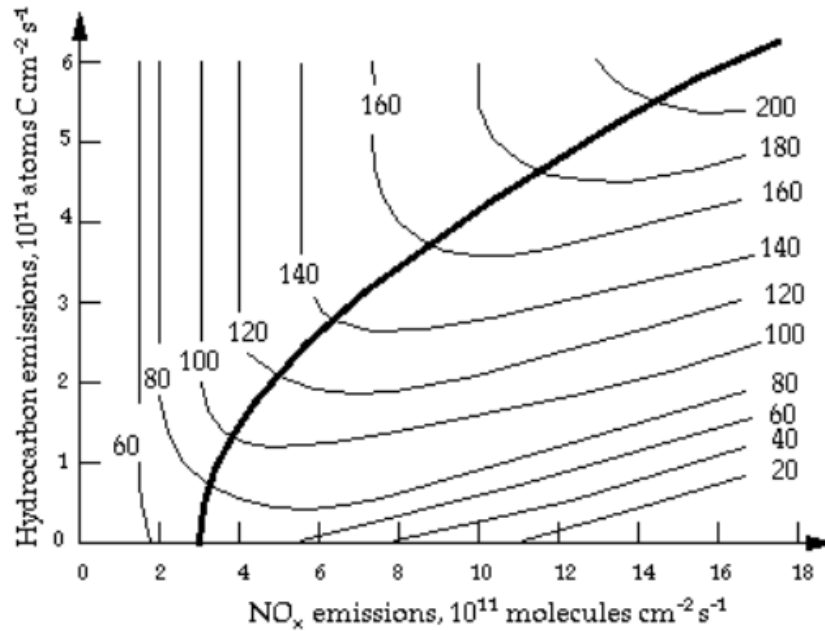


Figure 4 Chemical model calculation of simulated O₃ concentrations in the United States showing the two distinct regimes of O₃ production: NO_x-limited (top left) and hydrocarbon-limited (bottom right). The thick line represents the boundary between the two regimes. Concentration of O₃ are in units of ppbv. (Jacob, 1999)

The thick line in the center divides the NO_x-limited regime (top left) and the hydrocarbon-limited regime (bottom right). In the NO_x-limited regime, where hydrocarbon concentrations are typically high and NO_x concentrations are typically low, any addition of hydrocarbon emissions will not change the concentration of O₃. The NO_x-limited regime is sensitive to NO_x emissions, meaning that an increase in NO_x emissions will increase the concentration of O₃, as follows (Jacob, 1999):

$$P_{O_3} \propto [NO].$$

In the hydrocarbon-limited regime, where NO_x concentrations tend to be high and hydrocarbon concentrations tend to be low, addition of hydrocarbon emissions will increase the concentration of O₃ significantly. What is interesting about the hydrocarbon-limited regime is if one increases NO_x emissions, concentrations of O₃ will slowly decrease. However, if one decreases NO_x emissions in a hydrocarbon-limited regime, concentrations of O₃ will slowly increase (Jacob, 1999):

$$P_{O_3} \propto \frac{[RH]}{[NO_2]}.$$

It was initially thought that O₃ production in the United States was primarily hydrocarbon-limited, when in reality, it is primarily NO_x-limited (Jacob, 1999). Early models lead to this misconception because they underestimated emissions of hydrocarbons from automobiles and did not account for vast natural emissions of biogenic hydrocarbons (Jacob, 1999). In fact, natural emissions of isoprene (the principal biogenic hydrocarbon contributing to O₃ production) in the United States are larger than the sum of all anthropogenic hydrocarbon emissions (Jacob, 1999). It is said that even without anthropogenic hydrocarbons, isoprene emissions would be sufficient to make O₃ production NO_x-limited everywhere except in large urban centers, where NO_x emissions dominate (Jacob, 1999). In large urban centers, levels of NO_x are high, which puts one on the right side of the thick line in Figure 3. Without any knowledge of which regime one is in, large urban centers may have regulations that require NO_x emissions to decrease, but this will increase O₃ concentrations locally, without appropriate hydrocarbon controls. This is why automobile emissions are regulated also for CO, as are

industrial volatile organic compound (VOC) emissions. In reality, NO_x reductions in cities help to reduce O₃ production downstream of urban centers.

Typical ambient concentrations of O₃ can be from 30 to 40 ppb, whereas in rural-suburban areas, O₃ can reach concentrations of 80 to 150 ppb (Finlayson-Pitts & Pitts, 2000). In the most highly polluted urban regions, O₃ can even reach concentrations as high as 500 ppb (Finlayson-Pitts & Pitts, 2000). Halifax-specific concentrations are discussed in Section 1.2. O₃ is also measurable by the OP-FTIR technique.

1.1.7. Particulate Matter

Atmospheric particulate matter (PM), also known as aerosols, refers to solid or liquid particles that are suspended in the atmosphere for short (larger particles) or long (smaller particles) periods of time with diameters between ~0.002 and ~100 μm (Finlayson-Pitts & Pitts, 2000). PM is important to include as an air pollutant because of its health effects and its potential to form acid rain. Unlike gas molecules, PM can be present in a variety of sizes, and one uses their size to categorize them into PM_{2.5} (particulates smaller than 2.5 μm in diameter) and PM₁₀ (particulates between 2.5 and 10 μm in diameter) (Houtman et al., 2013). One can have PM larger than 10 μm in diameter, but they are not as common in the atmosphere because they are larger and will settle out faster than those of smaller sizes. Solid phase examples of PM include soot, dust, ash, and pollen. Liquid phase examples include sulfates and nitrates.

Major anthropogenic sources of PM include burning coal in power and industrial plants (~40%), burning diesel and other fuels in vehicles (~17%), and agriculture,

unpaved roads, and construction accounting for the rest (Miller & Hackett, 2014). Power plants that burn fossil fuels with sulfur compounds can emit SO₂ gas, which eventually converts to aqueous sulfate and coagulates into droplets (PM) (Miller & Hackett, 2014). These sulfates may then be scavenged by precipitation and deposited on the Earth's surface as acid rain. Along with O₃, PM is also a major component of smog, where smog is defined as hazy air pollution at the Earth's surface that reduces visibility (Houtman et al., 2013).

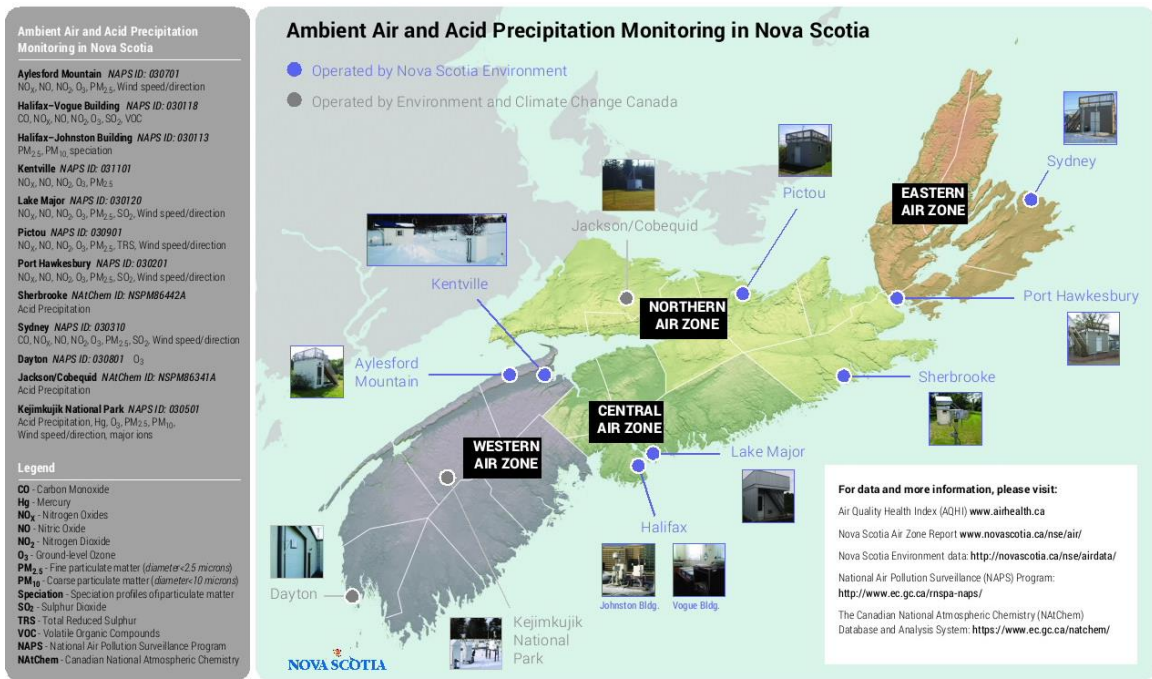
As mentioned earlier, PM can cause many health problems, but the severity depends on the size of the particle. PM₁₀ can collect in the respiratory system and irritate tissue in the lungs, whereas PM_{2.5} can enter cells and the bloodstream if breathed in because it is so small in size (Houtman et al., 2013; Reyes, Díaz, Tobias, Montero, & Linares, 2014). Therefore, it is important to not only monitor gaseous air pollutants, but solid and liquid air pollutants in the form of PM as well.

Mass concentrations of PM₁₀ in urban regions around the world have been reported as high as 300 micrograms per cubic meter (µg/m³), although, more typical mass concentrations in urban centers are from 20 to 100 µg/m³ (Finlayson-Pitts & Pitts, 2000). In rural areas, mass concentrations of PM_{2.5} can be from 1 to 50 µg/m³, whereas typical mass concentrations in urban regions can be from 50 to 80 µg/m³ (Finlayson-Pitts & Pitts, 2000). Halifax-specific concentrations are discussed in Section 1.2. The OP-FTIR spectrometer does not measure particulates, only their gas phase precursors, in the case of liquid aerosols.

1.2. Air Pollution – Halifax Context

1.2.1. Regulated Compounds

The provincial agency Nova Scotia Environment (NSE) operates nine ambient air monitoring stations across the province (two in Halifax) and currently continuously monitors CO, NO_x, NO, NO₂, O₃, SO₂, PM_{2.5}, and total reduced sulfur (TRS). In addition, air is sampled for 24 hours in Halifax on a weekly basis and analyzed for many chemicals, including more than 167 volatile organic compounds. The federal agency Environment and Climate Change Canada (ECCC) collects and analyzes information on acid precipitation, O₃, Hg and particulates at three stations in the province. The recently updated sites and the air pollutants monitored at each site, as of 2016, are depicted in Figure 5, with NSE operated sites labelled in blue.



March 2016

Figure 5 A new map of Nova Scotia's Ambient Air Quality Monitoring Network for 2016. Included is a list of pollutants monitored, monitoring equipment, organizations involved, and air pollutants measured at a particular site. The locations marked in blue represent sites operated by NSE and locations marked in grey represent sites operated by ECC. (F. Di Cesare, personal communication, May 11, 2016).

Prior to these recent changes in monitoring activities, VOC monitoring was operated also at Granton and Kejimkujik. The station on Sable Island is no longer active. Other changes in individual site activity include the addition of NO_x, NO, NO₂, and PM_{2.5} monitoring in Kentville (now operated by NSE) and the removal of polycyclic aromatic hydrocarbons (PAH), lead (Pb), NO_x, NO_y (another chemical family), PM, and VOC monitoring from Kejimkujik (with the addition of monitoring “major ions” at that site).

Nova Scotia and National standards are different in some of their gas concentration threshold values and stringency regarding these thresholds. “Maximum acceptable level” and “maximum permissible ground level concentration” are the terminologies used by the National Ambient Air Quality Objectives (NAAQO) and the

Nova Scotia Air Quality Regulations, respectively, and are the same, apart from differences arising from conversions/units. The lower “maximum desirable level” is an innovation of the NAAQO values, although these are only used as guidelines, whereas Nova Scotia Air Quality Regulations are legally binding in the province (NSE, AQB, 2009). Table 3 shows the maximum permissible ground-level concentration (82 ppb), maximum acceptable level (80 ppb), and maximum desirable level (50 ppb) for O₃ and also for the other five regulated air contaminants in ambient air.

Table 3 Summary of ambient air quality criteria for the six air contaminants regulated in Nova Scotia. (NSE, AQB, 2009)

Air Quality Criteria		Nova Scotia Air Quality Regulations		National Ambient Air Quality Objectives (NAAQO)			
Air Contaminant	Averaging Period	Maximum Permissible Ground Level Concentration		Maximum Acceptable Level		Maximum Desirable Level	
		(ppb)*	(µg/m ³)	(ppb)*	(µg/m ³)	(ppb)*	(µg/m ³)
O ₃	1 hour	82	160	80	160	50	100
TSP	24 hour	—	120	—	120	—	—
	1 Year	—	70 (geometric mean)	—	70	—	60
CO	1 hour	30 ppm	34.6 mg/m ³	31 ppm	35 mg/m ³	13 ppm	15 mg/m ³
	8 hours	11 ppm	12.7 mg/m ³	13 ppm	15 mg/m ³	5 ppm	6 mg/m ³
NO ₂	1 hour	210	400	210	400	—	—
	1 year	50	100	50	100	30	60
SO ₂	1 hour	340	900	340	900	170	450
	24 hour	110	300	110	300	60	150
	1 year	20	60	20	60	10	30
H ₂ S	1 hour	30	42	—	—	—	—
	24 hour	6	8	—	—	—	—

The table shows 1-hour, 8-hour, 24-hour, and 1-year averaging periods, where the shorter periods capture higher short-term exposure concentrations and the longer periods capture lower but long-term exposure concentrations (NSE, AQB, 2009). The purpose of having different averaging times is to use them to protect the public against both acute and chronic effects of ambient gas concentrations by allowing higher concentrations for the former and lower concentrations for the latter (NSE, AQB, 2009).

In order to help further protect and improve outdoor air quality, in 2012, the Canadian Council of Ministers of the Environment (CCME) implemented the Air Quality Management System (AQMS) that uses, as a driver, the Canadian Ambient Air Quality Standards (CAAQS), which are slightly more stringent than the Canada Wide Standards (CWS) originally proposed in 2000 (Canadian Council of Ministers of the Environment, 2012). Currently there are only three CAAQS: PM_{2.5} (24-hour and annual averaging times) and O₃ (8-hour averaging time), all of which are actually based on 3-year averages involving 98th percentile values of PM_{2.5} and O₃ (CCME, 2012). The NAAQO and NSAQ regulations, on the other hand, concern concentrations strictly in 1-hour, 8-hour, 24-hour, and in some cases, 1-year averages of TSP (which includes, but is not equal to, PM_{2.5}) and O₃, but also CO, NO₂, SO₂, and H₂S (see Table 3). The CAAQS are designed to highlight long-term changes in highest observed concentrations, unlike the NAAQS, which average all observations. For example, the NAAQO allow 70 µg/m³ of TSP in a 1-year average, whereas the CAAQS red-flag 10 µg/m³ of only the relevant PM_{2.5} in a 3-year average of 98th percentile values.

NSE delineated four Air Zones based on common ambient air quality characteristics and administrative structure for management: Western, Central, Northern, and Eastern (NSE, AQB, 2015). Figure 6 illustrates the four Air Zones in Nova Scotia together with ambient air monitoring station locations.

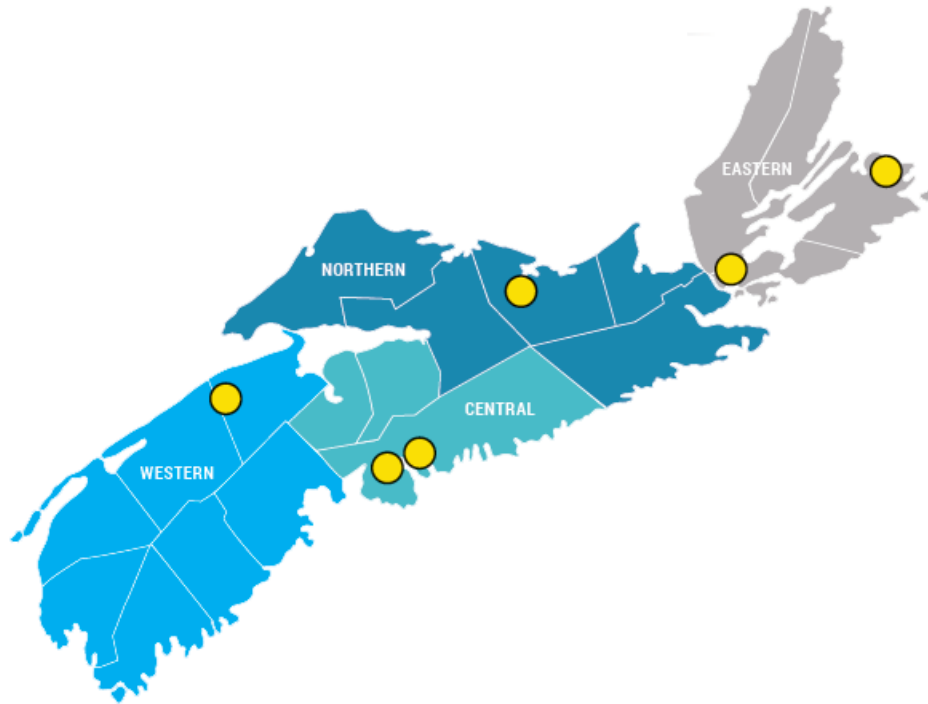






Figure 6 A map of Nova Scotia's four Air Zones with yellow dots indicating the location of ambient air monitoring station sites. (NSE, AQB, 2015)

For each air zone, now covering rural areas in addition to only populated areas, NSE will monitor $PM_{2.5}$ and O_3 concentrations and release the results in an Air Zone Management Report. The CCME is currently developing CAAQS for NO_2 and SO_2 for future addition to the AQMS as well, to match NAAQO values defined for these gases. The Air Zone Management Framework (AZMF) has colour-coded air management threshold values that determine what stage the zone is at in terms of air quality and how to act upon it (NSE, AQB, 2015). The air management threshold values and actions are listed in Table 4.

















Table 4 The Air Quality Management Framework and associated threshold values. (NSE, AQB, 2015)

Management Level	Management Actions	Air Management Threshold Values		
		8-hour Ozone (ppb)	PM _{2.5} 24-hour (µg/m ³)	PM _{2.5} Annual (µg/m ³)
 Red ^{††}	Actions for Achieving Air Zone CAAQS	63	28	10
 Orange	Actions for Preventing CAAQS Exceedance	56	19	6.4
 Yellow	Actions for Preventing Air Quality Deterioration	50	10	4
 Green	Actions for Keeping Clean Areas Clean	0	0	0

†† The threshold values for the 'Red' management level are equal to the numerical values of the Canadian Ambient Air Quality Standards (CAAQS).

Nova Scotia's first Air Zone Management Report came out in 2014, and the results for years 2012 to 2014 are shown in Table 5.

Table 5 Nova Scotia air zone management levels and CAAQS achievement results for air zone monitoring (2012-2014 average). (NSE, AQB, 2015)

Air Zone	Management Level*	Management Actions	Driver†	Results		
				Ozone 8-hour (ppb)	PM _{2.5} 24-hour (µg/m ³)	PM _{2.5} Annual (µg/m ³)
Central	 Yellow	Actions for Preventing AQ Deterioration	Ozone	 52	 14	 6.0
Eastern	 Orange	Actions for Preventing CAAQS Exceedance	PM _{2.5} annual	 50	 16	 6.9
Northern	 Orange	Actions for Preventing CAAQS Exceedance	PM _{2.5} 24-hr and annual	 45	 21	 7.5
Western	 Orange	Actions for Preventing CAAQS Exceedance	Ozone	 59	 12	 4.8

* Management levels for each air zone are determined by the "Driver." These levels have continuous improvement as a priority and require more stringent actions as the driver approaches CAAQS limit.

† "Driver" means the pollutant that has the highest measurement relative to the CAAQS (Measurement CAAQS) within each air zone. There can be more than one driver in an air zone if relative measurements are equal. For example, in the 2014 reporting year the Northern Air Zone has two drivers because each are equal to 75% of the CAAQS ($21/28 = 0.75$ and $7.5/10 = 0.75$)

For the Central Air Zone, which includes Halifax, the "yellow" management level indicates that this zone needs to act in order to prevent air quality deterioration. The "driver" is O₃, which was assigned a management level of "yellow", but 24-hour PM_{2.5} and annual PM_{2.5} measurements also received a management level of "yellow". The reason O₃ is the "driver" when the others have been assigned the same management level is because O₃ has the highest measurement relative to its CAAQS limit. The O₃ measurement is at ~83% of its CAAQS limit of 63 ppb ($52/63 \approx 0.83$), whereas 24-hour PM_{2.5} and annual PM_{2.5} measurements are at 50% ($14/28 = 0.5$) and 60% ($6/10 = 0.6$) of their CAAQS limits, respectively. For the other three air zones, because there is at least one management level result of "orange" for each air zone, actions need to be taken to prevent CAAQS exceedance of PM_{2.5} and O₃. Notably, O₃ in the Northern Air Zone is at a

green management level. All air zones in Nova Scotia achieved the CAAQS for PM_{2.5} and O₃ for 2012-2014.

With stringent air quality standards and the implementation of a new Air Zone Management System, Nova Scotia strives to continue protecting the health of citizens and the environment. It should be noted that the AQMS, in addition to air zone management, also comprises regulating mobile sources (vehicles) and industrial emitters, as well as airshed coordination, which requires multiple governments working together (NSE, AQB, 2015).

1.2.2. National Air Pollution Surveillance (NAPS) Data

The National Air Pollution Surveillance (NAPS) program is a cooperative agreement between the federal government, the provinces, territories, and some municipal governments with the goal of providing accurate and long-term air quality data of a uniform standard across Canada. Nova Scotia joined the NAPS program when it was established in 1969 to monitor and assess the quality of ambient air in the populated regions of Canada (Environment and Climate Change Canada, 2013). The Canada-wide Air Quality Database (CWAQD) is the national archive, managed by NAPS, for validated air quality data submitted by NAPS partners, i.e., NSE. All air quality measurements by NSE from monitoring sites across Nova Scotia are shared with the larger NAPS network and are available to the public along with other air quality measurements from across the country at <http://www.ec.gc.ca/rnsps-naps/>. This data is used to determine achievement of the CAAQS, report the Air Quality Health Index (AQHI), assess air quality

trends, determine the effectiveness of regulations, assess the impacts of air quality on health and the environment, and support strategies to reduce air emissions and manage air quality. It is interesting to note that industrial emitters (with permits) locate and maintain ambient air stations as well as perform their own dispersion modelling to measure their impact on ambient air directly, as opposed to the integrated picture that the NSE network is designed to provide (NSE, AQB, 2015). Air quality measurements specific to Nova Scotia can be found on the NSE ambient air quality website (<https://novascotia.ca/nse/airdata/>), which is also available to the public. The NSE data portal contains a combination of validated and “raw” near-real-time data.

Using NAPS data, the Air Quality Branch of NSE produced its latest air quality report called “The Air We Breathe”, released in 2009. It is a data summary of the major air pollutants in Nova Scotia from 2000 to 2007, with emphasis on GLO (O₃), PM, CO, NO₂, SO₂, volatile organic compounds (VOCs), and acid precipitation (NSE, AQB, 2009). Typical global concentrations of O₃, PM, CO, NO₂, and SO₂ were briefly discussed in earlier sections, but now to take a closer look at typical concentrations in Nova Scotia, with a focus on the city of Halifax.

According to Nova Scotia’s air quality report, O₃ levels were higher in the western region, but lower in urban regions (Halifax and Sydney) because of higher levels of traffic (Nova Scotia Environment, Air Quality Branch, 2009). This may seem counterintuitive, but follows from Figure 4 and the hydrocarbon-limited regime in which O₃ decreases with an increase in NO_x. Figure 7 shows the diurnal variation of O₃ and NO₂ concentrations for Halifax in 2006, indicating that Halifax is in a hydrocarbon-limited regime when it comes to O₃ production.

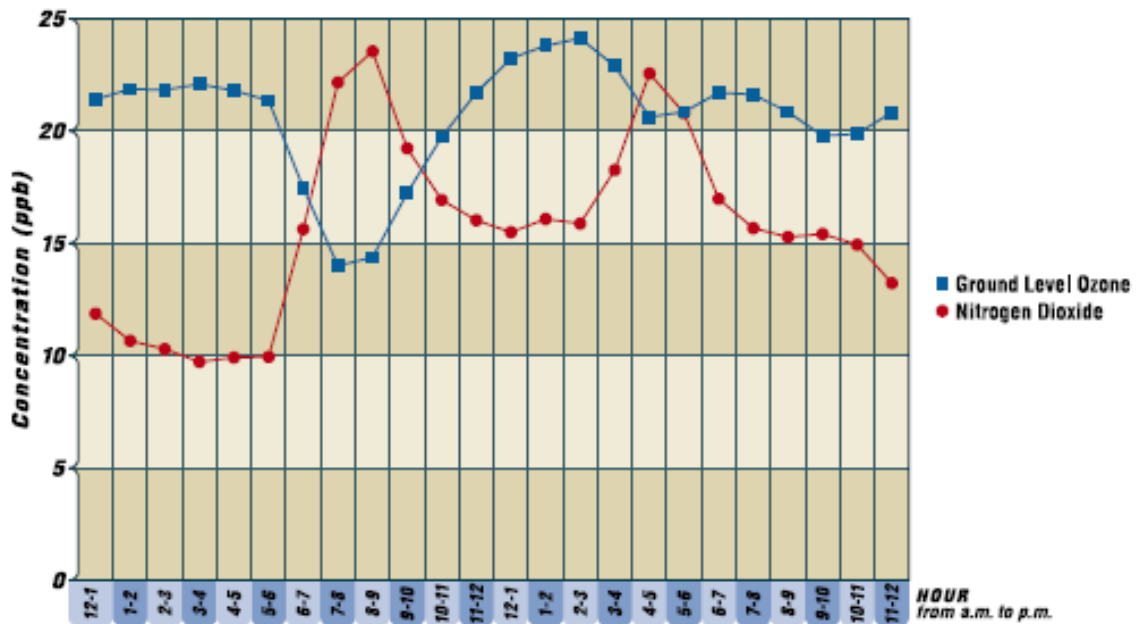


Figure 7 Diurnal variation of O₃ and NO₂ concentrations in ppb for the city of Halifax based on data from 2006. (NSE, AQB, 2009)

Figure 8 was created by downloading and plotting more recent O₃ concentration data from NSE’s ambient air quality website, and it shows annual 1-hour averages of O₃ concentrations for years 2004 to 2014.

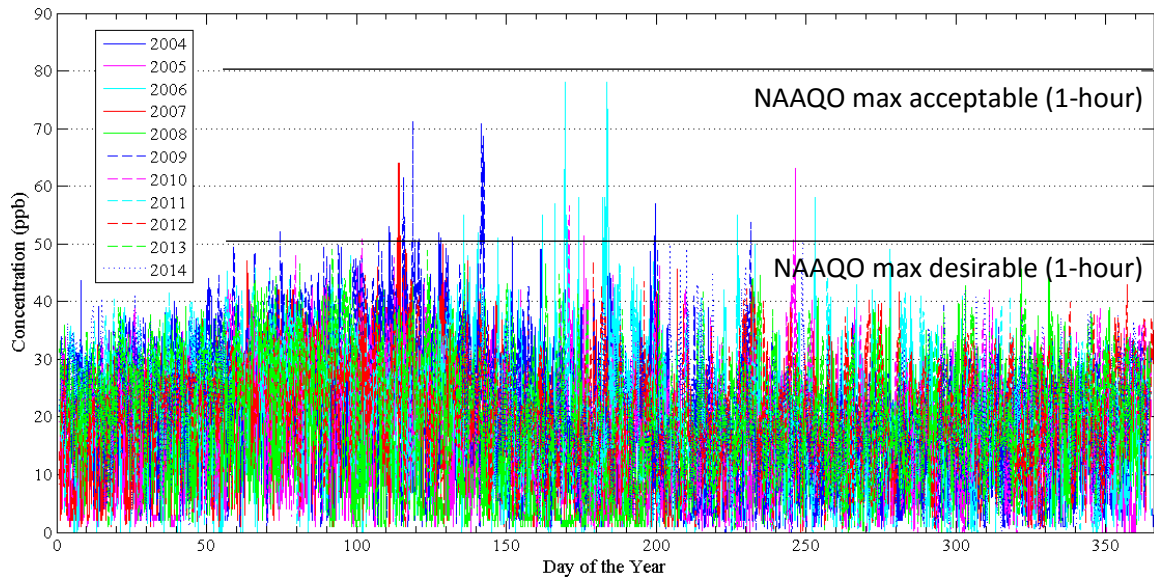


Figure 8 Annual 1-hour averages of NAPS O₃ concentrations measured on Barrington Street in Halifax for years 2004 to 2014. January 1st is day 1 and December 31st is day 365 (x-axis).

The data shows a clear rise in baseline O₃ concentrations in the springtime and exceedances of the 1-hour “maximum desirable level” of 50 ppb in summer months.

Measurement results of PM are presented in three ways in the provincial report: continuous monitoring of PM_{2.5}, intermittent monitoring of PM_{2.5} and PM₁₀, and monitoring of total suspended particulates (TSP) (NSE, AQB, 2009). Filter-based TSP sampling was terminated after 2004 and replaced with continuous monitoring of PM_{2.5} and PM₁₀. Continuous monitoring of PM_{2.5} in Halifax began mid-2006, therefore, continuous PM_{2.5} measurements are only available for the year 2007 (NSE, AQB, 2009). Figure 9 shows the annual maximum one-hour average PM_{2.5} concentrations for each station from 2000 to 2007 (NSE, AQB, 2009).

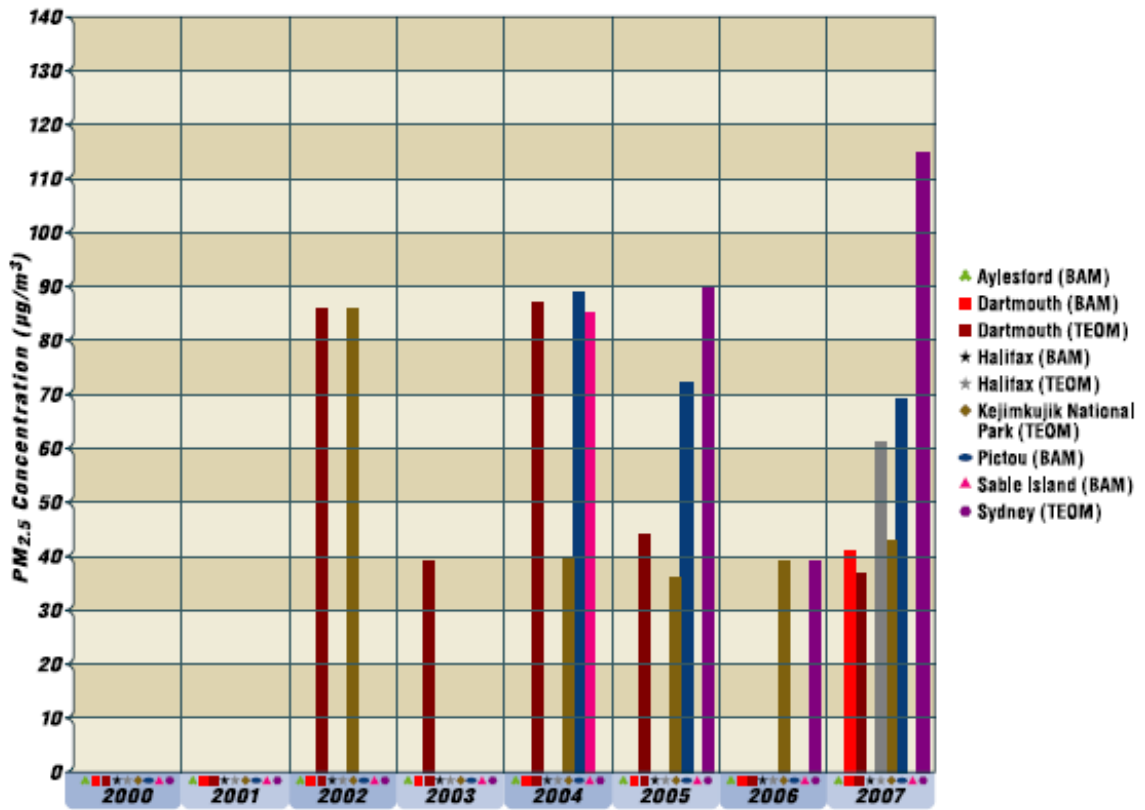


Figure 9 Annual maximum 1-hour average PM_{2.5} concentrations from 2000 to 2007 for multiple stations in Nova Scotia. BAM and TEOM refer to two PM_{2.5} aerosol sampling instruments. (NSE, AQB, 2009)

Overall, the max 1-hour average PM_{2.5} data is limited, especially for Aylesford, Dartmouth, Halifax, and Sable Island. However, there was sufficient data to calculate the maximum 24-hour average and the annual average of TSP in Halifax and Sydney for years 2000 to 2004 (Figure 10). TSP includes PM_{2.5} and PM₁₀, along with any other suspended particulates captured in a filter.

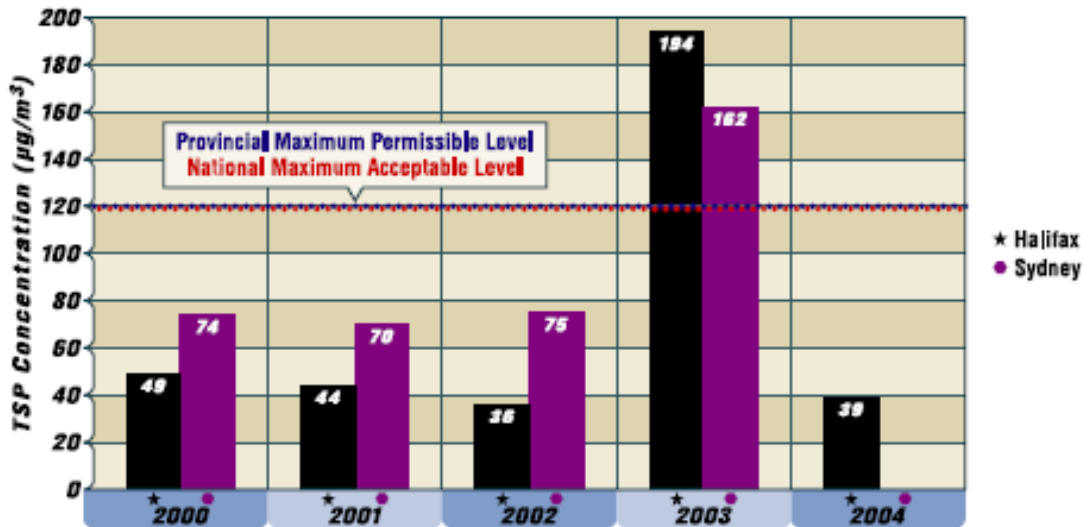


Figure 10 Annual maximum 24-hour average TSP concentration for years 2000 to 2004 in Halifax and Sydney, Nova Scotia. (NSE, AQB, 2009)

In 2003, Halifax and Sydney annual maximum 24-hour average TSP concentrations exceeded both the provincial maximum permissible level and the national maximum acceptable level, but it must be noted that the exceedance occurred only once at both stations. Accordingly, Figure 11 shows the annual average TSP concentration for each year in Halifax and Sydney as well below permissible, and even desirable levels, for all five years.

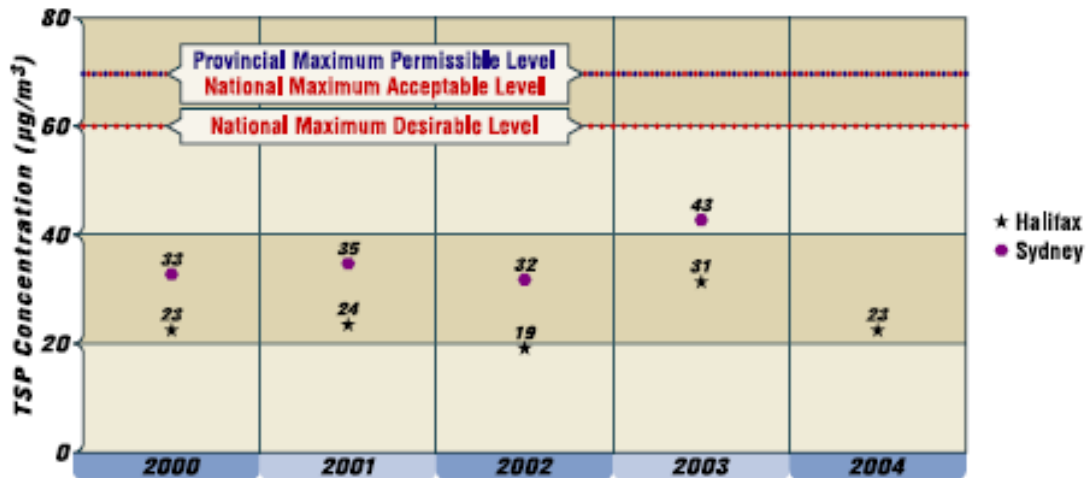


Figure 11 Annual average TSP concentration for years 2000 to 2004 in Halifax and Sydney, Nova Scotia. (NSE, AQB, 2009)

In Halifax, CO has been monitored since 1990, and since September, 2005 also in Sydney (NSE, AQB, 2009). Figure 12 and Figure 13 show the annual maximum 1-hour and annual maximum 8-hour average CO concentrations for years 2000 to 2007, respectively.

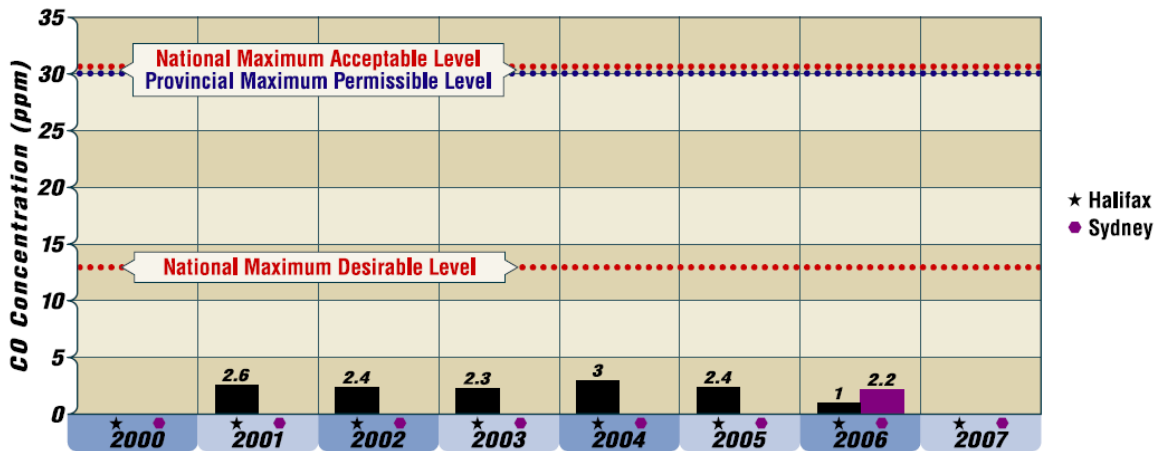


Figure 12 Annual maximum 1-hour average CO concentrations for years 2000 to 2007 for Halifax and Sydney, Nova Scotia. There is no data for Halifax in years 2000 and 2007 or for Sydney in years 2005 and 2007 due to insufficient data. (NSE, AQB, 2009)

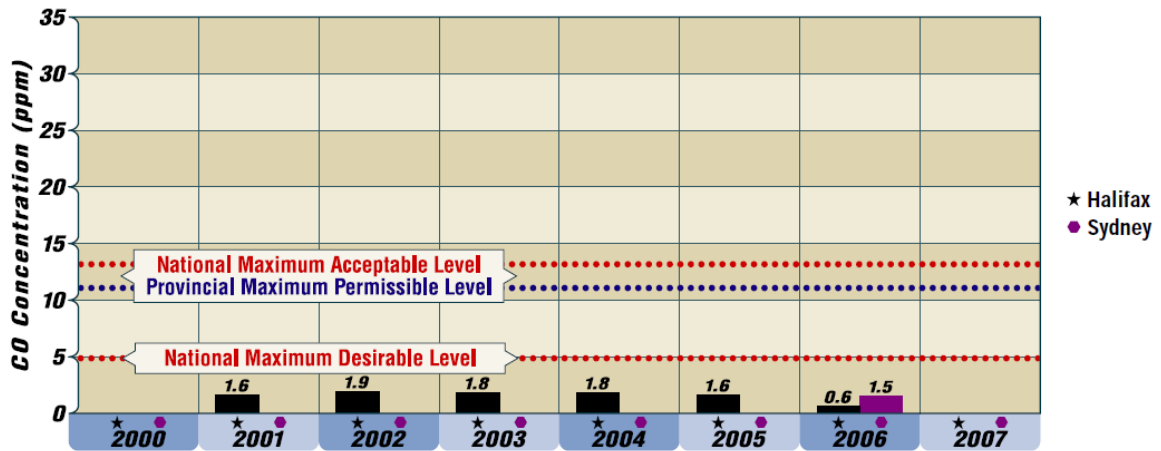


Figure 13 Annual maximum 8-hour average CO concentrations for years 2000 to 2007 for Halifax and Sydney, Nova Scotia. There is no data for Halifax in years 2000 and 2007 or for Sydney in years 2005 and 2007 due to insufficient data. (NSE, AQB, 2009)

CO concentrations in both cities were well below provincial and national standards for both annual maximum 1-hour averages and annual maximum 8-hour averages, with the annual average concentrations of CO from 2000 to 2007 even lower at less than 1 ppm (NSE, AQB, 2009).

Figure 14 is a continuation of Figure 12 with annual maximum 1-hour averages of CO in Halifax for years 2004 to 2015.

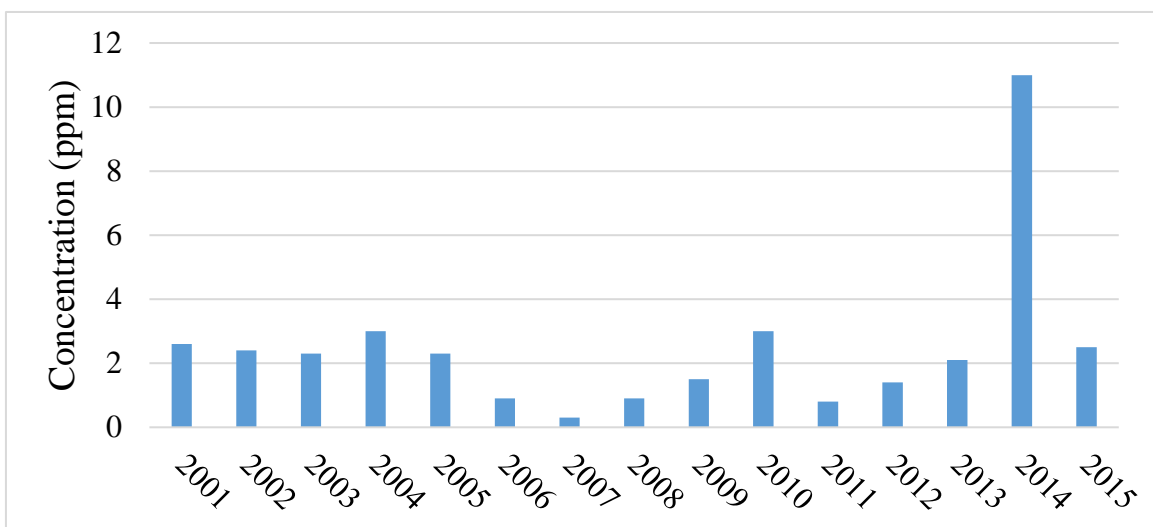


Figure 14 Annual maximum 1-hour average NAPS CO concentrations measured on Barrington Street in Halifax for years 2004 to 2015.

No clear trends in time emerge, but in 2014, CO concentrations were measured on Barrington Street in Halifax at a maximum of 11 ppm.

Figure 15 was created by downloading and plotting more recent CO concentration data from NSE's ambient air quality website, and it shows 1-hour averages of CO concentrations for years 2004 to 2014.

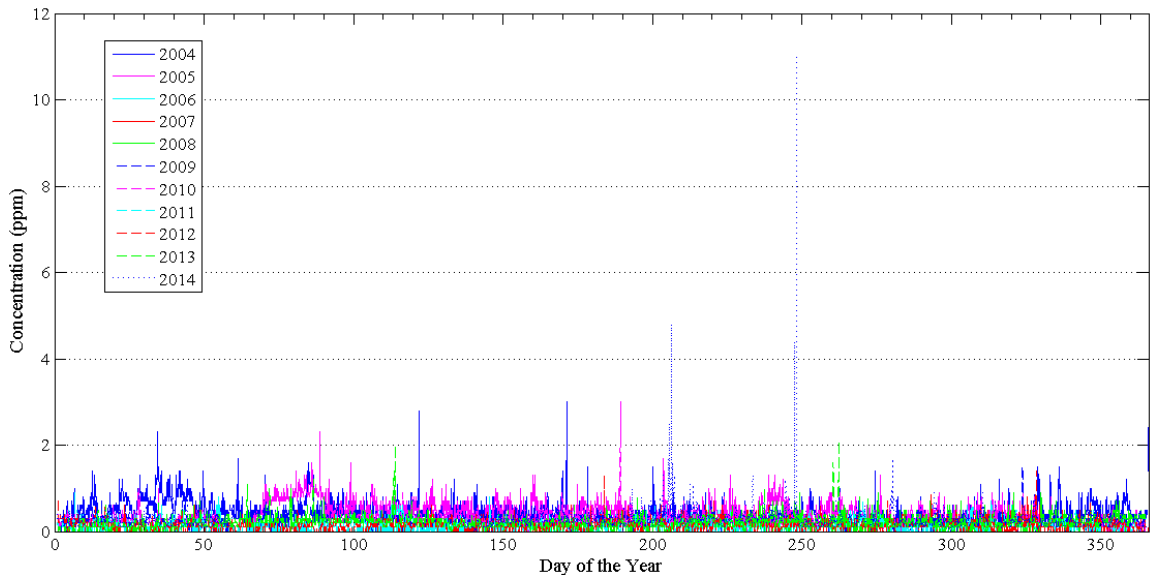


Figure 15 One-hour averages of NAPS CO concentrations measured on Barrington Street in Halifax for years 2004 to 2014. January 1st is day 1 and December 31st is day 365 (x-axis).

The data gives an idea of hourly mean concentrations of CO and the frequency and level of high CO concentrations in the span of a year. Although there are times when CO concentrations reach up to 11 ppm, they have still remained well below what is permitted to occur in one hour (30 ppm) and also below maximum desirable 1-hour levels (13 ppm). Baseline CO concentrations also become slightly elevated in February and March, which is shown in the data for 2004 (blue) and 2005 (pink), respectively.

In terms of NO₂, only the data from Halifax, Dartmouth, and Sable Island were sufficient enough to include in the report (NSE, AQB, 2009). Figure 16 shows the diurnal variation of NO₂ concentrations at these three sites for the year 2007.

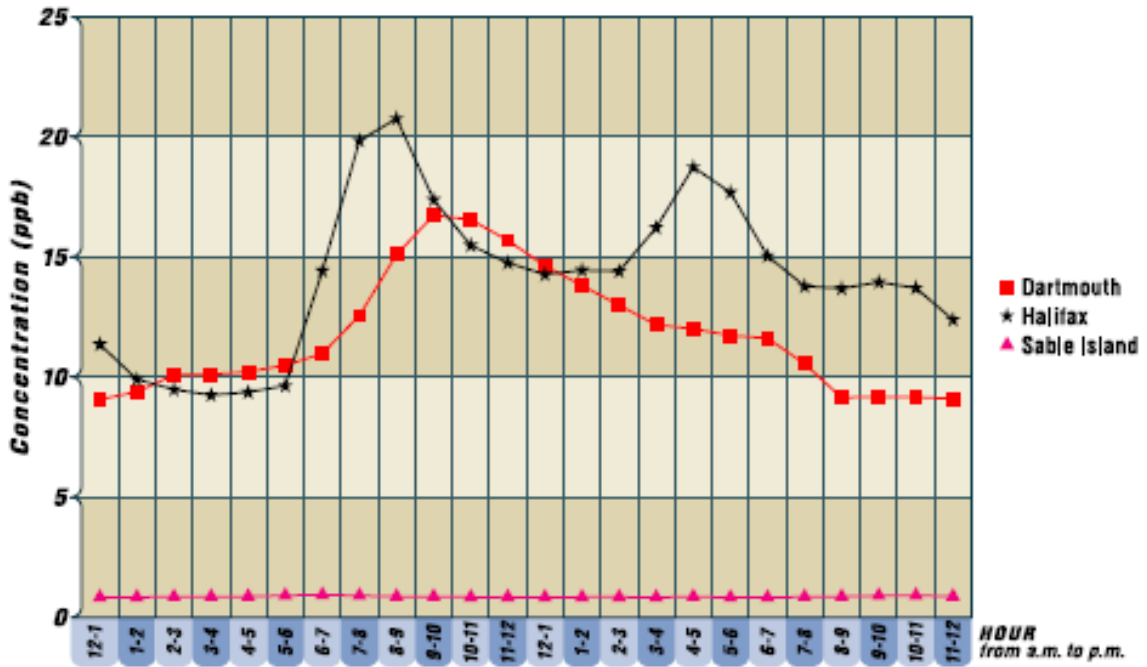


Figure 16 Diurnal variation of NO₂ concentrations at the Dartmouth, Halifax, and Sable Island monitoring stations based on data from 2007. (NSE, AQB, 2009)

For Halifax, one can see that NO₂ concentrations are higher in the morning and afternoon during rush hours. However, the trend is not as obvious in Dartmouth and is non-existent on Sable Island because it is isolated from traffic emissions.

Last, but not least, SO₂ concentrations were lower than the provincial and national standards from 2000 to 2007 except for in Halifax, where concentrations exceeded the 1-hour national maximum desirable level (170 ppb) for only two hours, and the annual national maximum desirable level (10 ppb) for two years in 2001 and 2002 (NSE, AQB, 2009). However, all locations had 1-hour, 24-hour, and annual SO₂

concentrations well below the provincial maximum permissible level and the national maximum acceptable level (NSE, AQB, 2009).

Because the latest provincial air quality report was only released in 2009, it does not include pollutant concentration measurements for the years 2008 to 2015. This new data is currently available on NSE's ambient air quality website, and therefore, the data for O₃, SO₂, NO, NO₂, NO_x, and PM_{2.5} concentrations were downloaded and plotted for analysis. Figure 17 shows annual maximum 1-hour average concentrations of O₃, SO₂, NO, NO₂, NO_x, and PM_{2.5} for the years 2004 to 2015.

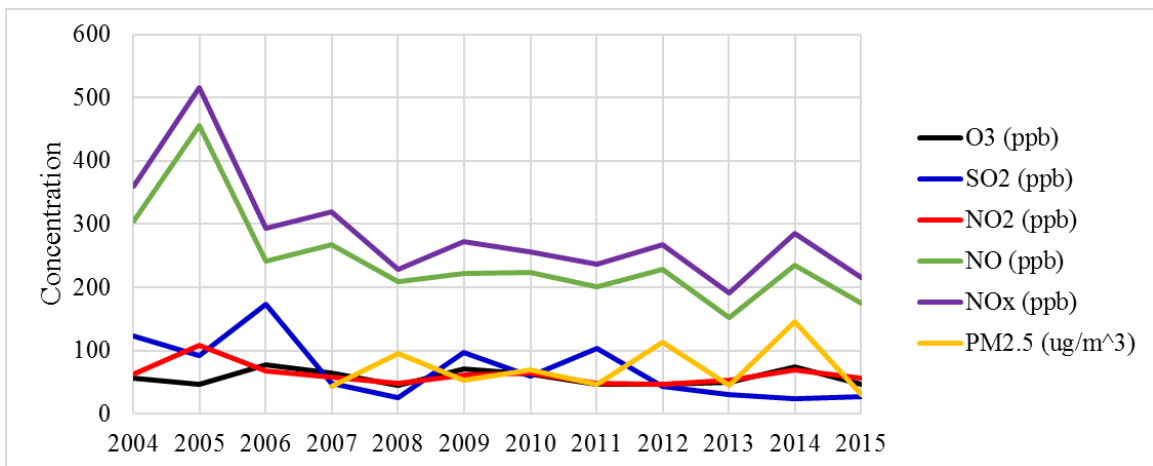


Figure 17 Annual maximum 1-hour average concentrations of O₃, SO₂, NO, NO₂, NO_x, and PM_{2.5} measured on Barrington Street in Halifax from 2004 to 2015.

Results show a slight decrease in maximum 1-hour average NO and NO_x concentrations after 2005, however, all other pollutants seem to have been steady at ~75 ppb (~75 µg/m³ for PM_{2.5}). This implies that emission sources responsible for annual maximum 1-hour average concentrations are holding steady, or that large emitters are decreasing, with small sources on the rise.

1.2.3. Other Sources of Air Quality Measurements

NSE and NAPS are not the only sources of air quality measurements for Nova Scotia. University-based researchers in the field of air pollution and air quality go out and measure trace gas concentrations or use atmospheric model calculations for their own work as well. One such researcher in the field in Atlantic Canada is Dr. Mark Gibson from the Department of Process Engineering and Applied Science at Dalhousie University. Some of his work involves dispersion model evaluation of different air pollutants and others involve direct passive sampling techniques (Gibson, Kundu, & Satish, 2013; Gibson et al., 2009). One of his studies involved using nitrite-impregnated passive samplers to measure long-term GLO concentrations in the rural Annapolis Valley, Nova Scotia (Gibson et al., 2009). Gibson et al. (2009) observed minimum, maximum, and mean ambient annual GLO concentrations of 7.7, 72.1, and 34.3 ± 10.1 ppbv, respectively, from August 2006 to September 2007. In another study, Gibson and coauthors used the AERMOD Gaussian plume air dispersion model to evaluate $PM_{2.5}$, NO_x , and SO_2 from point and major line sources in Nova Scotia (Gibson, Kundu, & Satish, 2013). They state that typical average concentrations of $PM_{2.5}$, NO_2 , and SO_2 in rural Nova Scotia are $0.1 \mu\text{g}/\text{m}^3$, 0.05 ppb, and 0.06 ppb, whereas typical concentrations in urban Halifax are $2.5 \mu\text{g}/\text{m}^3$, 2.1 ppb, and 0.4 ppb, respectively (Gibson, Kundu, & Satish, 2013).

Another researcher in the field, Dylan Millet, looked at the chemical characteristics of North American surface layer outflow from the United States over Chebogue Point, Nova Scotia during outflow periods (Millet et al., 2006). Using output

from a 3-D model of atmospheric composition, Millet et al. (2006) estimated that CO directly emitted from U.S. pollution sources account for up to 28% of the total CO observed at Chebogue Point during outflow periods.

These are a few examples of air pollution research in Nova Scotia, and for the most part it is limited compared to research in other parts of the world. This lack of information, especially concerning measurements of CO and other trace gases, is, in part, what motivates this honours thesis work.

2 Experimental Methods and Materials

2.1. Molecular Spectroscopy

Molecular spectroscopy can be described as the study of the interaction of electromagnetic waves (electromagnetic radiation) and matter (Banwell & McCash, 1994). In the case of this honours thesis work, it allows one to identify gases in the atmosphere, and their concentrations, based on their fingerprint in the electromagnetic spectrum. However, to have a better understanding of how this works, there are a few basic concepts that need to be explained first.

The Earth's main source of energy is the Sun, which emits electromagnetic radiation, of which the majority is in the form of visible light and heat. The continuum of electromagnetic radiation is referred to as the electromagnetic spectrum, which is shown in Figure 18.

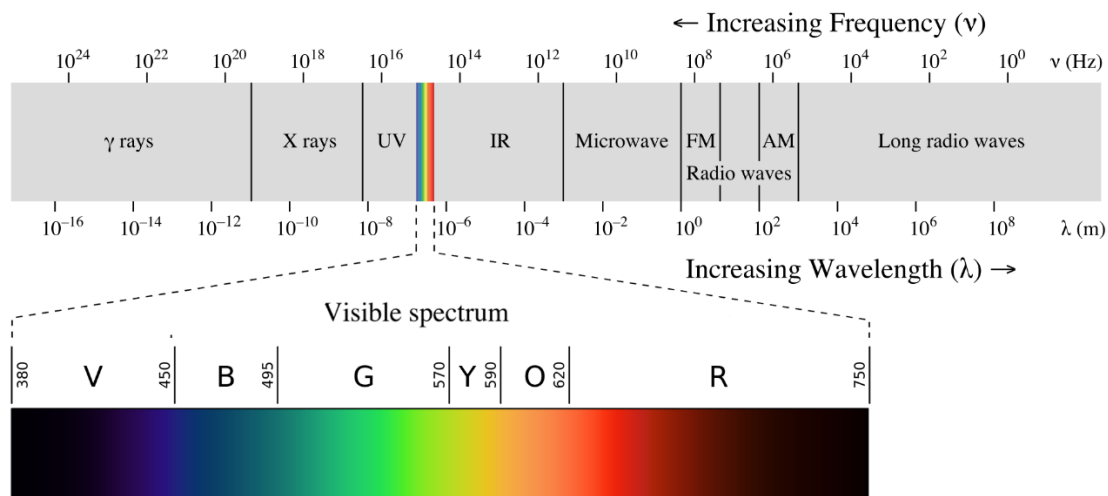


Figure 18 The electromagnetic spectrum in terms of frequency (top axis) and wavelength (bottom axis). [Untitled image of the electromagnetic spectrum]

The light that one sees (visible electromagnetic radiation) is a small fraction of the whole electromagnetic spectrum, meaning that most radiation is invisible. It is common for electromagnetic radiation to be characterized in terms of wavelength (λ), but it may also be characterized in terms of frequency (ν) or wavenumber ($\bar{\nu}$), which is equal to the mathematical inverse of the wavelength ($1/\lambda$) (Banwell & McCash, 1994). Wavenumber represents the number of wave crests or troughs per unit length, and as such, it is directly proportional to frequency. The full spectrum in Figure 18 is characterized in terms of wavelength in meters, and the visible portion of the spectrum in the expanded section is shown in nanometers (nm). Radiation at a given wavelength will also have an associated frequency, which is given by the wave equation:

$$c = \lambda\nu = \frac{c}{\bar{\nu}}, \quad (2.1)$$

where c is the speed of light and ν is in units of Hertz, Hz (sec^{-1}) (Banwell & McCash, 1994).

When electromagnetic radiation interacts with a molecule, a portion of it can be absorbed at a wavelength specific to the molecule that it interacts with. All molecules have unique quantized electronic energy states and, additionally, a particular molecule can exist in a variety of vibrational and rotational energy levels (Banwell & McCash, 1994). A molecule's electronic energy is determined by the configuration of electrons around the nucleus, and its vibrational-rotational energy is determined by the configuration of atoms in the molecule (Banwell & McCash, 1994). Figure 19 illustrates the vibrational modes of CO_2 , for example. Rotation of a molecule is also important in the characterization of its energy state and superimposes itself on the vibrational state.

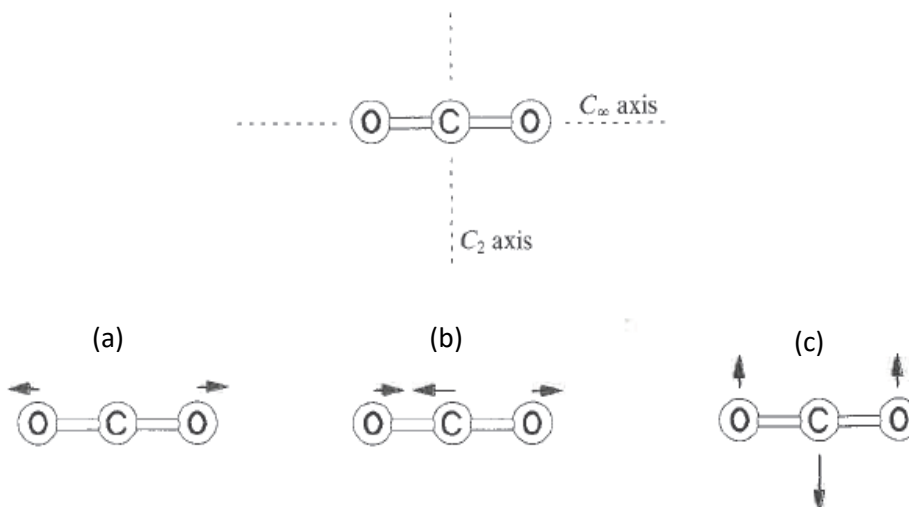


Figure 19 Symmetry and fundamental vibrations of the carbon dioxide molecule. (a) Symmetric stretching, (b) antisymmetric stretching, and (c) bending mode. (Banwell & McCash, 1994)

These different energy states of a given molecule are quantized, meaning that only a finite amount of energy unique to that molecule can interact with it and excite it (Banwell & McCash, 1994). Exciting a molecule involves absorption of radiation at a specific wavelength that corresponds to the finite amount of energy (ΔE) required to cause the molecule to jump from its ground state electronic energy level (non-excited) to its excited state electronic energy level, or to similarly excite its vibrational-rotational state (Banwell & McCash, 1994). Once that finite amount of energy is absorbed, it can later be emitted, allowing the molecule to go from its excited state to its ground state again. Physicist Max Planck showed that the frequency and energy of such absorbed or emitted quanta are related by

$$v = \Delta E / h, \tag{2.2}$$

where ΔE is in units of Joules (J), and h is a universal constant – Planck’s constant (Banwell & McCash, 1994). These finite energies absorbed by a molecule at specific

wavelengths represent the fingerprint of that molecule in the electromagnetic spectrum of radiation incident on it.

Many laboratory studies of gas absorption have been conducted, e.g., Rothman et al. (2013). Based on where absorption occurs in the electromagnetic spectrum, and the intensity of the absorption, it is possible to identify a gas in the atmosphere and its concentration, respectively.

2.2. Open-Path Fourier Transform Infrared (OP-FTIR) Spectrometer

One of many techniques used to identify gases and their concentrations in the atmosphere involves the use of an Open-Path Fourier Transform Infrared (OP-FTIR) spectrometer. The OP-FTIR spectrometer system used for this honours thesis work is manufactured by Bruker Corporation and consists of a spectrometer, a telescope, and a PLX retroreflector array™ (Bruker Corporation, 2015; PLX Innovative Optical Systems, n.d.). The instrumentation also comes with a spectral analysis software called OPUS-RS (Bruker Corporation, 2015). Figure 20 shows a simplified diagram of the open-path system (OPS) optics.

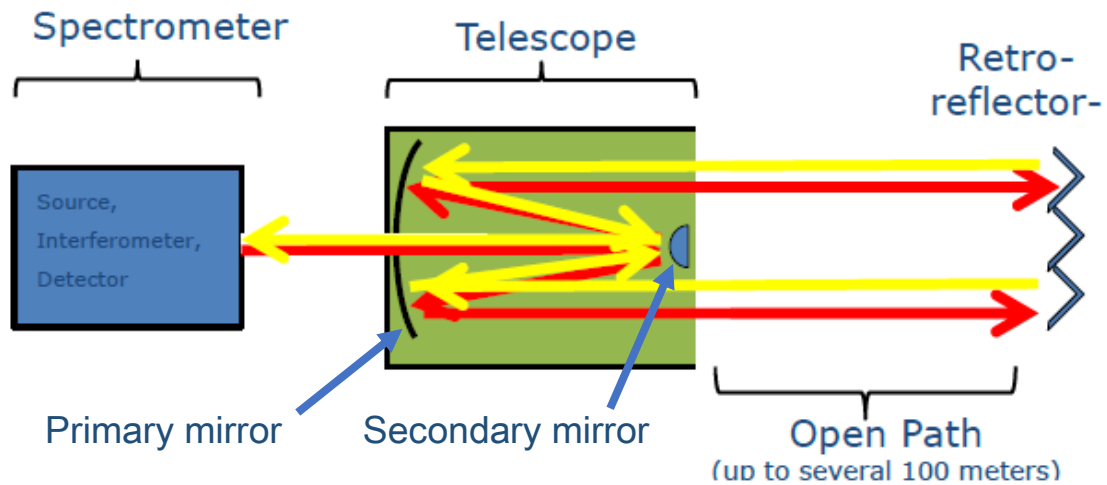


Figure 20 A simplified diagram showing the components of the OPS by Bruker. The red and yellow arrows represent the return-light path through the system, originating from the spectrometer. (Bruker Corporation, 2015)

The spectrometer housing includes a global™ radiation source, which emits in the mid-infrared (MIR) spectral range ($\sim 400\text{-}4000\text{ cm}^{-1}$), an interferometer, which modulates this radiation into an interferogram, and a detector, which records the

returned radiation after it has traversed the open path (Bruker Corporation, 2015; Griffiths & de Haseth, 2007).

The interferometer is the Bruker RockSolid™ pendulum interferometer, which accomplishes the same task as the classic (and simpler to follow) Michelson interferometer, as shown in Figure 21, which consists of two arms: the fixed mirror arm and the moving mirror arm.

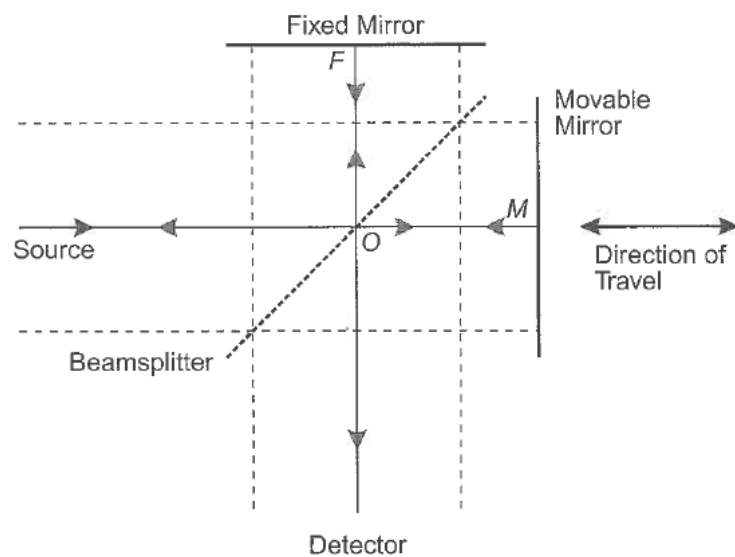


Figure 21 A classic Michelson interferometer. (Griffiths & de Haseth, 2007)

The beam from the globar enters the interferometer from one end and strikes a beamsplitter, which is designed to transmit half of the radiation that strikes it and reflect the other half (Smith, 1996). One beam will strike the fixed mirror arm, the other beam will strike the moving mirror arm, and then the two beams will recombine at the beamsplitter (Smith, 1996). The difference in distance between the moving mirror and the beamsplitter inside the interferometer (Figure 21) compared to the distance between the stationary mirror and this same beamsplitter is called the optical path

difference (OPD) (Smith, 1996). A change in the OPD will change how the two radiation beams derived from the source interfere with one another once they recombine (Smith, 1996). The two beams will either interfere constructively or destructively. Although the global™ light source in a OP-FTIR spectrometer is broadband in practice, a monochromatic (single wavelength) light source best illustrates the concept of wave interference. Constructive interference occurs when two monochromatic light beams recombine with an OPD of λ and produce a light beam whose amplitude is two times the amplitude of each of the individual beams (Smith, 1996). Destructive interference occurs when two monochromatic light beams recombine with an OPD of $\lambda/2$, such that wave crests align exactly with wave troughs and the resultant beam amplitude is zero (Smith, 1996). The interference that occurs inside the interferometer for all wavelengths produces the modulation of the broadband beam, which is later useful for distinguishing return light that originated in the spectrometer from ever-present atmospheric emissions, which are not modulated in this way (A. Wiacek, personal communication, March 2, 2016). The interferometer, within the spectrometer box, is a key component of the OPS because it creates the “interferogram”. An interferogram is a plot of radiation intensity against OPD in the spectrometer. The incoming radiation produces an electrical response in the detector based on the radiation intensity after it has traversed the open path. As the moving mirror in the interferometer scans back and forth, different intensities are recorded. The interferogram created by a monochromatic source, in Figure 22(a), looks like a simple cosine wave, but the interferogram created by a broadband infrared source, in Figure 22(b), looks like a spike of greatest intensity at zero

path difference (ZPD) with a decrease in intensity as the OPD increases towards its maximum OPD. This is because most component wavelengths are in phase at ZPD, but most are out of phase at OPD_{max} .

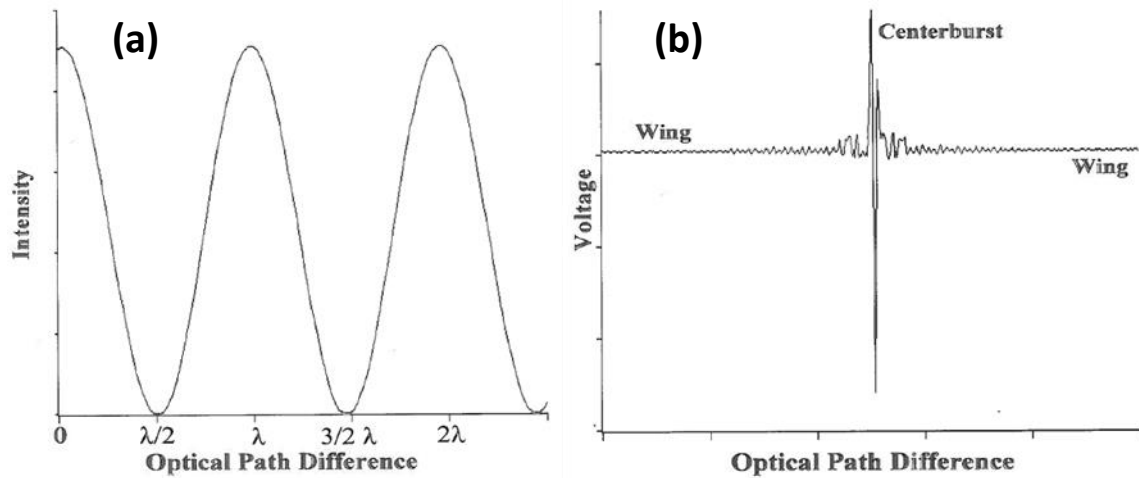


Figure 22 (a) Interferogram of a monochromatic radiation source of wavelength λ . (b) Interferogram of a broadband infrared source. The y-axis represents voltage because this is the unit in which the detector produces an electrical response. (Smith, 1996)

Figure 22(a) indicates that maximum intensity (constructive interference) occurs at an OPD where the two light beams are in phase. This is summarized in equation form as follows:

$$\delta = n\lambda, \quad (2.3)$$

where δ is the OPD and n is any integer (Smith, 1996). Figure 22(a) also indicates that minimum intensity (destructive interference) occurs at an OPD where the two light beams are out of phase by half of a wavelength of the beam. This is summarized in equation form as follows:

$$\delta = (n + 1/2)\lambda. \quad (2.4)$$

The radiation source used in the spectrometer is a broadband infrared source, which means the source gives off radiation at a continuum of wavelengths. Each wavelength gives rise to a different cosine wave interferogram, but the total interferogram measured by the detector is the sum of all of the interferograms from all the different infrared wavelengths (Smith, 1996). The intensity spike in the center of the interferogram in Figure 22(b) is called the centerburst and the regions on either side of the centerburst where intensities are lower at greater OPDs are called wings. The centerburst occurs as a result of all wavelengths constructively interfering at ZPD, while the wings occur because most wavelengths interfere destructively away from ZPD. What is advantageous in an FTIR spectrometer over other techniques is that the interferogram encodes the intensity and wavelength information so that all of the data can be measured at once (Smith, 1996). The analysis of an interferogram is discussed further below.

Once the beam traverses through the open path, strikes the retroreflector, and returns through the open path, it will hit the detector inside the spectrometer after a second pass through an additional beamsplitter (external to the interferometer), as shown in Figure 23.

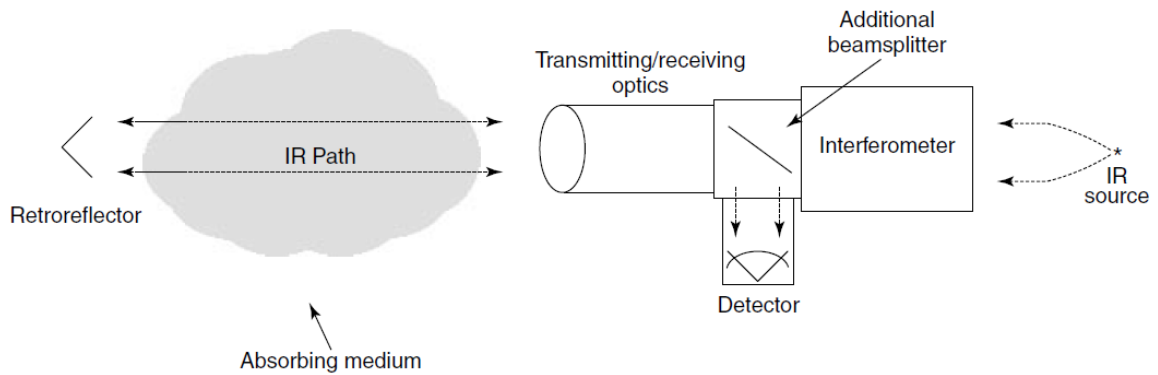


Figure 23 Configuration of the OPS used for this honours thesis work. (Russwurm & Childers, 2002)

Lastly, the detector is the part of the spectrometer that measures the variation of radiation intensity with OPD once the beam has travelled through the open path, providing the electronic signal (information on beam intensities) that creates the interferogram.

The telescope is the part of the system where the radiation is collimated before it is sent out towards the retroreflector. Collimation of the beam modifies it so that the light rays travel parallel to one another, minimizing divergence of the beam in the open path. Illustrated in Figure 20 and Figure 24(b), the 12-inch diameter Schmidt-Cassegrain telescope consists of a large primary mirror at the back side, and a small adjustable secondary mirror at the front (Bruker Corporation, 2015). The radiation will exit the interferometer and enter the telescope through the external beamsplitter, first hitting the adjustable secondary mirror and then reflecting onto the primary mirror, from which it is sent out towards the retroreflector (Bruker Corporation, 2015). A small loss of radiation occurs because of the suspension of the secondary mirror, but it is necessary for collimating and later collimating the beam. After interaction with gases in the open path, the returning radiation enters the telescope and strikes the external beamsplitter

again (Figure 23) that directs 50% of the beam towards the detector (Russwurm & Childers, 2002). The spectrometer and the telescope are permanently aligned to one another on a modular aluminum rack, as shown in Figure 24(a).

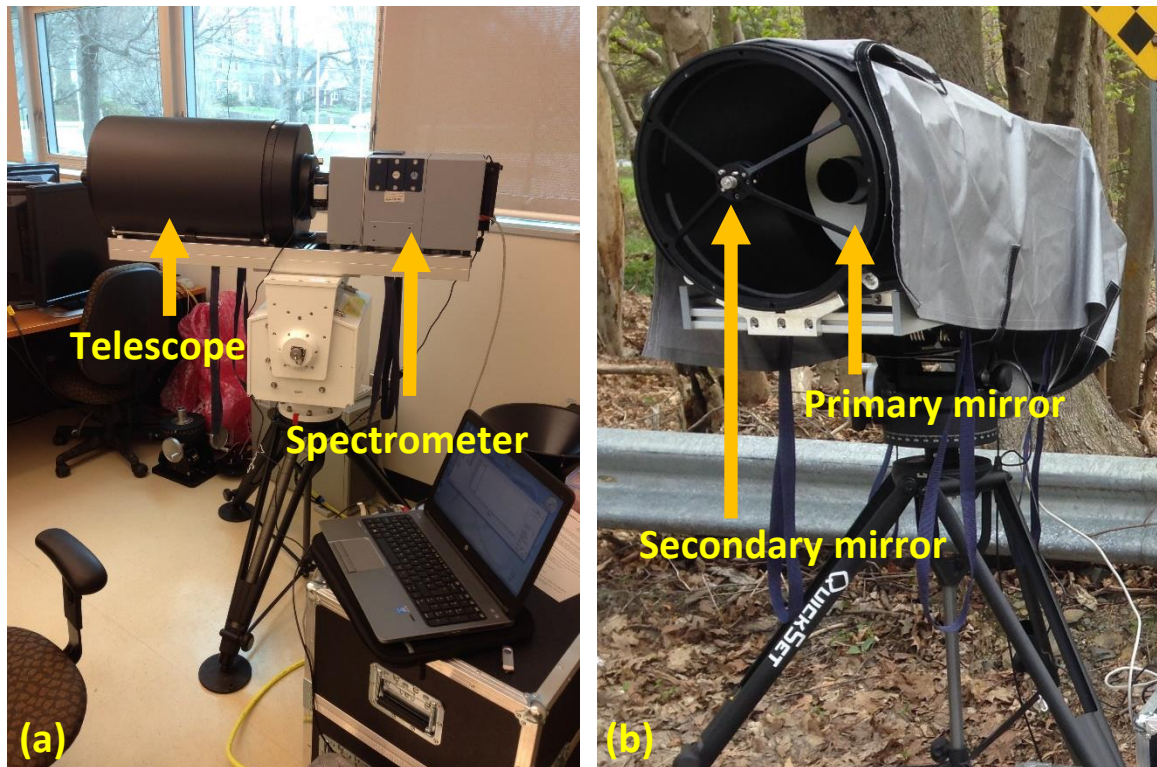


Figure 24 (a) The OP-FTIR spectrometer on its tripod and pan-tilt head. (b) The telescope of the OP-FTIR spectrometer with its primary and secondary mirrors.

The retroreflector array is a separate unit that is positioned in-line with the OP-FTIR spectrometer at the far end of the open path that is being probed. The retroreflector is a device that will reflect radiation very nearly back along a vector parallel to the incident radiation for input angles of roughly $\pm 30^\circ$, although in practice, one aligns to within a few degrees by eye. This allows for the spectrometer to be imperfectly aligned with the retroreflector, whereas a flat mirror would only be aligned to return incident radiation back in a single, precise orientation. The retroreflector used

for this honours thesis work has a deviation angle no worse than 20 arc seconds from a 180° return angle (PLX Innovative Optical Systems, n.d.). The retroreflector is a “honeycomb” array of cube corner mirrors, as shown in Figure 25, with each mirror reflecting a portion of the telescope’s beam. The reason this is done is because manufacturing big mirrors that are optically flat and aligning the corners well enough to have an angle of deviation less than 20 arc seconds is difficult. It is much easier to manufacture an array of smaller cubes with well-aligned corners.



Figure 25 The retroreflector array on a tripod.

Pointing the spectrometer at the retroreflector involves the use of a visible camera attached between the spectrometer and the telescope, as shown in Figure 26 (Bruker Corporation, 2015). The camera points at a movable mirror that can be placed to intersect the axis of the MIR beam of the spectrometer, enabling the user to observe

through the telescope along that MIR beam axis (Bruker Corporation, 2015). The movable mirror is double-sided so that when the camera views through the telescope, the spectrometer simultaneously looks at the “mini-retro” used for calibration purposes (not shown in Figure 26).

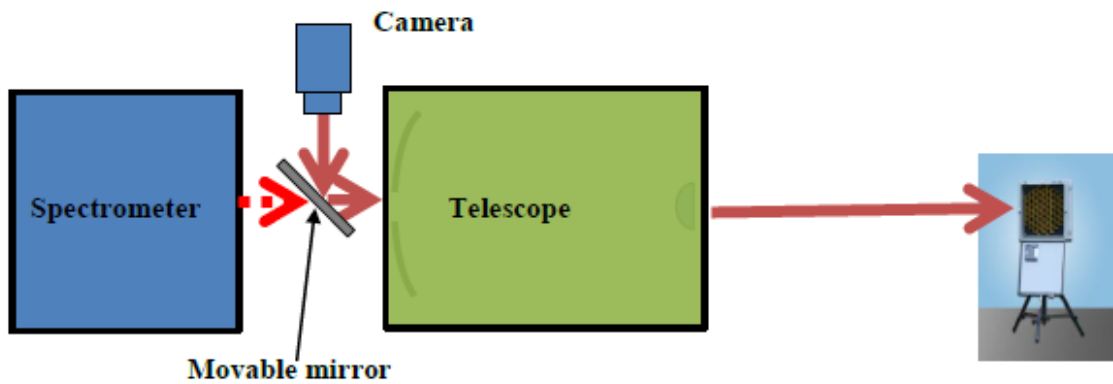


Figure 26 Setup for alignment of the spectrometer and telescope with the retroreflector on the other side of the open path. A camera points at the movable mirror in-line with the MIR beam axis. (Bruker Corporation, 2015)

The camera is connected to a laptop, which displays the spectrometer’s line of sight.

Figure 27 shows a sample image of the line-of-sight across the open path that the camera captured when trying to align the spectrometer.

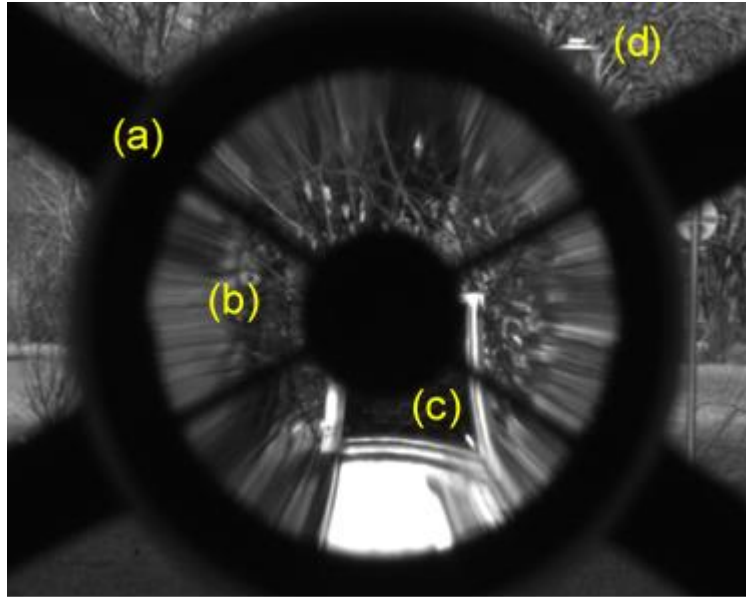


Figure 27 (a) The outline of the secondary mirror and its four suspension legs, (b) the magnified scene in the secondary mirror at the front of the telescope, (c) the retroreflector, with its lid down, at a distance away from the spectrometer as observed by the camera through the telescope, and (d) the rest of the scene in the view of the camera, not magnified. (Bruker Corporation, 2015)

The scene in the secondary mirror, which can be seen in the central part of Figure 27, is what is used to align the spectrometer in order to focus the maximum MIR radiation on the retroreflector, which in turn maximizes the return signal to the detector (Bruker Corporation, 2015). The spectrometer's half field-of-view (FOV) is 21.739 milliradians (mrads), meaning that the divergence of the beam from the line-of-sight axis is ± 21.739 mrads as it enters the telescope (Bruker Corporation, 2015). By simple right-angle triangle trigonometry, this corresponds to the beam spreading outside the area of the retroreflector after only approximately 12 meters of path. In practice, the telescope reduces this beam divergence so that it begins to overfill the retroreflector at approximately 280 meters, which corresponds to an "effective" beam divergence of only ± 1 mrad. In relation to the retroreflector's deviation from a perfect 180° reflection

angle, which the manufacturer lists at 0.097 mrad (20 arc seconds), the spread of the beam in the spectrometer/telescope system is larger.

Above, the source, the detector, and the optics of the open path, as well as the inner workings of the interferometer and the creation of interferograms have been discussed. Although an interferogram contains the information on all trace gases present in the atmosphere, it is not trivial to obtain results by just looking at it; something needs to be done to the interferogram in order to know what information it has encoded. The way one obtains results from an interferogram is by applying to it a mathematical function called the Fourier transform. Joseph Fourier, a mathematician and physicist, developed a theorem that said any mathematical function can be expressed as an infinite sum of sinusoidal waves (Smith, 1996). An interferogram is a sum of sinusoidal waves, each of which contains information about the intensity of a given infrared wavelength (Smith, 1996). Therefore, the Fourier transform function can be applied to the interferogram, resulting in a new mathematical function; i.e., the spectrum, which shows results otherwise “hidden” within the interferogram. One property of the Fourier transform function is that it yields the inverse of the x-axis input unit (Smith, 1996). In the case of interferograms, the x-axis unit is a unit of linear distance for the OPD (cm). Therefore, the Fourier transform will output a spectrum with x-axis units of inverse centimeters (cm^{-1}), or wavenumbers, with a physical spectral resolution of $1/\text{OPD}_{\text{max}}$ (Griffiths & de Haseth, 2007). A sample raw spectrum created with the OPUS-RS software is shown in Figure 28. Because the OP-FTIR spectrometer

measures in the MIR region of the electromagnetic spectrum, the absorption spectrum calculated by OPUS-RS only has a wavenumber range of ~ 500 to 7000 cm^{-1} .

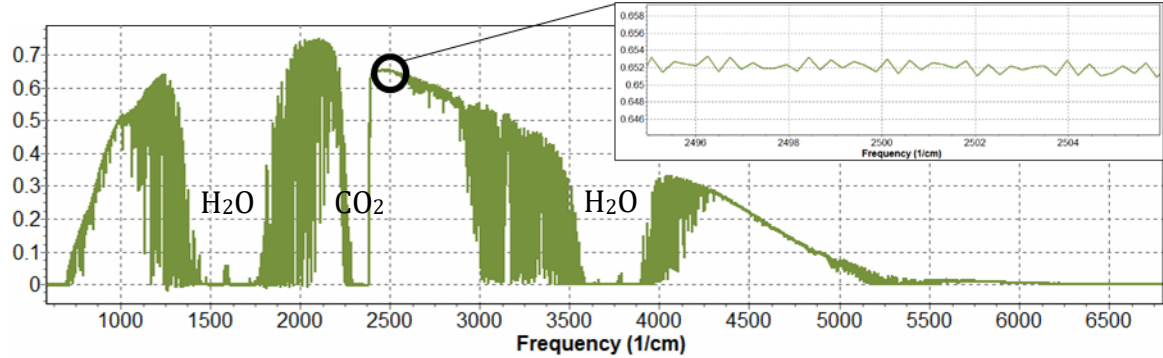


Figure 28 The whole recorded absorption spectrum as calculated from the interferogram. The x-axis is in wavenumbers and the y-axis represents the intensity of radiation after traversing the open path twice. Three regions of the spectrum are labelled with strong-absorbing gases, H_2O and CO_2 , that cause intensity to be zero. The inset is a zoomed region of the intensity around 2500 cm^{-1} . (Bruker Corporation, 2015)

The Fourier transform is a crucial step in being able to analyze measurement results, but before the interferogram is Fourier transformed, it needs to be multiplied by an apodization function. Apodization of an interferogram is a computational step that will reduce noise in the final calculated spectrum by smoothing it. A Fourier transform calculation involves performing a mathematical integral on the interferogram, where by definition, the limits of the integral are plus and minus infinity (Smith, 1996). However, this would mean that the OPD can go from minus infinity to plus infinity, which is impossible to achieve in a practical instrument. A real digitized interferogram has an abrupt transition in recorded intensity from a finite value at maximum OPD to zero just beyond maximum OPD, which leads to artefacts in the Fourier-transformed spectrum that manifest as a sinusoidal oscillation at the maximum resolution of the measurement (0.5 cm^{-1} in the system used for this honours thesis work). These oscillations are often

called “ringing” or “noise” (Smith, 1996). To reduce this effect in the spectrum, the interferogram is gradually, numerically attenuated to zero at the maximum OPD along the x-axis, which is called apodization (Smith, 1996). This term comes from Latin and means to remove the feet of the lineshape (A. Wiacek, personal communication, March 2, 2016). There are multiple types of apodization functions, including the triangular apodization function, which is a popular apodization function used in Fourier transform infrared spectrometry (Griffiths & de Haseth, 2007). In summary, apodization reduces numerical artifacts in the transformed spectrum due to a finite maximum path difference in the interferogram. However, this comes at the cost of a small reduction in the resolution of the spectra, i.e., a line broadening.

Another type of noise is random noise in the instrument itself. One feature of the OPUS-RS software is that it allows one to reduce random noise and improve the signal-to-noise ratio (SNR) by averaging multiple interferograms together in a process called co-adding. This means that each spectrum calculated is a result of a single Fourier transform applied to a number of co-added interferograms, as the user chooses. Co-adding improves the SNR of the spectrum, and the relationship between the SNR and the number of coadds (N) is as follows (Smith, 1996):

$$SNR \propto (N)^{1/2}. \quad (2.5)$$

The signal (S) is the intensity and the noise (N) is the size of ripples in the spectrum. For the OP-FTIR spectrometer, the number of interferogram co-adds is driven by the time it takes to record one interferogram. For example, the spectrometer can measure four samples per second, meaning it can scan through four interferograms at maximum OPD

every second. For this honours thesis work, the number of co-adds was chosen to be 240, which corresponds to one minute of co-adding. If one sets the number of co-adds to be 400, it would take 100 seconds to record the interferograms. The SNR loss as a result of choosing 240 co-adds over 400 co-adds is 30%, and is represented mathematically as follows:

$$\frac{SNR_{400}}{SNR_{240}} = \frac{\sqrt{400}}{\sqrt{240}} = \sqrt{\frac{5}{3}} = 1.3.$$

If one were to increase the SNR by two from 240 co-adds, one would need 960 co-adds, corresponding to four minutes per spectrum:

$$\frac{SNR_{960}}{SNR_{240}} = \frac{\sqrt{960}}{\sqrt{240}} = \sqrt{\frac{12}{3}} = 2.$$

The reason for choosing 240 co-adds as opposed to co-adding for a longer period of time to increase the SNR is to avoid losing peaks of CO concentration in time through excessive averaging. However, the SNR of the spectra is not a limiting issue. The inset in Figure 28 zooms in on a region of the raw spectrum around 2500 cm^{-1} , and from this, one is able to estimate the rough SNR of the instrument. The signal is ~ 0.652 and the noise is ~ 0.001 , indicating an estimated SNR of 652 ($0.652/0.001 = 652$).

As mentioned earlier, quantitative analysis of gases in the atmosphere can be done using many techniques, with OP-FTIR spectroscopy being one of them. Air quality experts use different techniques for different reasons. Advantages of the OP-FTIR spectrometer include being able to measure absorbance of radiation over a continuum of wavelengths rather than a single wavelength or a narrow range, which allows the

quantification of many IR-active gases at the same time. High speed of spectra acquisition and high SNR of spectra is another advantage (A. Wiacek, personal communication, March 2, 2016). Some disadvantages of this technique include only partial and/or somewhat cumbersome mobility and not being able to analyze complex mixtures (A. Wiacek, personal communication, March 2, 2016; Smith, 1996). The latter happens when a region of the spectrum of interest is saturated with a strongly absorbing molecule, such as water vapour ($\text{H}_2\text{O}_{(g)}$), or more than one molecule in the air absorbs radiation at the same wavenumber. Looking back at Figure 28, there are three regions of the spectrum that are considered “saturated”, meaning that there are strong absorbers of MIR radiation present in the atmosphere that bring the intensity of the returning beam to zero. If absorption in a region is saturated by H_2O , and one wants to measure another gas in that spectral region, there is no way to know how much absorption is due to H_2O and how much is due to the gas of interest because the transmission is already zero in that region. This is a big problem in Halifax, Nova Scotia as one is located near the ocean, resulting in more water vapour in the air. The problem is similar for analyzing complex mixtures of gases. If one is trying to measure multiple gases that all absorb at the same wavenumber, it becomes challenging to determine how much radiation is absorbed by each gas. However, the main disadvantage of this technique is that the spectrometer has relatively low detection limits, as compared to other techniques that may be tuned to one gas and can detect low concentrations of that gas. The spectrometer used for this honours thesis work has limits of “a few ppb” because there are diminishing returns for longer open paths due to H_2O and CO_2 in the

air, and also because of the strength of absorptions in the IR region (A. Wiacek, personal communication, March 2, 2016).

2.3. Concentration Retrieval

2.3.1. MALT

Once a spectrum is calculated from co-adding a set number of interferograms and applying the Fourier transform, one needs a way to analyze the spectrum to determine the concentrations of the gases found absorbing radiation within a selected region of the spectrum, typically 100 cm^{-1} wide, which corresponds to $1\mu\text{m}$ at 1000 cm^{-1} . One does this through a “retrieval”, which is performed by iteratively re-simulating a calculated spectrum until a best match to the measured spectrum is found, given the random noise.

MALT (Multiple Atmospheric Layer Transmission) is a program developed by David Griffith (1996) for the simulation and fitting of infrared spectra. MALT does this by using an iterative non-linear least squares (NLLSQ) retrieval approach. MALT calculates spectra based on the HITRAN (High-resolution TRANsmission) spectral line parameter database, which provides a list of the line positions, strengths, widths, pressure shifts, and temperature dependences of absorption lines for 47 different molecules, plus their common isotopes (Griffith, 1996; Rothman et al., 2013; Harvard-Smithsonian Center for Astrophysics, 2015). What is varied in each iteration is the concentration of absorbing gases, as well as certain instrumental parameters that also affect the measured spectrum in a known way. MALT retrieval errors, including OP-FTIR spectrometer measurement errors, are no greater than 10% (Smith, Wooster, Tattaris, & Griffith, 2011).

Bruker's OPUS-RS is able to do this type of retrieval, however, for this honours thesis work concentration retrievals will be run iteratively with MALT. There are a few reasons as to why retrievals by MALT were chosen over retrievals by OPUS-RS. Whereas MALT calculates spectra based on parameters from the HITRAN database from first principles, OPUS-RS is currently set up to only scale spectra based on those measured by the PNNL (Pacific Northwest National Laboratory) laboratory (Bruker Corporation, 2015). The HITRAN and PNNL databases are two databases that contain different spectral information of a number of molecules, some overlapping in both databases. There are multiple differences between the two that relate to why one was chosen for retrievals over the other. The PNNL database contains previously measured spectra at temperatures of 5, 25, and 50°C for molecules of concentration 1 ppm across a one-meter path (1 ppm*m) (Sharpe et al., 2004). This is a good basis for reference spectra, but because there is only information for gas absorbance at three temperatures (sometimes only two), reference spectra need to be interpolated to other measurement temperatures, which introduces uncertainties. The HITRAN database contains information on the location of an absorption line, the strength of the line for one molecule, and parameters for how the absorption line varies as a function of temperature and pressure (Rothman et al., 2013; Harvard-Smithsonian Center for Astrophysics, 2015). Therefore, MALT allows one to directly input parameters (temperature, pressure, target gas, interfering gases, wavenumber range, etc.) from which it calculates the spectra from first principles, re-simulating it iteratively until it best matches the measured spectrum. Another reason why MALT was chosen over

OPUS-RS retrievals is MALT produces spectra with a spectral resolution of 0.017 cm^{-1} , whereas OPUS-RS works with spectra recorded with a resolution of 0.112 cm^{-1} at PNNL (Griffith, 2010; Sharpe et al., 2004).

2.3.2. Retrieval Parameters

The main parameters of interest within MALT input files are temperature, pressure, spectral range, path length, target gas, interfering gases, spectral resolution, apodization, FAP, and phase. A sample MALT input file used for concentration retrievals can be found in Appendix 5.1.

Temperature and pressure is logged with a pressure/temperature (PT) sensor simultaneously with the measurement of each spectrum, and one is able to input these parameters directly into MALT. The spectral range is an important parameter because it tells MALT where to look for the fingerprint of the target gas. The path length parameter is important too, as it tells MALT the length of the open path in which the gases were measured. Path length is double the distance between the spectrometer and the retroreflector, plus 3.7 meters, which is the distance the radiation has to travel within the spectrometer before it first exits the telescope and before it reaches the detector (Bruker Corporation, 2015). The amount of radiation absorbed by a gas is proportional to the distance the radiation travels (Beer's Law), therefore, without a path length parameter, MALT would not be able to simulate an accurate spectral fit (Smith, 1996). Another main set of parameters in MALT input files are the target gas (the gas, or gases, one is interested in measuring) and the interfering gases (the gases that are absorbers in

the same part of the spectrum where one's target gas, or gases, absorb). MALT allows you to select any of the 47 compounds (or their common isotopes) from the HITRAN database and requires the input of an initial guess for the concentrations of each compound in the air one is sampling through. The initial input of gas concentrations is a starting point for MALT in concentration retrievals. The spectral resolution parameter provides the resolution of the measured spectrum, which is much lower than the calculated spectrum resolution. The apodization parameter allows the choice of apodization in the calculated spectrum to match that used to produce the measured spectrum from the co-added interferograms being Fourier transformed. Lastly, FAP and phase are MALT input parameters specific to accounting for width problems and symmetry, respectively, with the measured spectrum in the simulated spectra. The FAP parameter is an additional apodization that accounts for symmetric instrument line broadening (Griffith, 1996). An FAP value of 0 is equivalent to the boxcar apodization function and a value of 1 is equivalent to the triangular apodization function (Griffith, 1996). The phase parameter (units of degrees) is a phase error simulation to account for asymmetry around ZPD in the interferogram, which introduces asymmetry in the instrument lineshape (Griffith, 1996). The first guess of phase is 0° , or having a symmetric interferogram for the spectrum calculated (A. Wiacek, personal communication, March 4, 2016).

When MALT simulates the first spectrum, using the input starting points, it will run a NLLSQ analysis between that spectrum and the measured spectrum. It is almost certain that the initial guess is incorrect, and based on the difference between the

simulated spectrum and the measured spectrum, MALT will make corrections and alter parameters before resimulating a new spectrum for comparison to the measured spectrum. It will continue this until the difference between the simulated spectrum and the measured spectrum is minimized. For this honours thesis work, all parameters used in the retrieval process are summarized in Table 6.

Table 6 Summary of MALT parameters used for simulation of calculated spectra and the retrieval of CO concentration.

Temperature	Variable (from PT sensor)
Pressure	Variable (from PT sensor)
Target gas	CO
Interfering gases	H ₂ O, CO ₂ , and N ₂ O
Spectral range	2050 – 2140 cm ⁻¹
Path length (two way)	Variable (343.7, 681.7, and 317.7 meters)
Spectral resolution	0.5 cm ⁻¹
Apodization function	Triangular
FAP	0 (boxcar apodization)
Phase	0° (symmetric)

Because multiple measurements were made, multiple different MALT input files were used, however, the only parameters that change for each measurement are the temperature, pressure, path length, and the file name. The remaining parameters are left as the MALT default parameters, and can be found within the input file in Appendix 5.1. A parameter can be fit (*t*) or unfit (*f*) in the retrieval, e.g., FAP = 0 can be fit or unfit, but it is always simulated, and so requires the initial guess. If it is fit, then it may not remain zero after the fit converges on a solution, meaning a bit of line broadening from the interferometer best explains the measured spectrum (A. Wiacek, personal communication, March 4, 2016). The instrumental parameters fitted in all retrievals for this thesis work were target and interfering gases, FAP, spectral shift, and phase.

2.3.3. *MATLAB*

Due to the large number of concentration retrievals that needed to be done for this honours thesis work, MATLAB® was used in order to externally drive MALT. MATLAB is a technical computing language and interactive environment that allows for data visualization, data analysis, and running external software, among others. Multiple MATLAB codes and corresponding functions were written by Dr. Li Li, a postdoctoral researcher in the Tropospheric Remote Sensing Laboratory (TRSL) at Saint Mary's University. Dr. Li Li's codes can be found in Appendices (5.2) through (5.7).

Each MATLAB code is specific to data analysis from the three different campaigns. Each code will take the multi-spectra files recorded by OPUS-RS, convert them to individual spectra, convert all corresponding PT files to a format readable by MALT, and then automatically run the MALT program to retrieve a concentration for each spectrum, pressure, and temperature. This is not trivial since MALT requires a different input file for each new temperature and pressure during the course of observation and MATLAB automatically writes all needed files. The concentrations are collected into a time series by MATLAB. Along with the best-fit spectrum figures and concentration time series plots, MATLAB also plots the spectral residual for each measurement and a time series of the root mean square (RMS) of the residuals. The residual is the difference between the measured spectrum and the retrieved spectrum and is plotted against wavenumber for each fit. Figure 29 shows a measured spectrum and a retrieved spectrum. The error in the fit is represented by a residual plot.

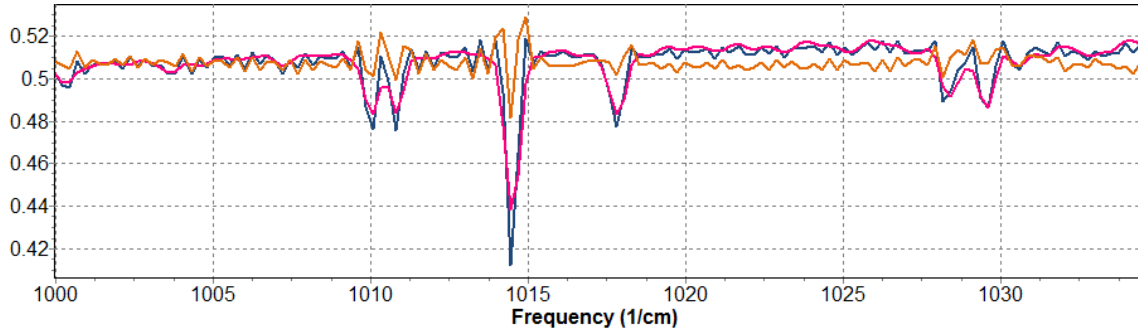


Figure 29 A fit between a retrieved spectrum (pink) and a measured spectrum (blue) with the residual plot (orange). The residual has been offset from zero to appear next to the calculated and measured spectrum. (Bruker Corporation, 2015)

The RMS is the square root of the mean of the squared residuals for each measurement.

The mathematical steps to calculating the RMS are:

$$\text{Residuals: } [r_1, r_2, \dots, r_n]$$

$$\text{Squared residuals: } [r_1^2, r_2^2, \dots, r_n^2]$$

$$\text{Mean of the squared residuals: } \frac{(r_1^2, r_2^2, \dots, r_n^2)}{n} = \frac{1}{n} \sum_{i=1}^n r_i^2$$

$$\text{RMS} = \left(\frac{1}{n} \sum_{i=1}^n r_i^2 \right)^{\frac{1}{2}}$$

where n is the number of spectral points in the retrieval “window”. If the RMS is smaller than 0.01 (or 1%), the fitted spectrum is generally considered a good fit to the measured spectrum. This RMS benchmark value is somewhat arbitrary and was agreed upon by the TRSL group at Saint Mary’s University for CO. Figure 30 illustrates an example of a residual plot for one spectrum and its corresponding single calculated RMS value.

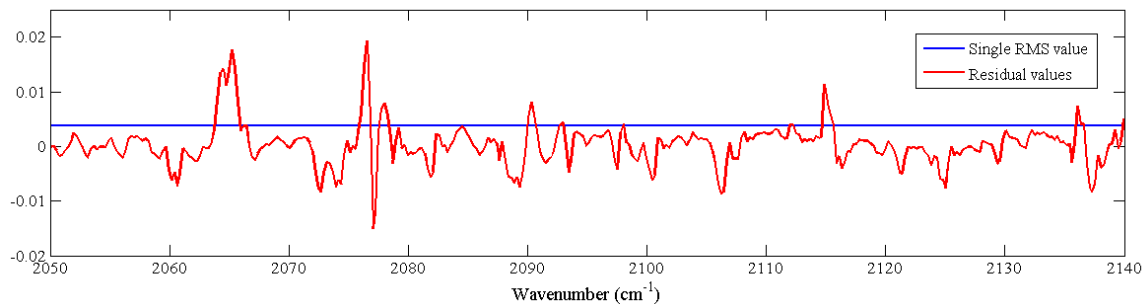


Figure 30 A residual plot (the difference between a measured spectrum and a retrieved spectrum) (red) along with its corresponding single calculated RMS value (blue). (Bruker Corporation, 2015)

Although there are residual values that exceed 0.01 (1%), the corresponding RMS value is still less than 0.01. Those residuals much in excess of the RMS value are indicative of systematic fitting problems, as will be discussed in detail in Section 3.

2.4. National Air Pollution Surveillance (NAPS) Measuring Station and Equipment

NSE currently measures NAPS trace gas data from the fourth floor of the Vogue Optical building at 1645 Barrington Street in Halifax (F. Di Cesare, personal communication, April 6, 2016). Air is sucked in through a glass inlet, which transports the air sample to the equipment. The measuring equipment used by NSE is a Teledyne API Model 300 CO Analyzer, which detects and measures CO concentration based on the absorption of infrared (IR) radiation by CO molecules at wavenumbers near 2128 cm^{-1} (Teledyne API, 2006). This is in the same band as our FTIR analysis. The IR beam is passed through a rotating Gas Filter Wheel, which modulates the beam for maximized detector SNR performance, then enters the multi-pass sample cell (Teledyne API, 2006). This sample cell uses folded optics to generate a 16-meter absorption path length (Teledyne API, 2006). Upon exiting the sample cell, the beam is filtered by a band-pass interference filter to limit the light to the wavenumber of interest and then strikes the detector, which outputs a modulated voltage signal (Teledyne API, 2006).

Table 7 lists the manufacturer specifications of the Model 300 CO Analyzer used for measuring air quality on Barrington Street.

Table 7 Specifications of the Teledyne API Model 300 CO Analyzer. (Teledyne API, 2006)

Ranges	User selectable to any full-scale range from 1 ppm
Zero Noise	< 0.025 ppm (rms)
Span Noise	< 0.5% of reading (rms)
Lower Detectable Limit	< 0.050 ppm
Zero Drift (24 hours)	* <0.1 ppm
Zero Drift (7 days)	* <0.2 ppm
Span Drift (7 days)	* 1% of reading
Linearity	1% FS
Precision	0.5% of reading
Lag Time	10 sec
Rise/Fall Time (95%)	<60 sec
Sample Flow Rate	800cc/min. \pm 10%
Temperature Range	5-40°C
Humidity Range	0-95% RH, non-condensing
Temp Coefficient	< 0.05 % per °C
Voltage Coefficient	< 0.05 % per V
Dimensions HxWxD	7"x 17"x 25" (178mm x 432mm x 660mm)
Weight	50 lbs (22.7 kg)
Power	110V~/60Hz, 220V~/50Hz., 240V~/50Hz. 250 Watts
Power, CE	230V~/50Hz, 2.5 A
Environmental Conditions	Installation Category (Overvoltage Category) II
Recorder Outputs	\pm 100 mV, \pm 1 V, \pm 5 V, \pm 10 V (Bi-Polar)
Status	12 status outputs from opto-isolators
* at constant temperature and voltage	

Based on the manufacturer specifications, the NAPS data was assigned an instrumental error of 10% in the absence of zero or span drift. This estimate does not include all sources of error in the measurement process or the process of converting voltage to a final CO concentration.

2.5. Campaigns

2.5.1. Robie Street Campaign

The Robie Street campaign was the first in which the OP-FTIR spectrometer was deployed. This campaign occurred on May 15th, 2015 in the median strip on Robie Street by Saint Mary's University with measurements of atmospheric gas concentrations between 12:11 pm and 2:00 pm. Figure 31 is an image from Google Maps indicating the location of the OP-FTIR spectrometer and the retroreflector on Robie Street. The distance between the spectrometer and retroreflector was 170 meters, providing an optical path length of 343.7 meters (double the distance plus 3.7 meters). The path length is actually measured on site using a range finder accurate to 1 meter.



Figure 31 Location of the retroreflector and the spectrometer on Robie Street.

The spectrometer was measuring continuously at 240 interferogram co-adds per spectrum for approximately two hours, resulting in 111 spectra at 0.5 cm^{-1} resolution and corresponding concentration time series points. The target gas for this honours thesis work is carbon monoxide (CO), and the purpose is to compare the measurements from the OP-FTIR spectrometer with NAPS data measured on Barrington Street in Halifax at the same time using a different technique. CO was chosen as the target gas because it has a strong absorption signature in a spectral region that is not blocked by H_2O or CO_2 saturation. This comparison is part of new instrument characterization. Figure 32(a) and (b) below are pictures taken on the day of the campaign on Robie Street. This location was chosen in an attempt to measure vehicle emissions during lunch hour, e.g., NO, NO_2 , CO, CH_4 , and others if possible.



Figure 32 (a) Graduate student Keane Tobin standing beside the retroreflector. Photo taken by Dr. Aldona Wiacek. (b) Honours thesis candidate, myself, setting up the OP-FTIR spectrometer. Photo taken by Dr. Aldona Wiacek.

2.5.2. Rice Campaign

The Rice campaign took place from August 13th to August 21st, 2015 on Saint Mary's campus. The spectrometer was located on the fourth floor of the Science Building (S425) pointing out of a window towards the retroreflector located on the roof of the Rice Building. Figure 33 is an image from Google Maps indicating the location of the OP-FTIR spectrometer and the retroreflector on Saint Mary's campus. The distance between the spectrometer and retroreflector was 339 meters, resulting in an optical path length of 681.7 meters.

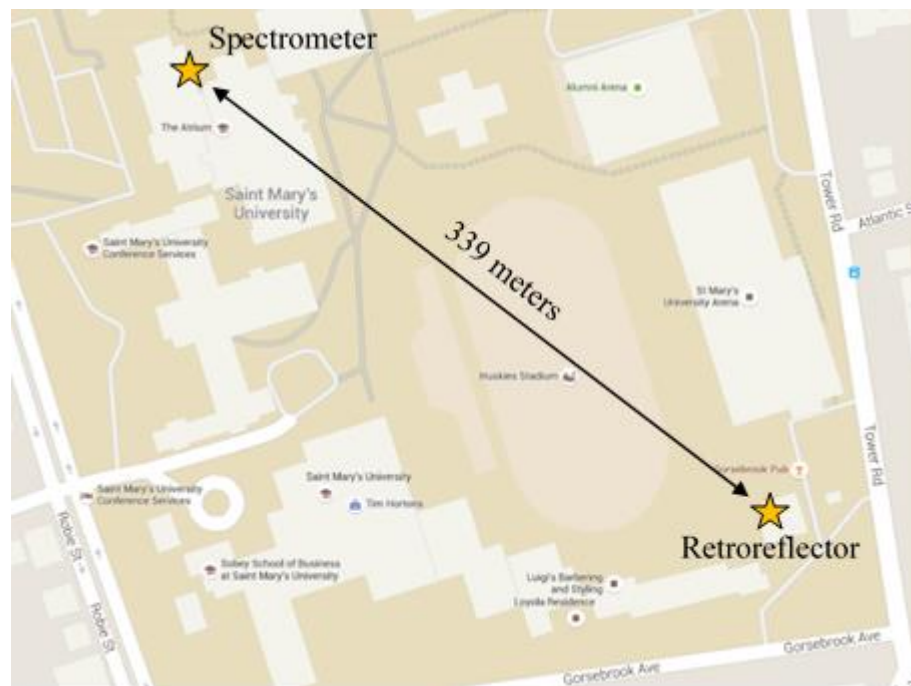


Figure 33 Location of the retroreflector and the spectrometer on Saint Mary's campus.

The spectrometer measured continuously at 240 interferogram co-adds per spectrum for nine days, with the exception of brief periods of time where the spectrometer was either manually stopped and started again on the 14th, 18th, 19th, and the 20th of August,

or where the spectrometer stopped measuring automatically for a few moments due to a bug in the controlling software that has been fixed with the manufacturer. The purpose of this campaign was to gather test data relating to atmospheric composition and air quality on Saint Mary's campus for at least a week. The data from this campaign was compared with NAPS data measured on Barrington Street in Halifax at the same time. Figure 34(a) and (b) are pictures taken on August 13th, 2015, the day the OP-FTIR spectrometer and retroreflector were setup.

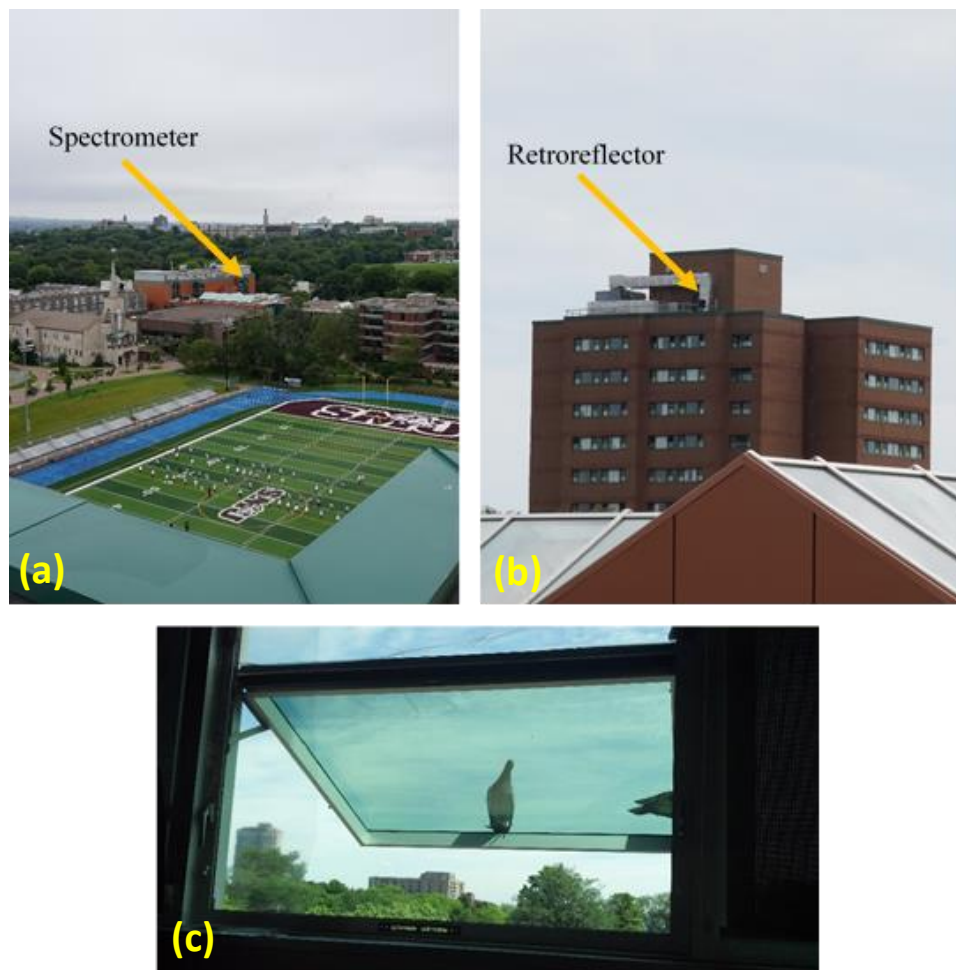


Figure 34 (a) View of the spectrometer from the top of the Rice Building on Saint Mary's campus where the retroreflector is located. (b) Slightly zoomed view of the retroreflector from the fourth floor of the Science Building on Saint Mary's campus where the spectrometer is located. (c) View of the window in room S425 that the spectrometer was pointing out of towards the retroreflector on the Rice Building. Photos taken by Dr. Aldona Wiacek.

Owing to its short cable, the PT sensor during this measurement period was located inside the room the spectrometer was located in (S425), meaning it recorded the temperature and pressure of the room instead of the air in the open path outside. Recorded temperatures and pressures were obtained from the Burke-Gaffney Observatory (BGO), located on campus on the roof of McNally Tower, which gives more representative PT values than indoor measurements, especially for temperature.

On average, 62 spectra and corresponding concentration time series points were recorded for each measurement block, which lasted approximately one hour, and there were 144 blocks completed, with ~8928 spectra and concentration time series points recorded during this campaign.

Out of the 144 blocks, 30 blocks, plus an additional 16 data points, were discarded due to the occurrence of heavy fog along the open path. These measurements were discarded as “foggy data” because fog creates more random noise within the spectrum and the overall transmittance is lower. Figure 35 illustrates the effect of fog on the measured spectrum.

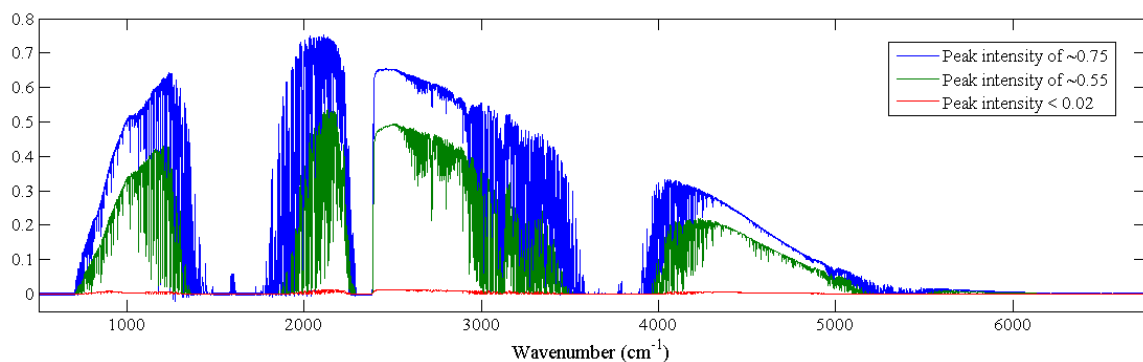


Figure 35 Comparison of three different measured spectra to illustrate the effect of fog on the intensity of the returning beam.

The blue spectrum is the same spectrum as depicted in Figure 28. From comparing the blue spectrum with the green and red spectra it is clear that the two spectra affected by fog have much lower intensities, among other differences. The fog adds more particles of water (droplets) suspended in the air and creates more interference by scattering the beam in the open path, which is why foggy data was discarded. The quantitative criteria used in order to identify and discard the foggy data in bulk was a peak intensity less than 0.02 at 2000 cm^{-1} and the failure of OPUS-RS to identify water in the spectrum. A few data points still remain in the dataset that do not meet the criteria because this was a manual process applied to a large number of data folders. Figure 36 shows the time series of CO concentration during the Rice campaign illustrating the effects of fog on retrieved CO concentrations.

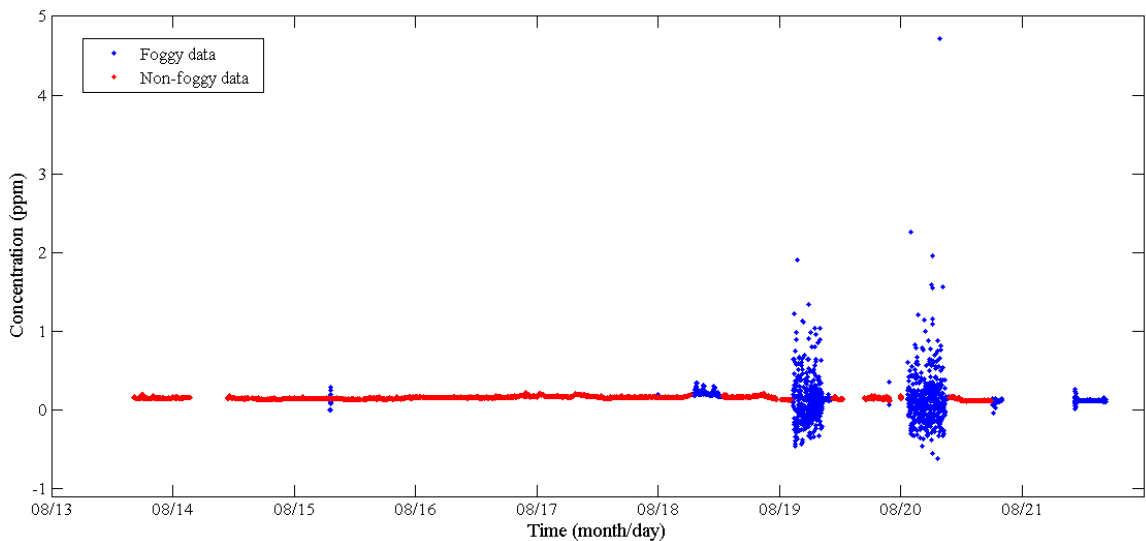


Figure 36 Effects of fog on retrieved CO concentrations. The data in red represents the non-foggy data and the data in blue represents the foggy data.

The data in red represents the data considered “non-foggy” based on the criteria used to discard the foggy data. The data in blue represents the foggy data and was discarded

from the Rice campaign dataset. Most of the data effected by fog represents a negative retrieved CO concentration, which is physically impossible.

2.5.3. Lake Major Campaign

The Lake Major campaign took place at the Lake Major Water Treatment Plant in Dartmouth from September 4th to September 10th, 2015. The spectrometer and retroreflector were located within a fenced-off area and were separated by a distance of 157 meters, resulting in an optical path length of 317.7 meters. Figure 37(a) is an aerial view of the Lake Major setup retrieved from Google Maps. Figure 37(b) and (c) are pictures taken on the first day of the Lake Major campaign.

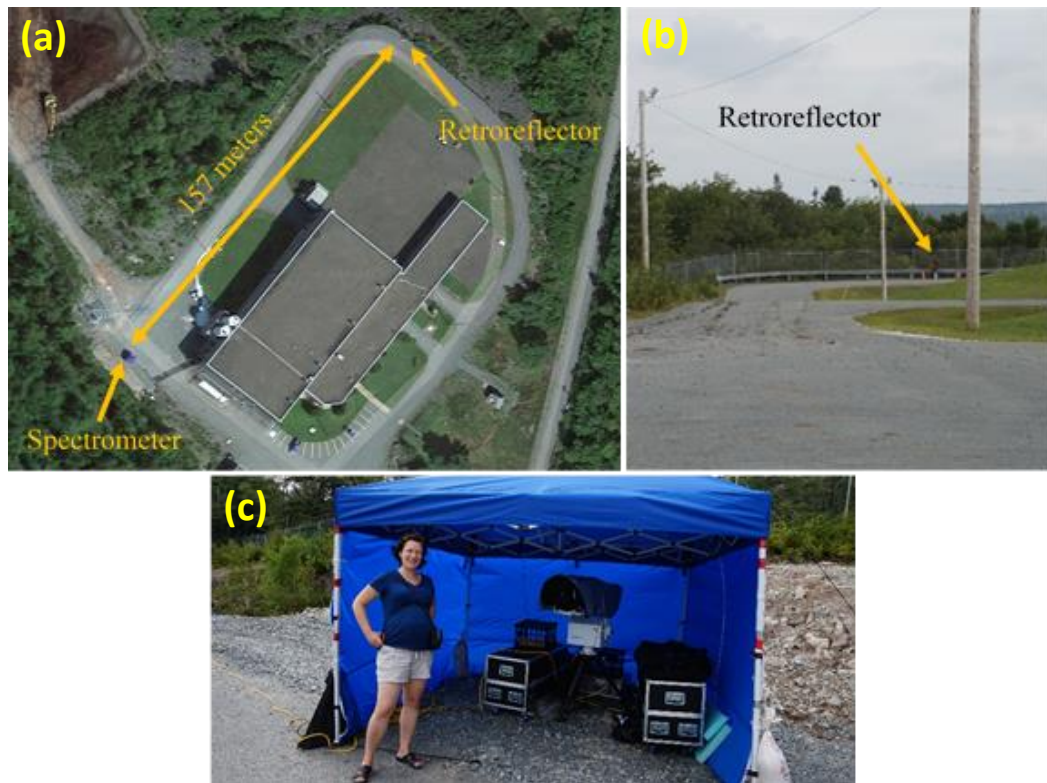


Figure 37 (a) Aerial view of the location of the spectrometer and the retroreflector during the Lake Major campaign. (b) View of the retroreflector from the spectrometer. Photo taken by Dr. Aldona Wiacek. (c) Dr. Aldona Wiacek standing beside the OP-FTIR spectrometer setup at Lake Major. Photo taken by Dr. Li Li.

The spectrometer measured continuously at 240 interferogram co-adds per spectrum for seven days, with the exception of a few hours on the 5th and the 9th of September. The purpose of this campaign was to measure air composition in a more rural, forested environment and compare retrieved concentrations of CO at Lake Major with CO concentrations in the more urban Halifax area.

On average, 62 spectra and corresponding concentration time series points were recorded for each measurement block, and there were 128 blocks completed, with ~7936 spectra and concentration time series points recorded during this campaign.

3 Results and Discussion

3.1. Comparison of MALT CO Concentration Retrievals and NAPS Data

3.1.1. Robie Street

Representative results derived from the Robie Street campaign are illustrated with a single fitted spectrum corresponding to an enhanced CO concentration. Before time series plots of CO concentration are discussed, one must examine a single spectrum to illustrate the retrieval process. Figure 38 is a transmittance spectrum (top panel) that corresponds to data collected at 12:59pm on May 15th, 2015. It is a product of MALT and was obtained by fitting to the measured spectrum obtained from Fourier transforming 240 co-added interferograms.

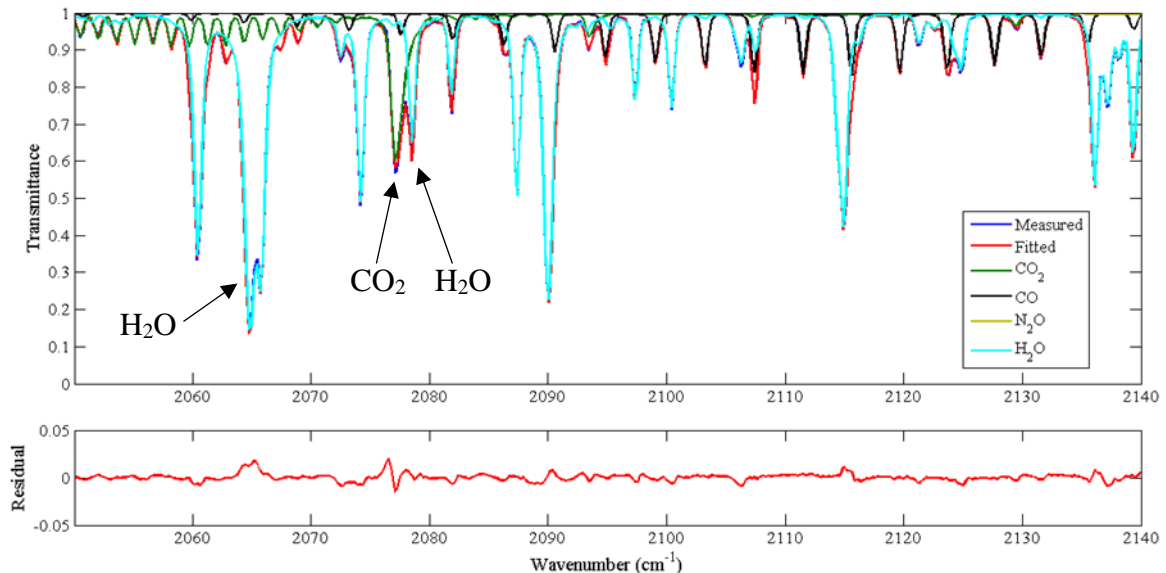


Figure 38 Retrieved transmittance spectrum corresponding to data collected at 12:59pm on May 15th, 2015 for the Robie Street campaign. The temperature, pressure, and relative humidity at this time was 22.6°C, 1020.8 mbar, and 45%, respectively. Top panel: Measured and fitted spectra, also showing the contribution of the target gas (CO) and interfering gases. Bottom panel: The residual plot obtained by taking the difference (measured – fitted spectrum). Absorptions mismatches greater than 1% are identified as H₂O and CO₂.

Some absorptions due to H₂O and CO₂ are already identified in Figure 38, and will be described further below. The residual plot (bottom panel) is essential not only for determining the overall fit error, but for identifying systematic features, such as over-fitting and under-fitting problems as a result of incorrect spectroscopic parameters. Between 2075 and 2080 cm⁻¹, a systematic feature in the residual plot with an amplitude of ~0.02 (2%) is clearly visible. This corresponds to the under-fitting and over-fitting of the measured spectrum at the CO₂ absorption line in the transmittance spectrum. Figure 39 illustrates the CO₂ microwindow within the full CO spectral window from Figure 38 and the corresponding residual plot.

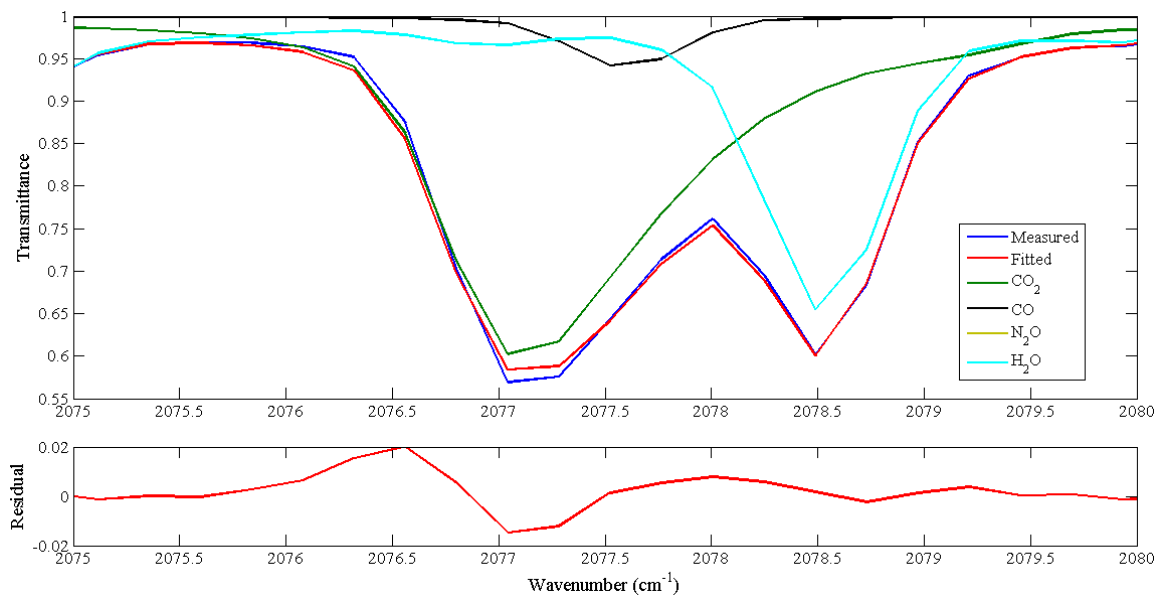


Figure 39 Top panel: Zoomed view of the CO₂ absorption line (2075–2080 cm⁻¹). Bottom panel: Zoomed view of the corresponding residual values.

The type of systematic feature in Figure 38 occurs near 2077 cm⁻¹ and is the largest residual for that spectrum. Another large residual of ~2% is found at 2065 cm⁻¹ and corresponds to a strong water absorption line. Due to the prominence of the

systematic CO₂ feature in the residual of Figure 38, additional analysis was done in order to determine whether this feature was most prominent in the residuals of all Robie Street spectra. Figure 40 is a plot of the maximum residual value for each CO spectrum recorded during the Robie Street campaign, along with the maximum residual value for the narrower CO₂ region.

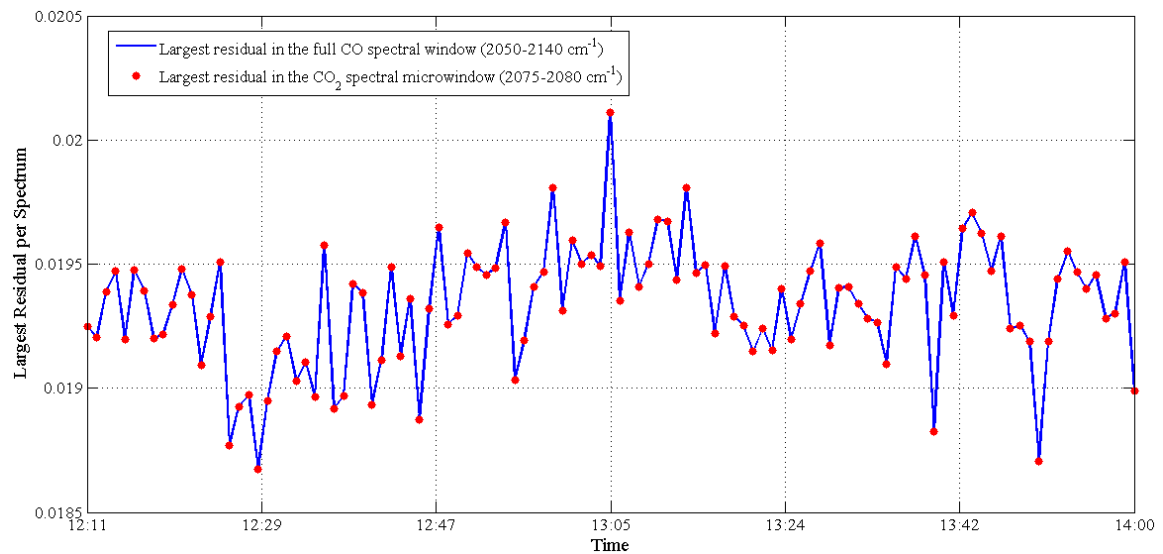
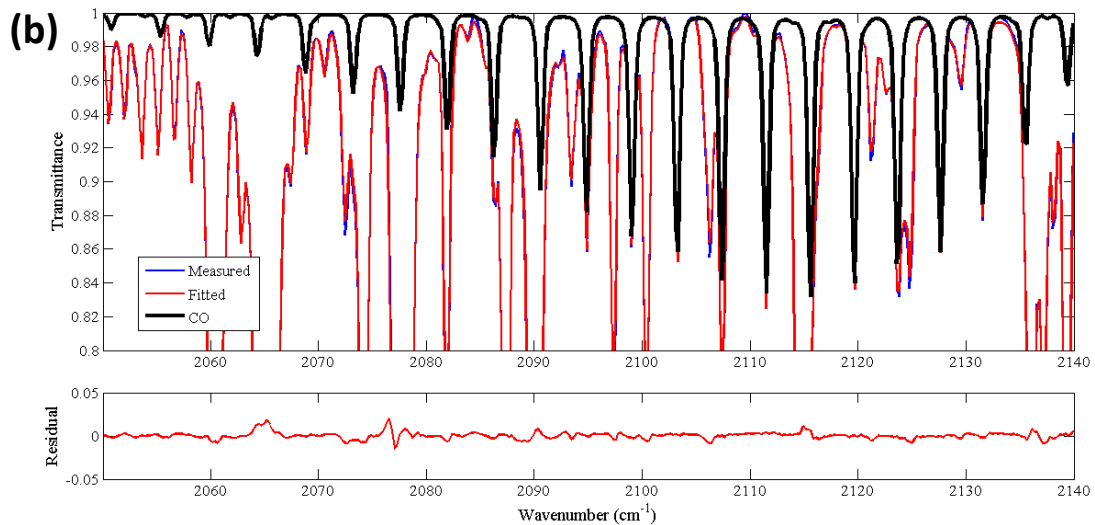
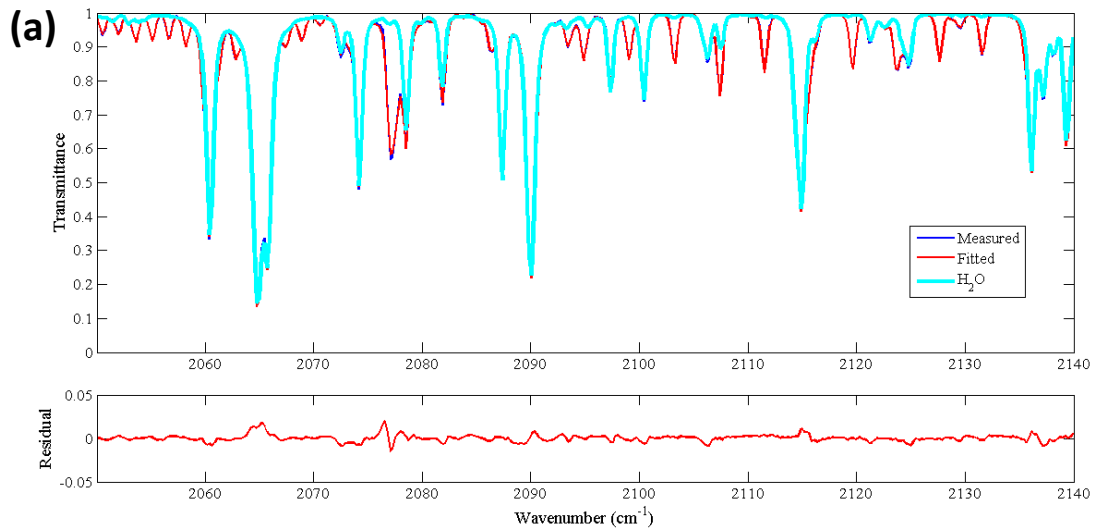


Figure 40 Maximum residual values for the full CO spectral window (blue line) and the CO₂ spectral microwindow (red dots) corresponding to the location of the systematic CO₂ feature in Figure 38 for the Robie Street campaign.

It shows the same maximum residual value for each spectrum in both the narrow and wide spectral interval, indicating that the largest residual in each spectrum of the Robie Street campaign is a result of the over fitting and under fitting of the measured spectrum near 2077 cm⁻¹ corresponding to the CO₂ feature. The other problem region corresponds to H₂O absorption (2065 cm⁻¹). There is no systematic over-fitting or under-fitting of the target gas CO (Figure 41(b)), which is a requirement for a final result, free of large systematic errors. Lastly, while somewhat arbitrary, retrievals with residuals of better than 1% are desirable; apart from the two problem regions, this is being achieved

in all spectra, as discussed below. Figure 41(a) through (d) illustrates the contribution of each gas (H_2O , CO , CO_2 , and N_2O) to the overall fitted spectrum in the last iteration of the retrieval. All four plots are a manipulation of Figure 38 and the residuals are the same in each plot because the measured spectrum and fitted spectrum are the same in each plot. Note changing vertical scale.



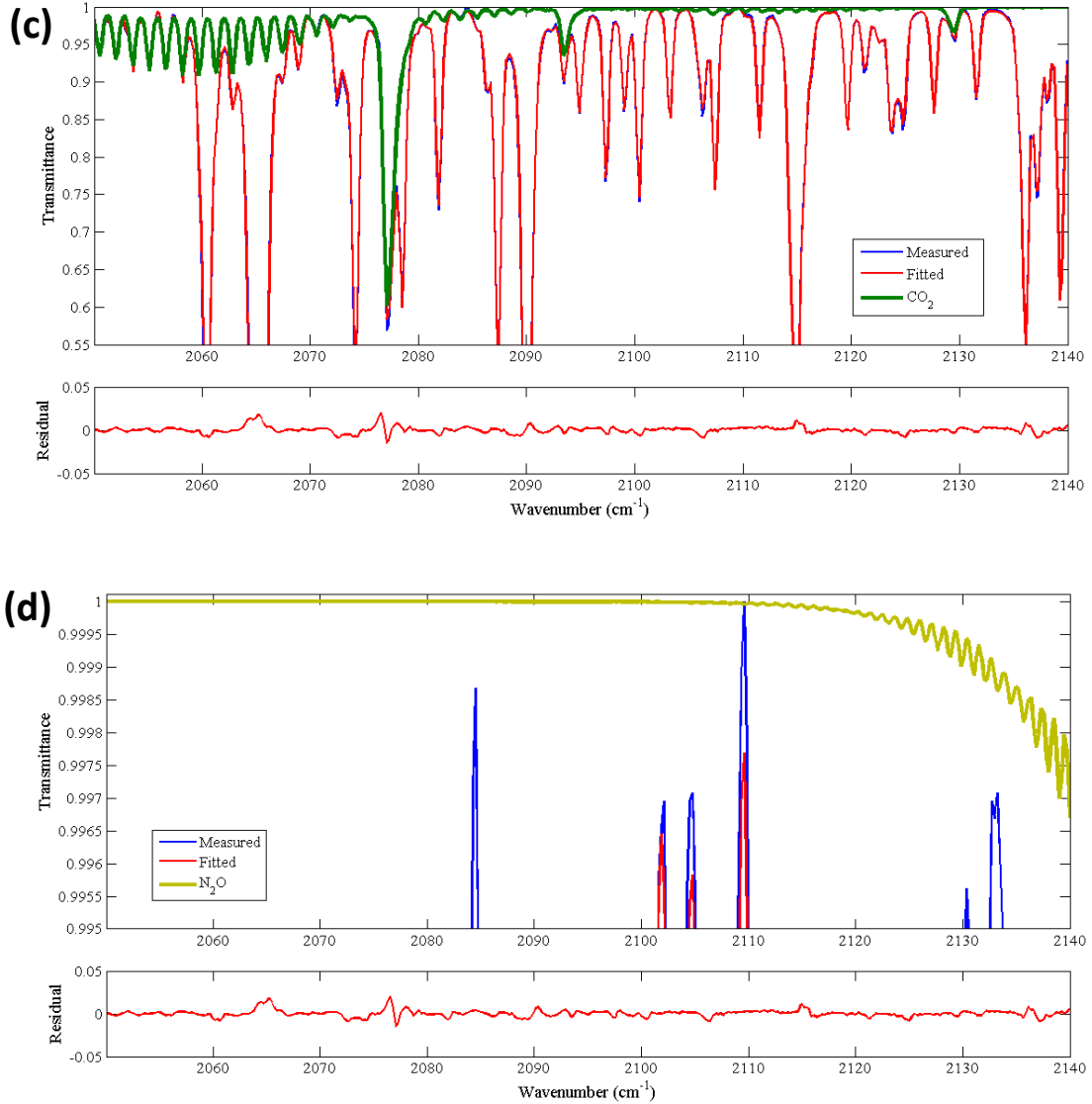


Figure 41 Contribution of: (a) H₂O, (b) CO, (c) CO₂, and (d) N₂O to absorption in the air across the open path and the overall measured absorption spectrum as fitted by MALT.

The gas that contributes most to the measured spectrum is H₂O because its absorption lines are strong and measured because of its high concentration in the air. Using temperature, pressure, and relative humidity, the concentration of H₂O was calculated to be 1.2% at the time corresponding to the spectrum in Figure 38. The H₂O absorption line at 2065 cm⁻¹ approaches 90% absorption, whereas CO₂, the second strongest absorbing gas, has a maximum absorption of 40%. The contribution of N₂O to the measured spectrum is the

smallest of all gases and reaches a maximum absorption of only 0.003%. N₂O could be omitted as an interfering gas, but it was not. The residual would need to be three times better than 0.003% in order to detect the highest absorption of N₂O in this spectral region, such that the N₂O absorption was three times greater than random noise levels in the spectrum.

Figure 42 shows a time series of retrieved CO concentrations throughout the two-hour measuring period on Robie Street, with a baseline concentration of ~0.15 ppm. Each data point represents one spectrum produced by transforming 240 co-added interferograms and has an associated error of at most 10%, including measurement errors and errors associated with MALT fitting (Smith et al., 2011). The bottom panel in Figure 42 is an RMS time series (see Section 2.3.3), where each RMS value is calculated from the spectral residual values for each retrieved transmittance spectrum. The spectral residual itself is just one diagnostic of a good fit to the measured spectrum, highlighting systematic features, such as under-fitting and over-fitting. The RMS is a one-number diagnostic that is somewhat better at showing the random noise in the measurement, assuming that a few systematic problems average out over the full spectral region of the fit. The random noise levels in undisturbed TRSL transmittance spectra are typically ~0.0015, with the signal-to-noise *ratio* depending somewhat on the open path length and humidity, as they both affect the *signal* levels. The RMS values in Figure 42 are ~0.004, and compare reasonably well to the ~0.0015 random noise levels. One would expect the RMS values to be higher than random noise because they incorporate systematic fitting errors in addition to random instrument noise.

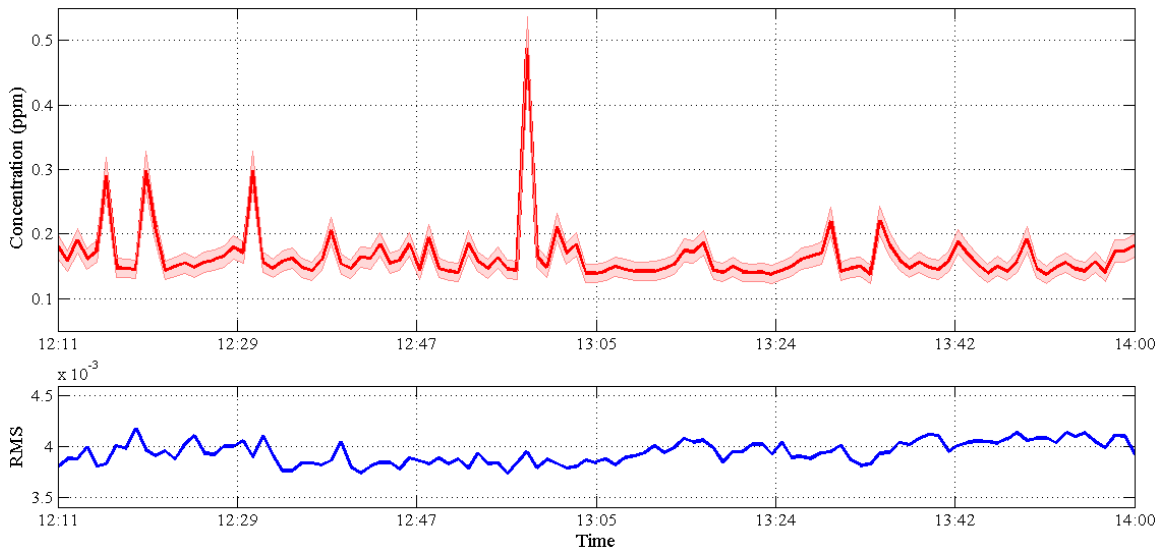


Figure 42 Time series of retrieved CO concentrations by MALT for the Robie Street campaign. The shaded region represents 10% uncertainty of OP-FTIR spectrometer data. A time series of RMS for each spectrum is included.

Four prominent enhancements in CO concentration were captured at 12:16pm, 12:20pm, 12:31pm, and 12:59pm. The corresponding RMS values for all four retrieved concentrations indicate that the measured spectrum has no increased random noise in it, which could indicate spurious results, e.g., due to a person blocking the open-path. If the spectrum was disturbed by someone standing or repeatedly walking in front of the beam, the random noise would not increase, but the signal would decrease, affecting the SNR and RMS. It is most likely that the enhancements in CO concentration during this campaign represent CO emissions from a large truck, bus, or a moment when the car density was high, as captured in a one-minute average over the one-way open path of 170 meters. Also, while conducting the campaign, no measurement interruptions were noted.

Figure 43 illustrates a comparison between OP-FTIR spectrometer retrieved CO concentrations and NAPS measured CO concentrations for the Robie Street campaign. NAPS data shown in this thesis has not yet been validated by NSE, meaning the data is raw and has not been through quality control (F. Di Cesare, personal communication, March 8, 2016). In the absence of zero and span drift, the error of the CO analyzer is 10% (Teledyne API, 2006). These 1-minute unvalidated NAPS datasets for all three campaigns were obtained from Frances Di Cesare.

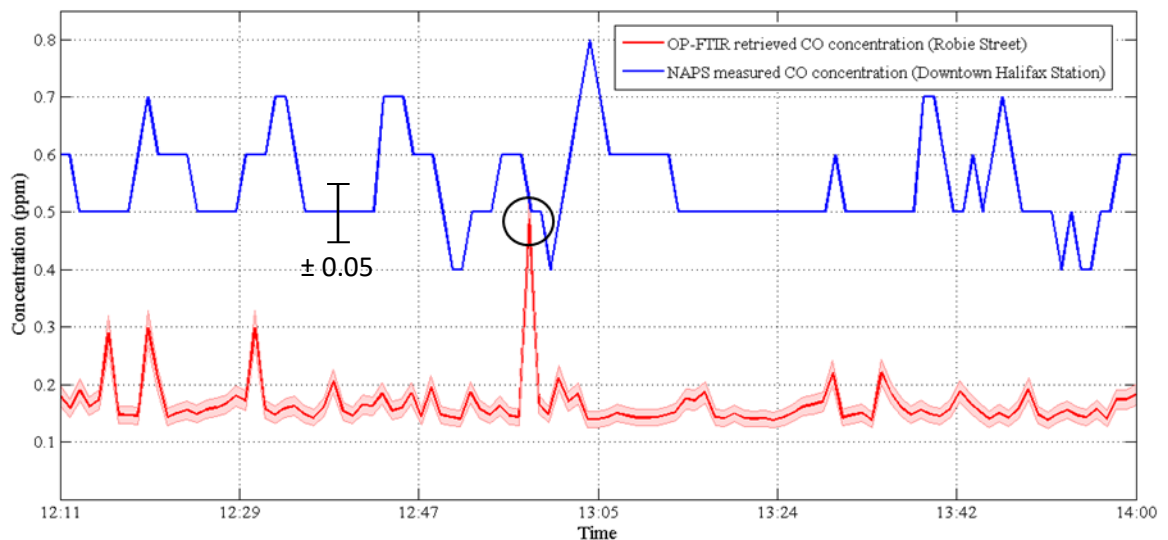


Figure 43 Comparison between OP-FTIR spectrometer retrieved CO concentrations on Robie Street and NAPS measured CO concentrations on Barrington Street. The shaded region represents 10% uncertainty on OP-FTIR spectrometer data. The NAPS measurement error is 10% and not shown. One representative 10% error bar is shown on the NAPS time series.

The results show a clear systematic bias between the two measurements. The OP-FTIR time series has a baseline concentration of ~ 0.15 ppm, whereas the NAPS time series has a baseline concentration of ~ 0.5 ppm. One reason for this bias may be that the NAPS data is not correct as it has not been through quality control (validation process), although this is suspected not to be the main cause. Another reason, and one that is

more likely, is that Barrington Street may be much busier than south Robie Street at lunch time. Because Barrington Street is a location of dense vehicle traffic and a hub for city buses, it is reasonable to attribute the bias that is present in the results to this. While one expects higher CO concentrations on Barrington Street, it is interesting that the OP-FTIR spectrometer measured CO at a concentration typical to Barrington Street levels just once. This is likely also caused by the spatial averaging effect of our measurements that tends to attenuate CO enhancements. In contrast to this, measurements on Barrington Street could be very enhanced by a single vehicle idling near the NAPS station air inlet.

The approximate distance between the NAPS station on Barrington Street and Robie/Inglis Street (southwest of Barrington Street) is 1.6 kilometers, which is not a long distance for air parcels to travel. Depending on the wind speed, transportation would not take long either. For example, a wind speed of 10 kilometers per hour (km/h) would transport air over a distance of 1.6 kilometers in just under 10 minutes. Wind speed and wind direction measurements were gathered from a nearby weather station on Francklyn Street to determine whether or not air from Barrington Street could have been transported to Robie Street at the time of this campaign, in which case our lower measurement values would be even harder to explain. The weather station on Francklyn Street, located approximately one kilometer southeast of the campaign site on Robie Street, was the closest station that had historical wind data available for this period of time (Weather Underground, 2015). Figure 44 illustrates the variation in wind

speed/gust and wind direction over the time of CO concentrations from NAPS and the OP-FTIR spectrometer.

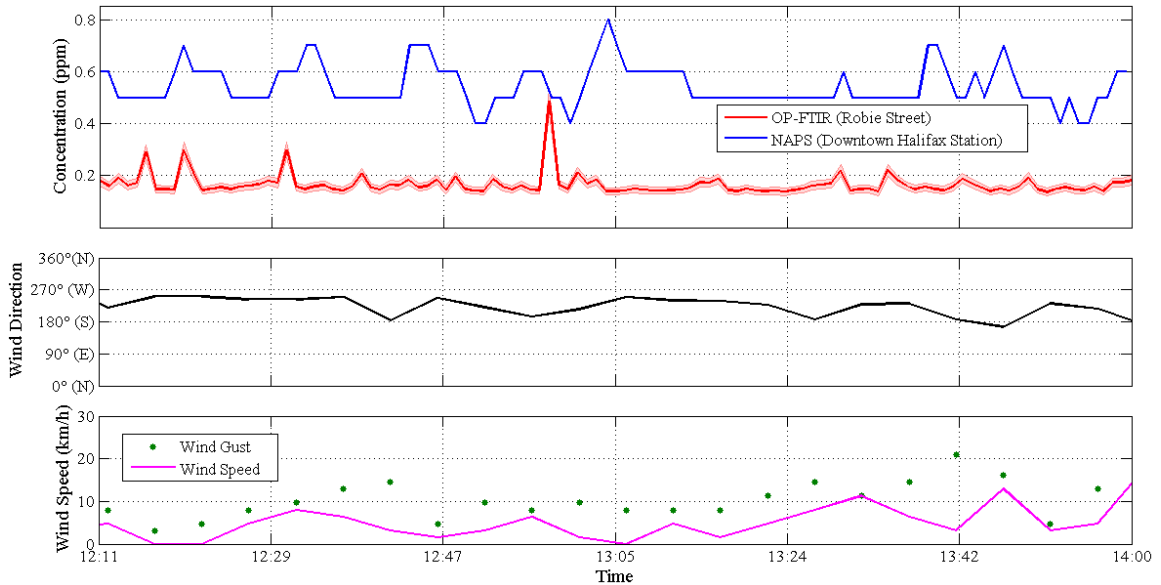


Figure 44 Wind speed/gust and wind direction measured at a weather station on Francklyn Street compared to the CO concentration time series. Wind direction represents the direction wind is coming from.

For the duration of the Robie Street campaign the wind is coming from the south/southwest direction. This means that the air sampled on Robie Street by the OP-FTIR spectrometer was not transported from Barrington Street, but from the Northwest Arm and Williams Lake. Sampling from an area with cleaner air on Robie Street helps to explain the bias between the two datasets. In addition to the traffic on Barrington Street, the NAPS station on Barrington Street is sampling air coming from the entire downtown core to the southwest (upwind direction). Figure 45 is an aerial view of the city of Halifax taken from Google Maps illustrating the location of the measuring sites and the weather station during the Robie Street campaign.

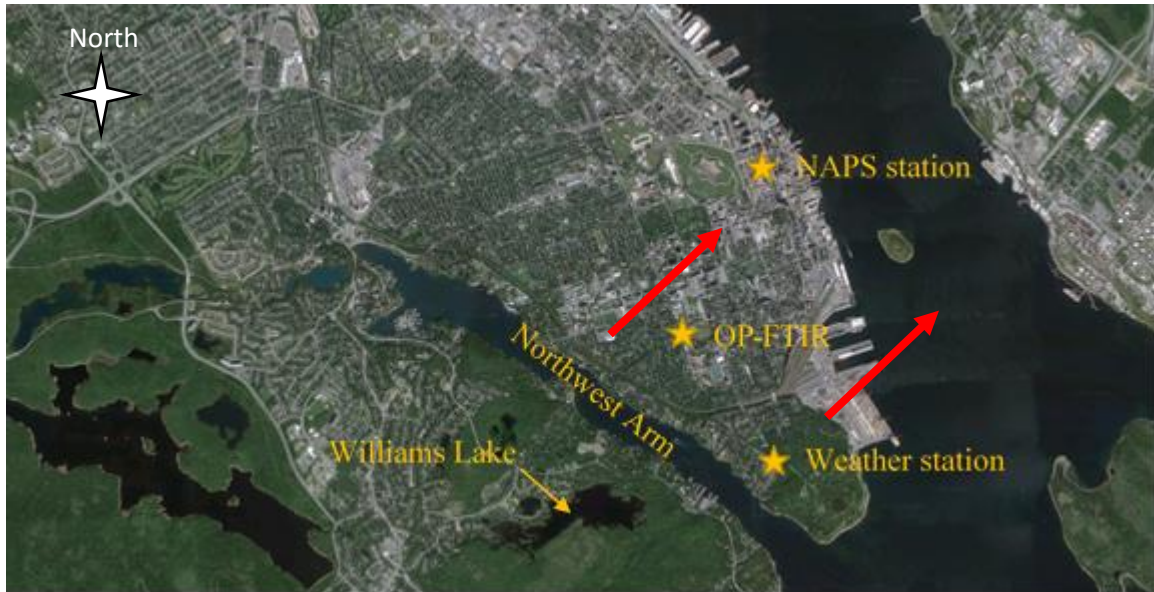


Figure 45 Aerial view of Halifax, including the location of the NAPS station on Barrington Street, the OP-FTIR spectrometer on Robie Street, and the weather station on Francklyn Street. The predominant wind direction is shown in red.

Another thing to consider is the way that each measuring system samples the air. In addition to the spatial averaging inherent in OP-FTIR measurements over point-sampling NAPS measurements, NAPS air samples are sucked in through a glass inlet from a fourth-floor window facing Barrington Street, whereas the OP-FTIR spectrometer averaged air along an open path in the median of Robie Street. The position of the glass inlet on Barrington Street, not being on the roof of a building, means that NAPS samples air at conditions for maximized CO concentrations at a given time because the inlet is closer to and pointed towards the sources of CO emissions. On the other hand, conditions for sampling maximized CO concentrations by the OP-FTIR spectrometer depend on wind direction with respect to the open path. Wind travelling parallel to the open path will carry CO along the open path from both sides of the road (resulting in maximized CO concentrations), whereas wind travelling perpendicular to the open path

will carry CO across the open path from only one side of the street (resulting in minimized CO concentrations). Robie Street runs roughly from the north to the south, therefore, the air in the median during the Robie Street campaign was subject to winds that were midway between parallel and perpendicular to the road, so not maximum, again helping to explain the higher baseline concentration of NAPS results (0.5 ppm vs. 0.15 ppm). To gain further insight into this bias, the TRSL group is currently planning a measurement campaign on Barrington Street near the NAPS station as a result of the findings of this work, as will be discussed in Section 4.

3.1.2. Rice

Unlike the Robie Street campaign, a lower baseline concentration and smaller enhancements in CO concentration with respect to NAPS measurements were expected as the open path extended across Saint Mary's campus and not the median of a busy city street. Figure 46 represents the first transmittance spectrum from the Rice campaign.

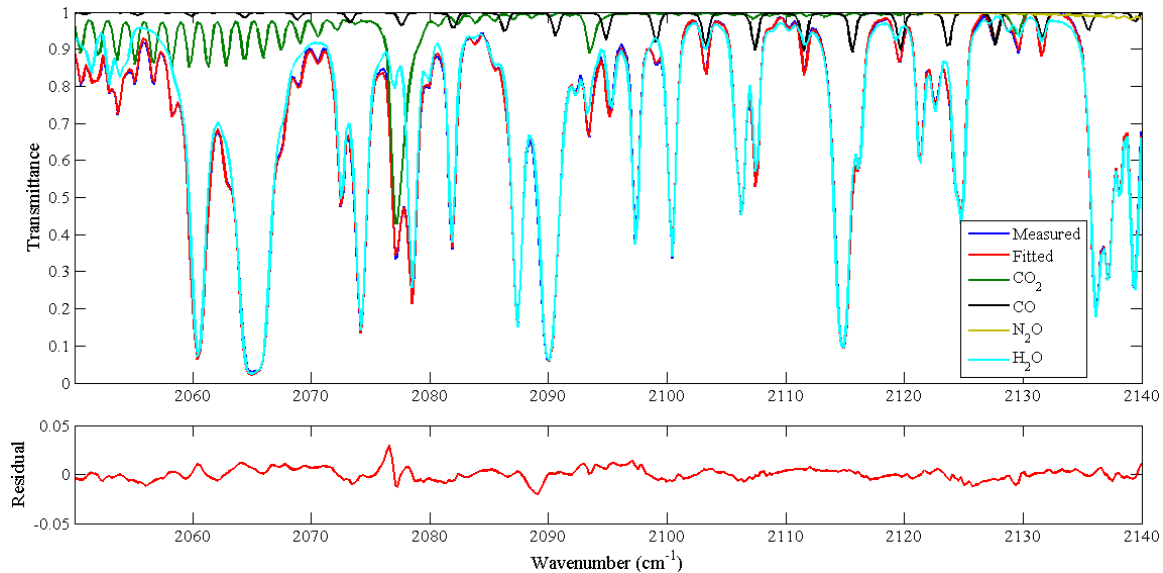


Figure 46 Retrieved transmittance spectrum of results corresponding to data collected at 4:11pm on August 13th, 2015 for the Rice campaign. The temperature, pressure, and relative humidity at this time was 22.6°C, 1005.3 mbar, and 93%, respectively. Top panel: Measured and fitted spectra, also showing the contribution of the target gas (CO) and interfering gases. Bottom panel: The residual plot obtained by taking the difference (measured – fitted spectrum).

One can quickly recognize the difference in H₂O absorption during the Rice campaign compared to that in spectra measured during the Robie Street campaign (Figure 38). The concentration of H₂O in the atmosphere (2.5%) was double that during the Robie Street campaign (1.2%). In August, the temperature is warmer than in May, and warmer air can hold exponentially more H₂O. Another factor in the lower transmittances is the length of the open path, which was nearly double the open path length on Robie Street. With a longer path comes more water vapour between the spectrometer and retroreflector, resulting in more radiation absorbed by H₂O. However, for lines already near saturation on Robie Street, doubling the concentration or path does not double the depth of absorption. The lines instead grow wider. This is an illustration of the breakdown of Beer's Law, which was briefly noted as linear in Section 2.3.2 with path and concentration.

Also visible is the same systematic feature in the residual due to CO₂ under-fitting and over-fitting near 2077 cm⁻¹ as in Figure 38, though not the one due to H₂O near 2065 cm⁻¹. Figure 47 is a plot of the maximum residual value (either positive or negative) for each spectrum recorded during the Rice campaign. Gaps in the data are due to equipment malfunction (14th) and heavy fog (19th-20th).

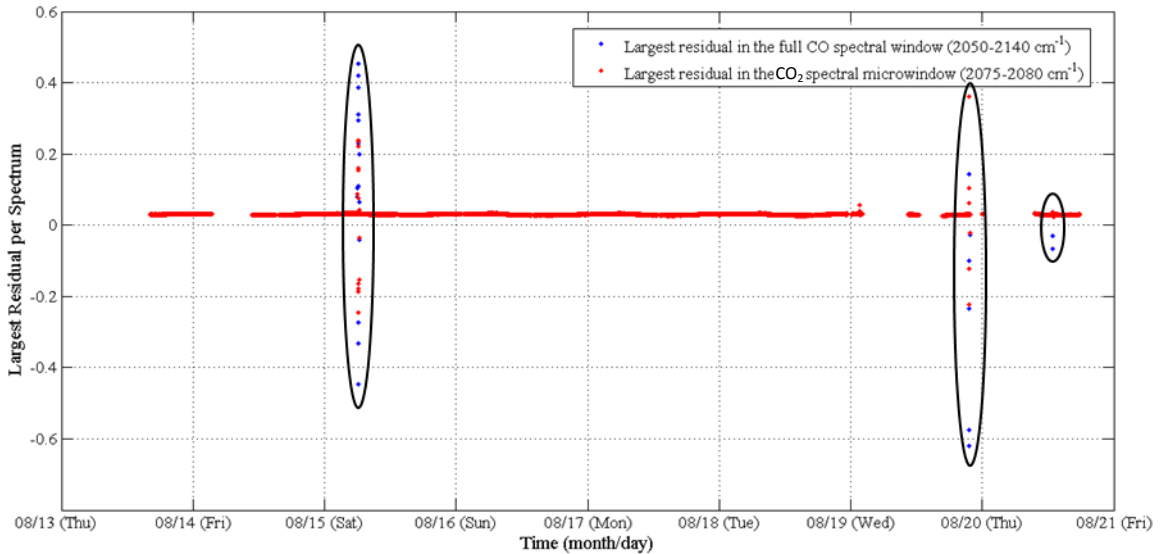


Figure 47 Maximum residual values for the full CO spectral window and the CO₂ spectral microwindow corresponding to the location of the systematic CO₂ feature for the Rice campaign. Circled residuals are those that do not correspond to the systematic CO₂ feature.

The red data represents the largest single residual value for each spectrum (not the RMS value) in the CO₂ spectral microwindow of 2075-2080 cm⁻¹ (targeting the systematic CO₂ feature) and the blue data represents the largest single residual value for each spectrum in the full CO spectral window of 2050-2140 cm⁻¹. Although it cannot be seen on this scale, the majority of the data indicates that the largest residual value for each spectrum is a result of misfitting near 2077 cm⁻¹. However, the largest residual values do not match up in the multiple spectra corresponding to ~7:30am on the 15th, ~10:00pm on

the 19th, and midday on the 20th. This means that something other than the systematic feature in the CO₂ microwindow of 2075-2080 cm⁻¹ caused the largest residual value. The very large residuals on three occasions also point to more serious problems in the recorded spectra beyond the systematic CO₂ under-fitting and over-fitting. On the 15th, the large residual values may correspond to interference of the beam by pigeons attempting to land on the window sill. The window was open for the duration of the campaign and at one point a pigeon had flown into the room from outside, as evidenced by shed feathers. The large residual values on the 19th at ~10:00pm may correspond to the onset of heavy fog because it precedes a gap in the data. As for the large residual values on the 20th, they may be due to interference by pigeons near the spectrometer, or it could be interference by a facilities management crew member walking in front of the retroreflector on the Rice Building.

Figure 48 is a time series of CO concentration for the duration of the Rice campaign at Saint Mary's University. The data affected by fog has been discarded from this plot, aside from a few data points that were missed during manual operator manipulation of the data. The criteria used for discarding the data was a peak intensity less than 0.02 at 2000 cm⁻¹ and the failure of OPUS-RS software to identify water in the spectrum.

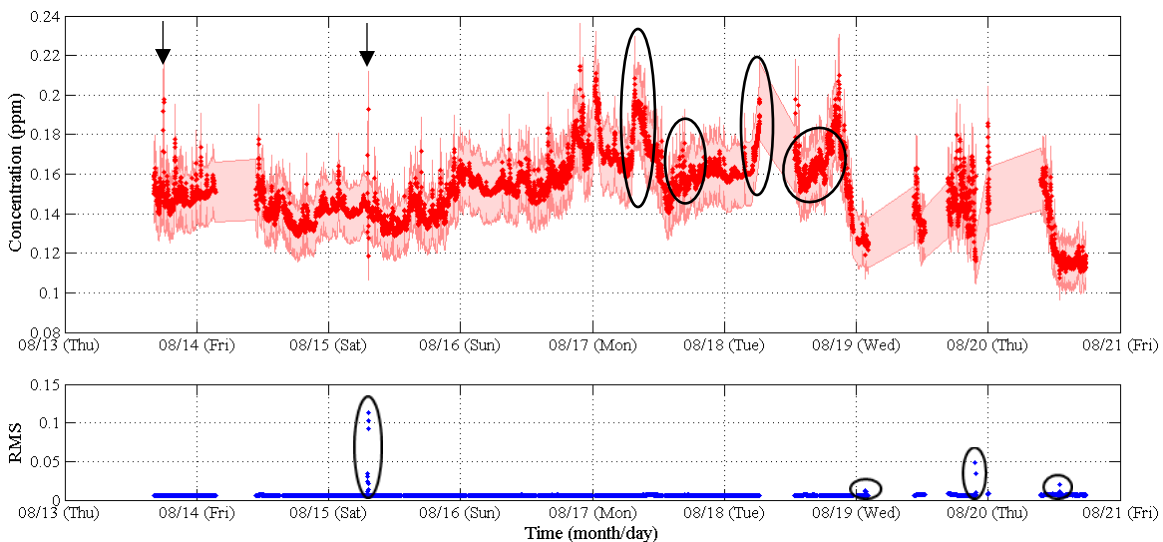


Figure 48 Time series of retrieved CO concentrations by MALT with an error of 10% for the Rice campaign. A time series of RMS for each spectrum is included. Circled enhancements in CO concentration in the top panel may correspond to rush hour traffic. Circled RMS values in the bottom panel are those above 0.01 (1%). Arrows point to enhancements detailed in Figure 51.

For the majority of the measurements, the RMS residual values are well below 0.01 (1%), except at four times, three of which correspond to the mismatched largest single residual values in Figure 47. Overall, there are approximately 13 spectra with an RMS value above 0.01. The RMS values above 0.01 at ~7:30am on the 15th, ~10:00pm on the 19th, and midday on the 20th correspond to the mismatched residual values in Figure 47, indicating that the RMS values are poor because of something other than incorrect spectroscopic parameters, e.g., perhaps interference by pigeons. At ~1:30am on the 19th, the RMS values above 0.01 correspond to a match in the single largest spectral residual value data from Figure 47, indicating that the misfit at 2077 cm⁻¹ is still the biggest issue, although, the spectrum is also noisier than average. However, these data points precede a gap in the data and their raw spectra all have intensities less than 0.02 at 2000 cm⁻¹ (i.e., they should have been discarded). This means there has been

interference, most likely fog, that lowers the overall intensity and decreases the SNR of each of the 13 raw spectra that have RMS values greater than 0.01.

The time series of CO concentration itself does not show any strong diurnal pattern, is quite variable, has an average baseline concentration of ~ 0.14 ppm, dropping to ~ 0.12 ppm on the last day of the campaign, and shows no clear correspondence with vehicle traffic. Although the spectrometer most likely detected CO emissions from vehicles, by the time CO emissions reached the open path they may have already diffused to a point where no sudden sharp enhancements in CO concentration were measured. Nevertheless, there are enhancements in CO concentration circled in the top panel of Figure 48 that may correspond to rush hour traffic, but they are not consistent throughout the work week. What would be expected is two CO concentration enhancements on each day of the work week at rush hour ($\sim 8:00$ am and $\sim 4:00$ pm), but this is not seen.

The drop in baseline concentration from ~ 0.14 ppm to ~ 0.12 ppm on the 20th may correspond to changes in weather, bringing in a cleaner air mass, as the last day of the campaign was cloudy and rainy. Figure 49 provides a closer look at the Rice campaign time series from the 16th to the 18th of August, with most continuous observations.

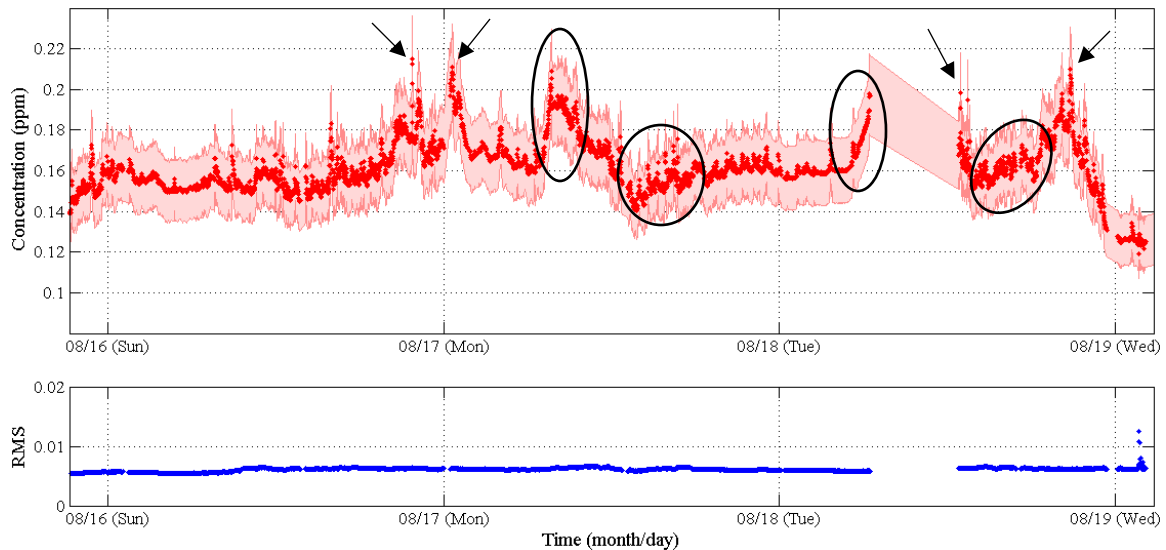


Figure 49 Zoomed-in CO concentration time series measured by the OP-FTIR spectrometer (top panel) and corresponding RMS values (bottom panel). Black circles represent events that may be related to rush hour traffic and black arrows point to unexplained overnight events.

On the morning of the 17th (Mon) and 18th (Tue) CO concentrations begin to rise and are most likely a result of morning rush hour traffic, but in the afternoon, CO concentrations enhance only slightly over a longer period of time. It is speculated, based on personal experience, that most people drive to work in the city at the same time (within the span of an hour), but leave work at different times (anywhere between 2:30pm and 5:30pm). This may be the reason why afternoon enhancement in CO concentrations are smaller than those in the morning. The highest values of CO concentration appear at ~9:30pm on the 16th and 18th, and ~12:30am on the 17th (black arrows), instead of during rush hour traffic. It is difficult to explain these events since CO emissions are primarily from vehicles, and vehicle traffic is generally least dense throughout the night. The near-midnight enhancements in CO concentration may be a result of temperature inversion and suppression of mixing. Also, Saint Mary's University has two smoke stacks on campus located behind the Loyola Building that may emit CO and other pollutants.

Figure 50 is a Google Maps aerial view of Saint Mary's University campus marking the location of the smoke stacks with respect to the spectrometer and retroreflector.

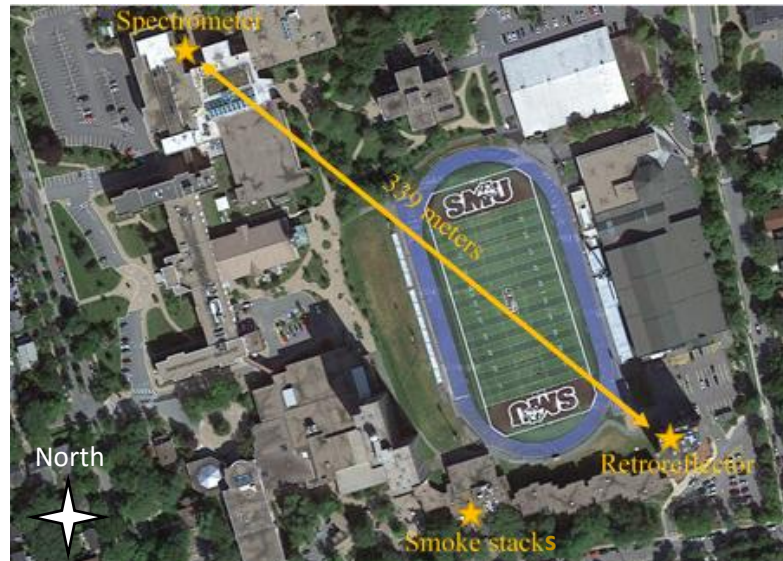


Figure 50 Aerial view of Saint Mary's University campus marking the location of the smoke stacks.

The location of the smoke stacks relative to the open path indicates that emissions from that source may have been detected throughout the campaign. Personal communication with Tom Strapps, Manager of Maintenance and Operations at Saint Mary's University, revealed the following:

- The smoke stacks are used for the main central heating plant, which supplies heat and hot water to all connected buildings on campus.
- The fuel used is natural gas, which has a small component of CO, however, the boilers are tuned regularly and serviced when required for peak efficiency, preventing inefficient combustion processes that would emit CO in excessive amounts.

- The boilers run 24/7 at load levels determined by ambient air and weather conditions, as well as demand for hot water.
- During the summer, load levels are very low, and even lower late at night.

Based on the information provided, it was determined that the nighttime enhancements in CO concentrations measured during the Rice campaign were most likely not a result of smoke stack emissions.

There are two notable enhancements in CO concentration at ~6:00pm on the 13th (Figure 51(a)) and ~7:30am on the 15th (Figure 51(b)), shown in full context in Figure 48. Although these enhancements are well above the baseline concentration, they occur suddenly and only for a few minutes. Each dot in Figure 51 is spaced one minute apart.

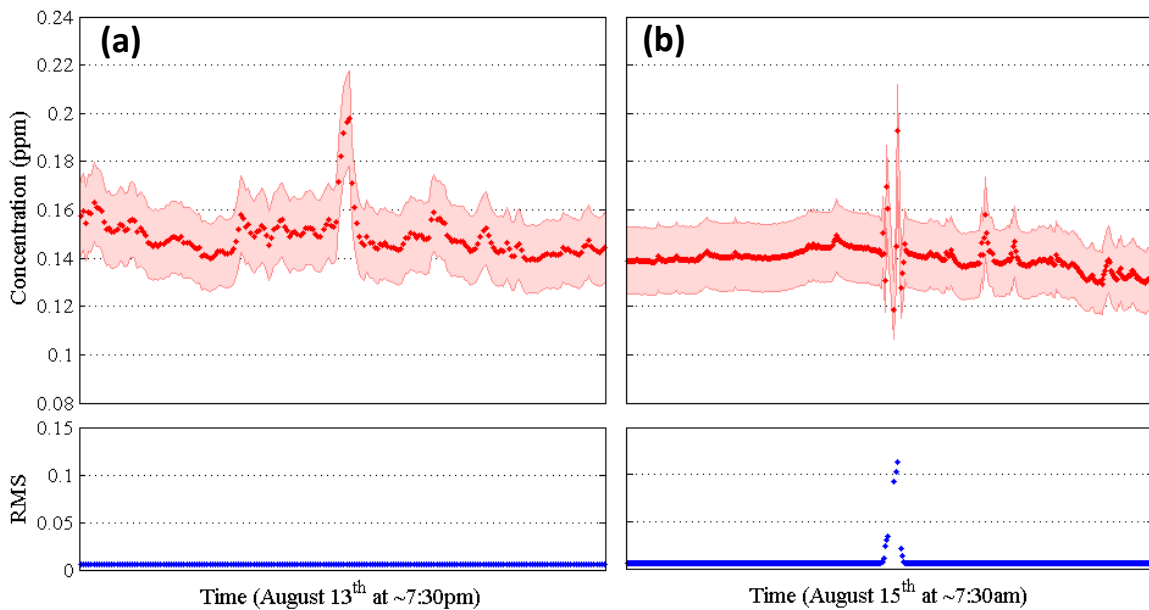


Figure 51 (a) Portion of the Rice campaign time series zoomed to real CO concentration enhancement at ~7:30pm on August 13th with corresponding RMS values. (b) Portion of the Rice campaign time series zoomed to spurious CO concentration enhancement at ~7:30am on August 15th with corresponding RMS values.

A closer look at the enhancement on the 13th and its corresponding RMS values clearly indicates a real enhancement in CO concentration (Figure 51(a)). The OP-FTIR spectrometer did measure a momentary increase in CO concentration, which then dropped back down to the baseline concentration. The RMS values are constant and below 0.01 for this event, meaning the enhancement is not spurious. The CO concentration enhancement on the 15th, on the other hand, varies above and below the baseline concentration for those few minutes before returning to the baseline concentration (Figure 51(b)). The corresponding RMS values are enhanced well above 0.01, and were discussed earlier (Figure 47) as interference by pigeons. Although these two enhancements appear to be of similar nature in Figure 48, a closer look reveals that the event on the 13th is a true enhancement and the event on the 15th is a spurious enhancement.

Similar to the Robie Street campaign, the Rice campaign was also compared to NAPS data. Figure 52 illustrates a comparison between OP-FTIR spectrometer retrieved CO concentrations and NAPS measured CO concentrations for the Rice campaign.

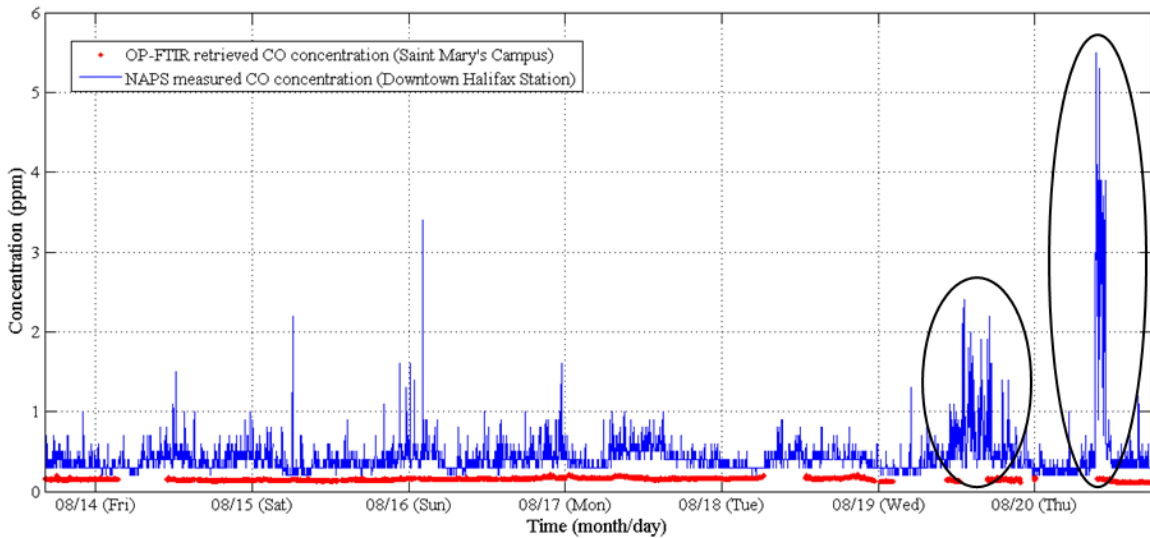


Figure 52 Comparison between OP-FTIR spectrometer retrieved CO concentrations on the Saint Mary's University campus and NAPS measured CO concentrations on Barrington Street. OP-FTIR spectrometer error bars of 10% were excluded as they are too small to be seen at this scale. Circled NAPS data are discussed in detail (see text).

There is a clear bias between the two datasets and the reason for this is likely the same as for the bias seen in the Robie Street comparison, i.e., transport, dispersion, and differences in CO emission sources. The baseline concentration for NAPS measurements is ~ 0.4 ppm vs. 0.14 ppm for OP-FTIR data and partly motivates an upcoming campaign on Barrington Street in April, 2016, to further study the bias. Throughout the campaign, there are multiple rises in measured CO concentrations by NAPS that reach ~ 1 ppm, however, the most prominent enhancements in CO concentration occur early afternoon on the 19th (Wednesday) from ~ 0.5 ppm to ~ 2.4 ppm and midday on the 20th (Thursday) from ~ 0.5 ppm to ~ 5.5 ppm on Barrington Street. The latter of these enhancements, which averages to ~ 3 ppm over one hour, exceeds all but one of the CO concentrations from the annual maximum 1-hour averages of CO concentrations in Figure 12, which is also 3 ppm for 2004. This is interesting to note because the maximum CO concentration NAPS measured in only one *week* at the time of the Rice campaign is comparable to

those measured by NAPS in one *year* for years 2000 to 2007. It should also be noted that the maximum desirable and acceptable CO levels in NAAQO are 13 ppm and 31 ppm, respectively (Table 3). Still, these features are highly localized enhancements and it is somewhat remarkable that the spectrometer did not detect any trace of these events at Saint Mary's University, only ~1.9 kilometers away. However, one reason for this may be the predominant wind direction at the time. Figure 53 is an aerial view of the city of Halifax taken from Google Maps illustrating the location of the measuring sites and the weather station during the Rice campaign.

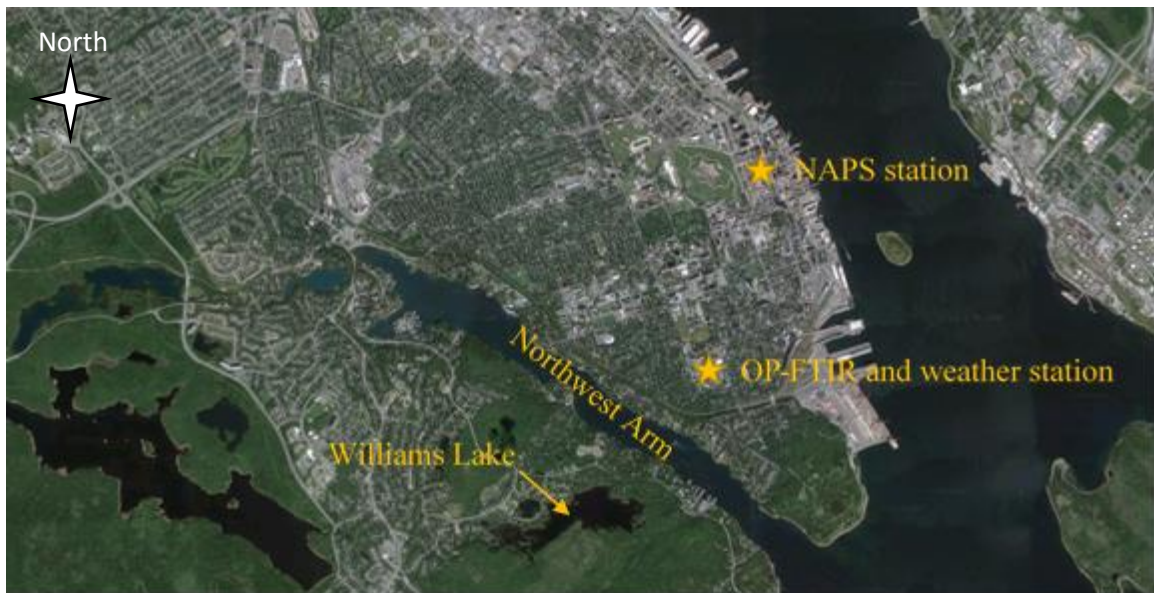


Figure 53 Aerial view of Halifax, including the location of the NAPS station on Barrington Street and the OP-FTIR spectrometer and the weather station on Saint Mary's University campus.

Figure 54 illustrates the variation in wind speed/gust and wind direction over the time of CO concentration measurements from NAPS and the OP-FTIR spectrometer. The wind data was downloaded from the Weather Underground website for the weather station on Saint Mary's University campus (2015).

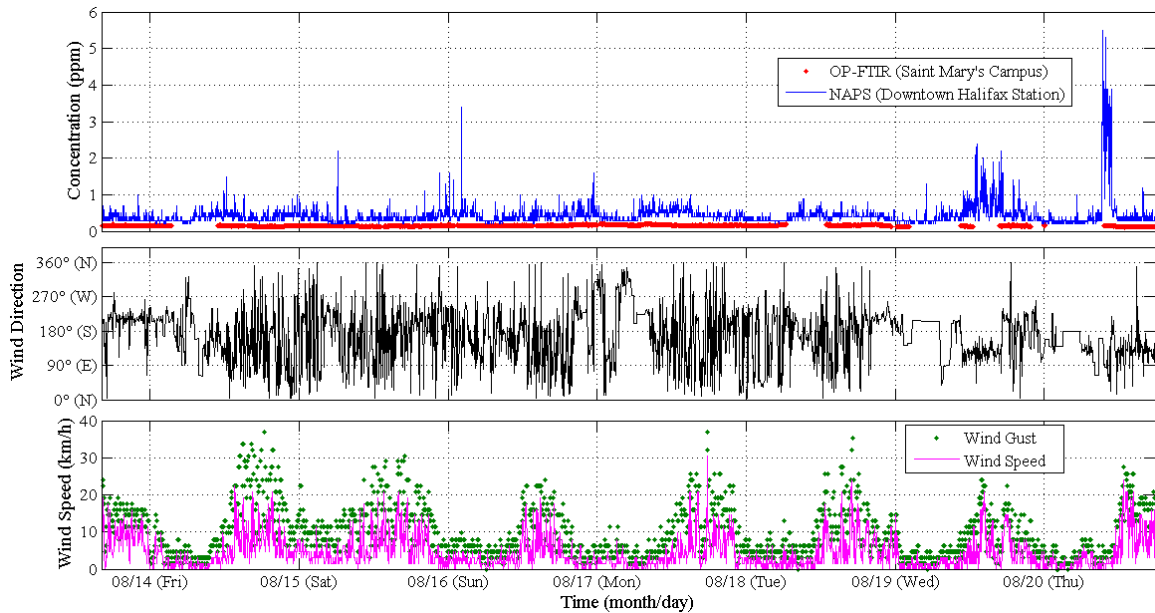


Figure 54 Wind speed/gust and wind direction measured at a weather station on Saint Mary's University campus compared to the CO concentration time series comparison between NAPS data and retrieved OP-FTIR spectrometer CO concentrations for the Rice campaign. Wind direction represents the direction wind is coming from.

Unfortunately, wind direction is quite variable, but wind speed/gust illustrates a clear diurnal pattern, where the lowest wind speeds/gusts occur overnight and in the morning (lowest temperatures) and the highest wind speeds/gusts occur in the afternoon, peaking at ~4:00pm (highest temperatures).

The enhancements in CO concentrations in the afternoon of the 19th and before noon on the 20th are interesting in that they are high, prolonged measurements of CO concentration, yet the OP-FTIR spectrometer did not detect any trace of these at Saint Mary's University. Figure 56 zooms in on these two events from Figure 54.

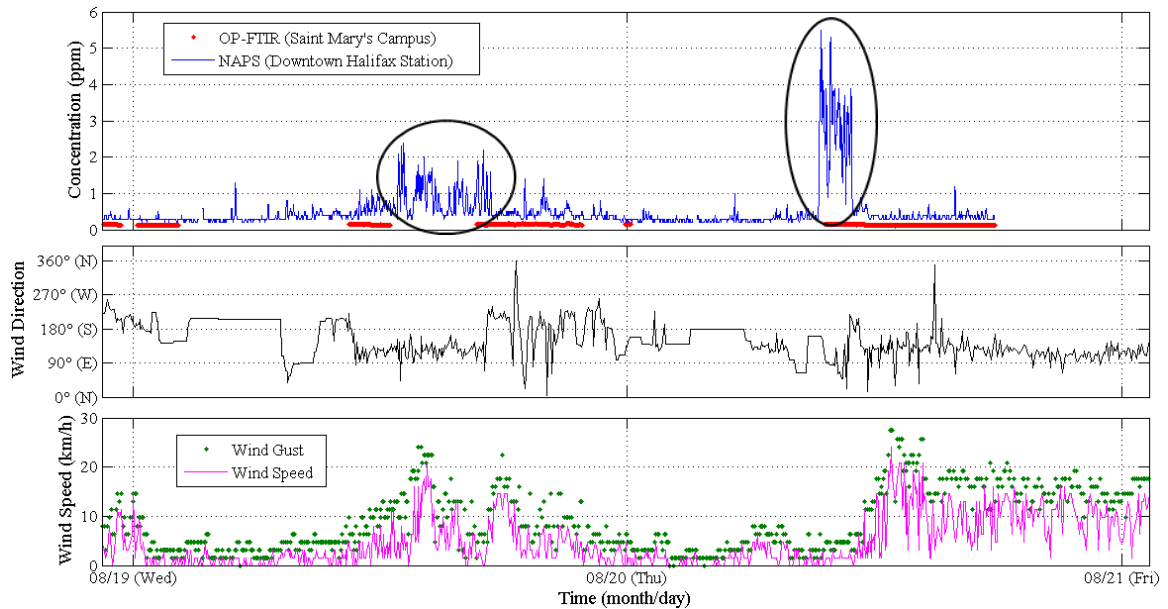


Figure 55 Zoomed time series showing measured CO concentrations (by NAPS and the OP-FTIR spectrometer), wind direction, and wind speed/gust for the two prolonged NAPS events on August 19th and 20th (circled in the top panel).

The enhancement in CO concentration on the 19th persists from ~1:00pm to ~5:00pm and reaches a maximum CO concentration of 2.4 ppm, whereas the CO concentration enhancement on the 20th only persists from ~9:00am to ~10:30am, but it reaches a maximum CO concentration of 5.5 ppm, possibly because of the very low wind speeds. The latter of the enhancements is interesting because the simultaneously measured CO concentrations by the OP-FTIR spectrometer were the lowest for the entire Rice campaign; however, the predominant wind direction at Saint Mary's University at that time was roughly southeast, meaning that the OP-FTIR spectrometer would not have sampled the same air as the NAPS station if the CO emissions originated from Barrington Street, unless the CO source was very extensive in space. Winds from the southeast could also transport to the NAPS station CO emissions from cruise ships or container ships entering, leaving, or docking at ports in the Halifax Harbour, without affecting the

OP-FTIR spectrometer. Further study is required to confirm this hypothesis by carefully tracking ship routes, but it currently stands as a reasonable explanation for the prolonged CO enhancements on August 20th. If the wind was blowing from the northeast, as it does once on the 20th during the time of the enhancement in CO concentration at the NAPS station, the air would then reach Saint Mary's University. Nevertheless, the spectrometer would probably not detect as high concentrations of CO as the NAPS station due to dispersion in transport. One could ask if these enhancements in CO concentration are the result of heavy bus traffic or industry. However, if they are a result of buses, why not see similar events every day? If they are a result of industrial emissions, what is the source southeast of the NAPS station given that the refinery in Dartmouth across the harbour is inactive? Is the oil terminal responsible? Many questions are still left unanswered, hence, the need for further study. The case of the smaller enhancement on August 19th under higher wind speeds is qualitatively similar, although the winds are much more consistently from the southeast, pointing clearly to sources in the harbour or on the Dartmouth coast near the old refinery.

Enhancements in NAPS CO concentrations at ~8:00am on the 15th and ~2:30am and ~11:30pm on the 16th (Figure 54) are not prolonged events and do not correspond to any enhancements in CO concentrations measured by the OP-FTIR spectrometer.

Figure 56 zooms in on these three events from Figure 54.

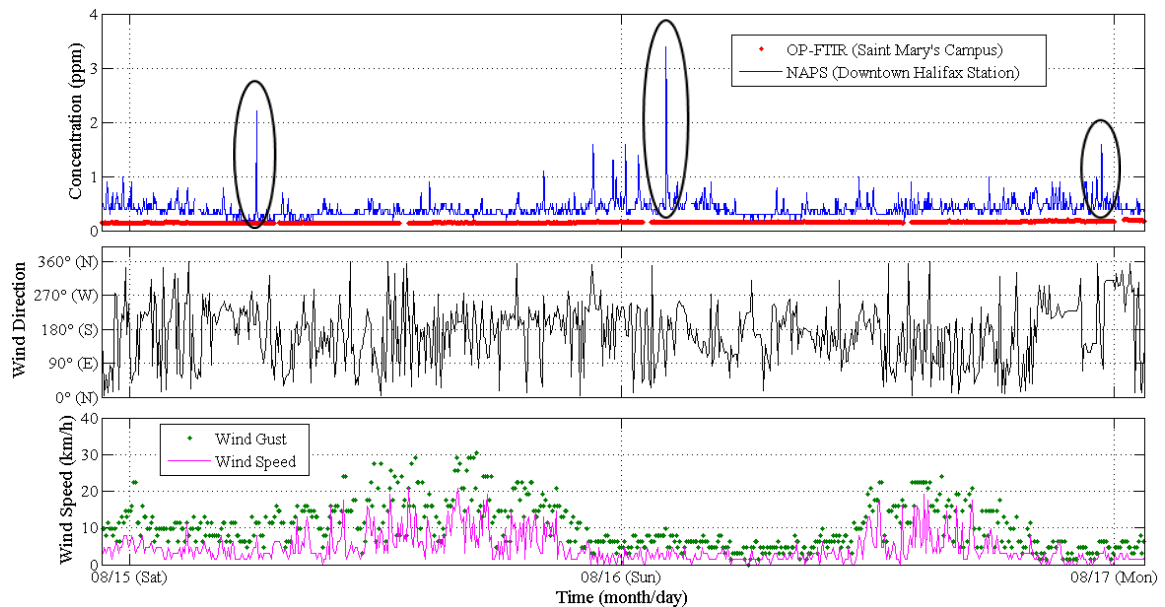


Figure 56 Zoomed time series showing measured CO concentrations (by NAPS and the OP-FTIR spectrometer), wind direction, and wind speed/gust for the three NAPS events on August 15th and 16th (circled in the top panel).

Because these three events are momentary, it is difficult to determine the emission source responsible for the CO concentration enhancements. They may be associated with a large truck or a bus driving by, but if this were the case, one would likely see these types of enhancements throughout the day, every day for the whole week, which is not the case.

3.1.3. Lake Major

The results from the Lake Major campaign are expected to have the lowest baseline concentration of all three campaigns as the environment is more rural than urban. This is indeed the case, as will be shown below. Figure 57 represents the first transmittance spectrum from the Lake Major campaign.

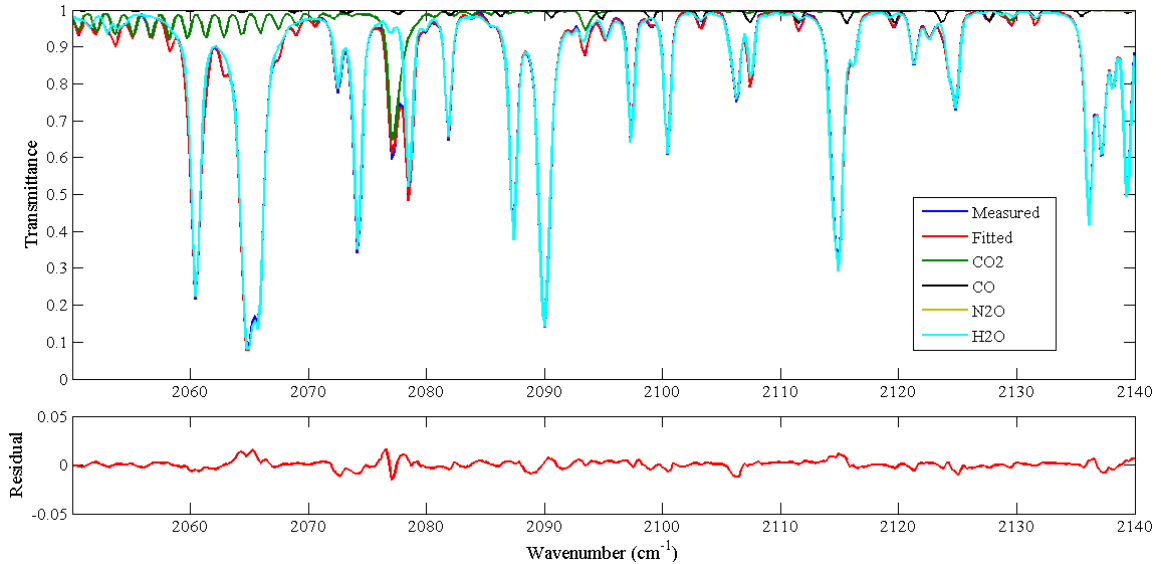


Figure 57 Retrieved transmittance spectrum corresponding to data collected at 5:43pm on September 4th, 2015 for the Lake Major campaign. The temperature, pressure, and relative humidity at this time was 21.3°C, 1014.5 mbar, and 66%, respectively. Top panel: Measured and fitted spectra, also showing the contribution of the target gas (CO) and interfering gases. Bottom panel: The residual plot obtained by taking the difference (measured – fitted spectrum).

Once again, the systematic feature is present in the residual plot of Figure 57, indicating a poor fit of the CO₂ absorption line near 2077 cm⁻¹. The concentration of H₂O at the time corresponding to this spectrum was 1.6%, which is lower than at Saint Mary's University during the Rice campaign (2.5%).

Figure 58 is a plot of the maximum residual value (either positive or negative) for each spectrum recorded during the Lake Major campaign.

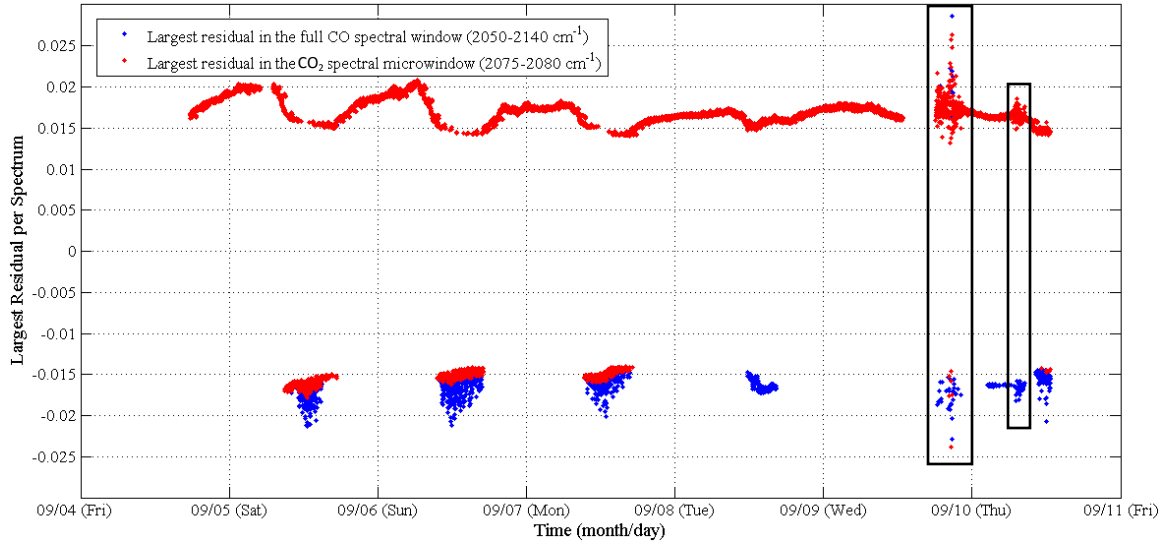


Figure 58 Maximum residual values for the full CO spectral window and the CO₂ spectral microwindow corresponding to the location of the systematic CO₂ feature for the Lake Major campaign. See text for discussion of boxed regions.

In the case of Lake Major residuals, the majority of the data indicates that the largest residual value per spectrum is a result of the systematic feature at 2077 cm⁻¹. There is a pattern of largest residuals switching to negative values and showing a mismatch in residual data points around noon on most days, indicating that these large and mostly negative residuals are a result of something other than the misfitting of the CO₂ absorption line. Randomly sampled spectra around noon on these days show a large negative systematic feature at the H₂O absorption line near 2107 cm⁻¹ with maximum spectral residual values around -0.022, which is consistent with the large negative mismatched residual values in Figure 58. The recurring pattern suggests that the cause is not related to incorrect spectroscopic parameters, which are constant in time. One obvious parameter that does change over time and experiences a diurnal cycle is temperature. Figure 59 is a time series plot of the spectral residual RMS values and the

temperature recorded by the PT sensor for each spectrum during the Lake Major campaign.

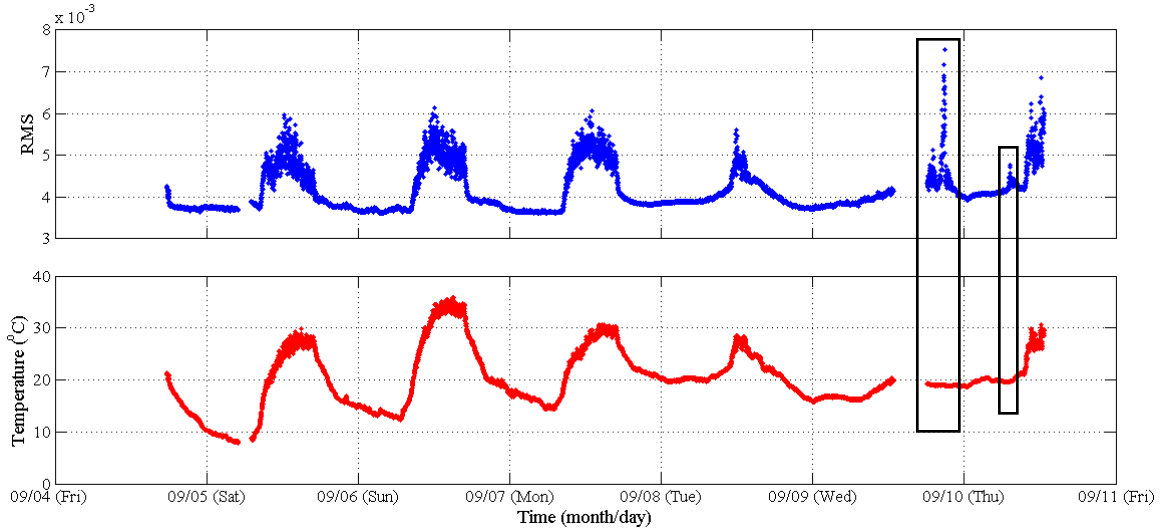


Figure 59 Time series of Lake Major RMS values and recorded temperature. Boxed RMS values show no correlation with temperature.

The RMS time series (top panel) illustrates a pattern of strongly increasing RMS values at midday on the 5th to the 8th, and the 10th, with a weak increase also on the 9th. Although all RMS values are below 0.01 (1%), there is still a degradation in fitting around noon and it is important to investigate where this pattern of increasing RMS values comes from.

According to Figure 59, the cause appears to be temperature-related. The PT sensor was located inside of a deep blue tent (Figure 37(c)) that protects the OP-FTIR spectrometer and related equipment from rain and high winds, but also acts as a heat trap, resulting in the elevated temperatures at noon, which are not representative of the air temperature in the open path. This incorrect temperature input to retrievals causes those absorption lines with a high sensitivity to temperature to be systematically misfit. On the 8th and 9th, solar intensity was reduced due to clouds, diminishing this effect. The only times when

there seems to be no correlation between RMS values and temperature and also the mismatch in data points are at ~9:30pm on the 9th and ~8:00am on the 10th (boxed regions in Figure 58 and Figure 59), which may be indicative of a random error in the measurement process or, more likely, interference by heavy fog. The problem area on the 9th, in particular, is qualitatively different (scattered residual values) and it follows a break in the data due to fog.

Figure 60 illustrates the time series of CO concentration (top panel) along with a time series of RMS values (bottom panel) for each spectrum recorded during the Lake Major campaign. The RMS time series shows the pattern discussed due to incorrect high recorded temperatures at midday. Since even these errors do not cause residuals to be greater than 1%, the effect does not map to a pattern in CO concentrations, which is reassuring. Overall, the time series of CO concentration measured by the OP-FTIR spectrometer is least variable for the Lake Major campaign, unlike those for the Robie Street and Rice campaigns.

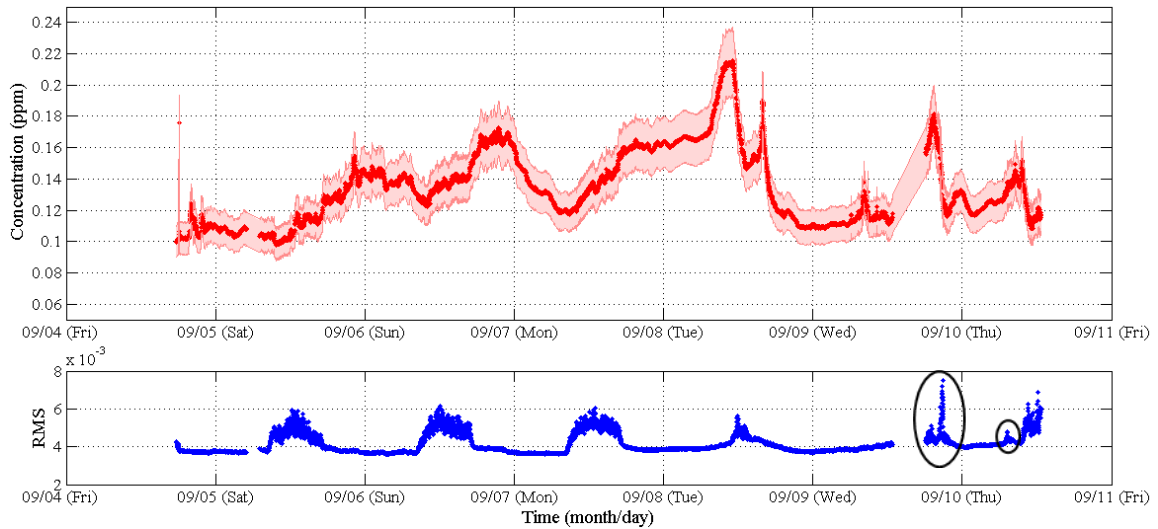


Figure 60 Time series of retrieved CO concentrations by MALT with an error of 10% for the Lake Major campaign. A time series of RMS for each spectrum is included. Circled RMS values are fog- not temperature-related.

There are a few interesting events that occur within this time series plot, including the enhancement in CO concentration from ~8:00am to ~12:00pm on the 8th (reaching up to 0.22 ppm) and the subsequent sharp enhancement at ~3:00pm of that same day from the baseline concentration of ~0.11 ppm. The CO peak before noon is interesting because it is similar to CO concentrations that were measured in the city. The environment at Lake Major is more rural, which typically consists of more biogenic compounds than anthropogenic compounds, such as CO. One possible explanation for the enhanced concentration of CO before noon is an idling delivery truck. Contacts at the Lake Major Water Treatment facility were asked if any deliveries were made to the facility on the 8th and the response was that at some point during the day a contractor arrived and worked for a few hours on a piece of equipment. The contractor was driving a pickup truck and possibly idled for a few hours beside the open path. However, this is unlikely because a point source, such as an idling truck, would have revealed more

random and instantaneous CO elevations in the time series, as a result of wind gusts. Instead, one sees a smooth, prolonged elevation. As for the subsequent sharp enhancement in CO concentration at ~3:00pm, the spectrometer may have detected CO emissions from employees smoking cigarettes or a single vehicle driving by/idling (possibly the contractor) near the open path for approximately 30 minutes. Another plausible explanation for these two strong enhancements in CO concentration on the 8th of September is Halifax Regional Municipality (HRM) traffic emissions from vehicles transporting kids to school (kindergarten to grade 12) for their first day after Labour Day Monday. Please see wind discussion further below.

Figure 61 illustrates a comparison between OP-FTIR spectrometer retrieved CO concentrations and NAPS measured CO concentrations during the Lake Major campaign. The latter were measured on Barrington Street in Halifax.

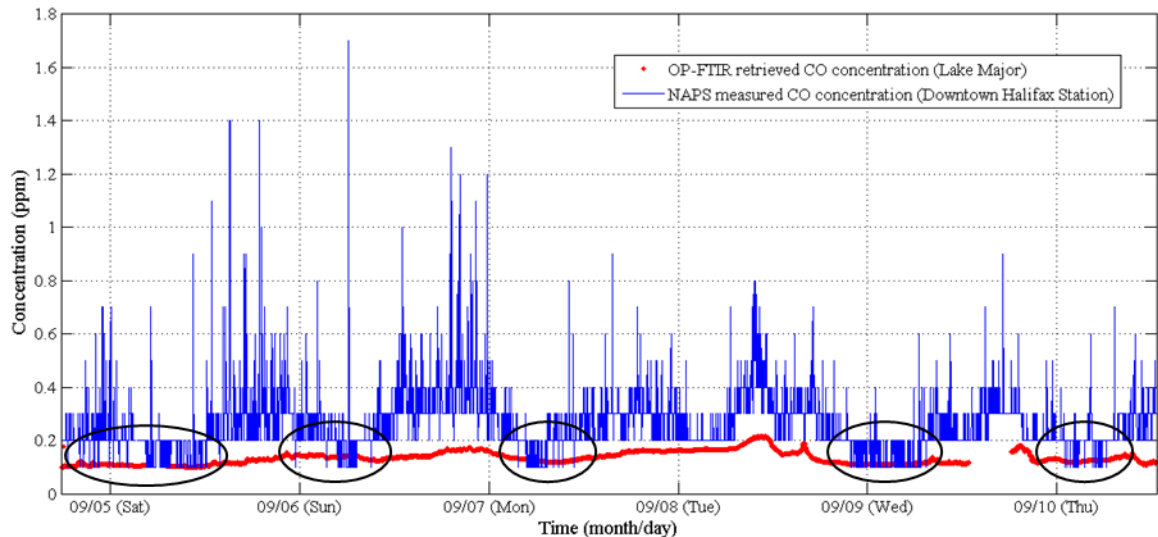


Figure 61 Comparison between OP-FTIR spectrometer retrieved CO concentrations at Lake Major and NAPS measured CO concentrations on Barrington Street. OP-FTIR spectrometer error bars of 10% were excluded as they are too small to be seen at this scale. Circled regions point to overlap in the two datasets.

Once again, there is a systematic bias between the two datasets, but in this case, there is overlap between the two datasets on all days for periods of time, as shown by the circled data points. During this campaign, the NAPS CO concentration time series has a baseline concentration of only ~ 0.2 ppm, which is low in comparison to the time series for the Robie Street (0.15 ppm) and Rice (0.14 - 0.12 ppm) campaigns. Why is there better agreement between NAPS data and OP-FTIR spectrometer data at this rural location? The answer is unknown at this time. Several explanations are proposed, such as the discontinuation of construction near the NAPS station on Barrington Street for Labour Day weekend/week, a possible cutback in cruise ship schedules, and the fact that all three NAPS datasets are unvalidated, meaning that the data may have an offset of up to 0.2 ppm in 7 days due to zero drift errors. Further study is required to answer this question.

To identify any OP-FTIR and NAPS correlation that may have resulted from transport of CO from Barrington Street in Halifax on September 8th, wind data needs to be analyzed. Figure 62 is an aerial view of Halifax and Dartmouth taken from Google Maps illustrating the location of the measuring sites and the weather station during the Lake Major campaign.

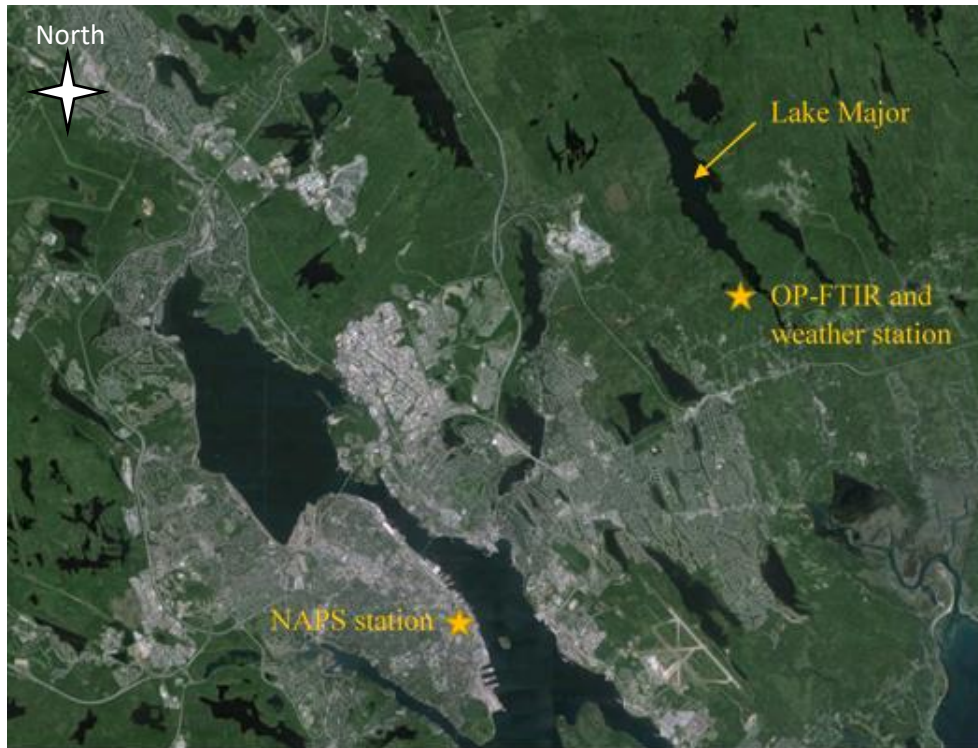


Figure 62 Aerial view of Halifax and Dartmouth, including the location of the NAPS station on Barrington Street and the OP-FTIR spectrometer and the weather station at Lake Major, which are separated by approximately 11 kilometers.

Figure 63 illustrates the variation in wind speed and wind direction over the entire time of CO concentration measurements from NAPS and by the OP-FTIR spectrometer. The wind data was measured on site at Lake Major by NSE and was obtained from Frances Di Cesare because it is otherwise unavailable at that temporal resolution.

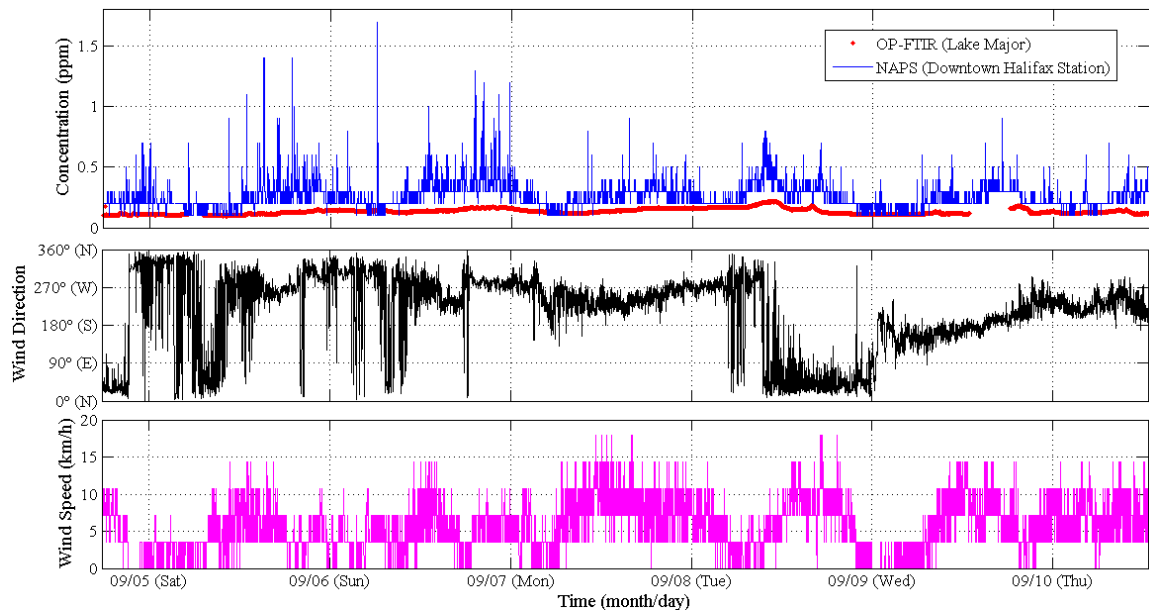


Figure 63 Wind speed and wind direction measured by Nova Scotia Environment at Lake Major compared to the CO concentration time series comparison between NAPS data and retrieved OP-FTIR spectrometer CO concentrations for the Lake Major campaign. Wind direction represents the direction wind is coming from.

After midnight on September 8th the wind direction is predominantly from the west, but becomes variable, and is not entirely clear at this scale, hence, Figure 64, which focuses only on September 8th.

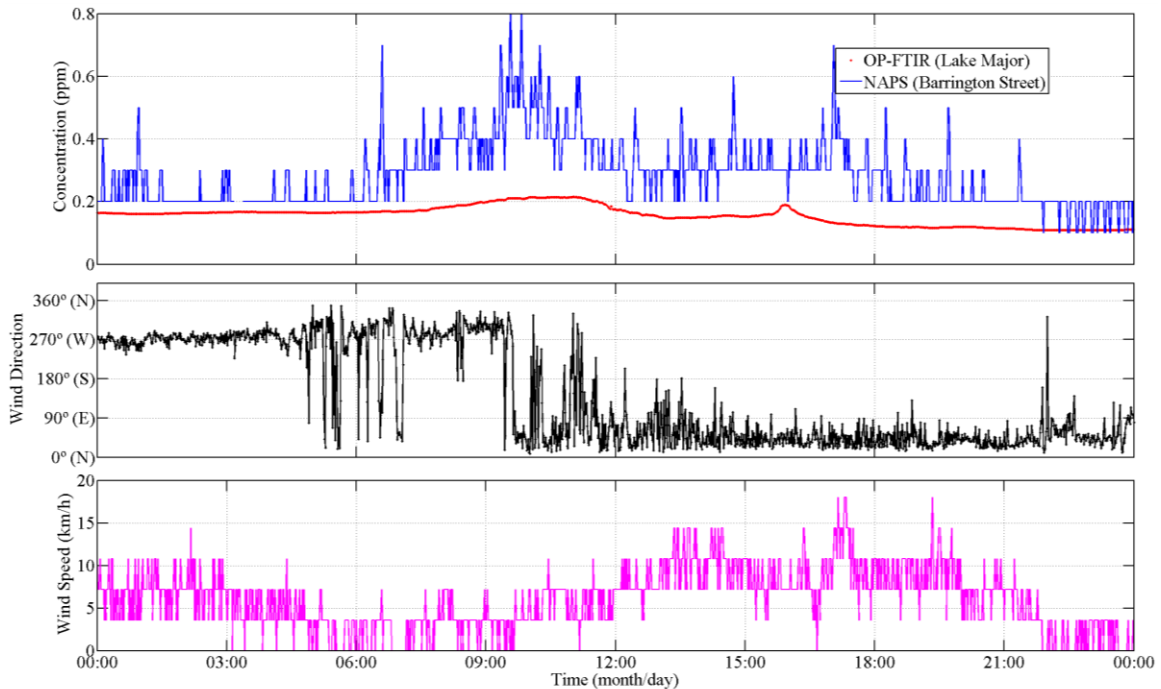


Figure 64 Zoomed-in plot of wind speed and wind direction measured by Nova Scotia Environment at Lake Major, on September 8th, compared to the CO concentration time series comparison between NAPS data and retrieved OP-FTIR spectrometer CO concentrations for the Lake Major campaign. Wind direction represents the direction wind is coming from.

In the early morning (~5:00am) the wind direction varies significantly for about two hours, but the wind speeds are low during this time. Relatively low wind speeds are also present from 8:00am to 12:00pm coinciding with the CO enhancement at Lake Major, and possibly leading to a build-up of CO. Afterwards, the wind switches progressively from west to northwest to northeast. These are all directions that would bring elevated CO concentrations to the NAPS station on Barrington Street, but cleaner air to Lake Major. Shortly after 9:00am, wind speed starts to increase and stabilizes at approximately 10 km/h just after noon; the point in time when CO returns to its base-level concentration. With the increase in wind speed, and wind direction from the northeast (from noon onwards), the wind is ventilating the Lake Major area of CO build-up from earlier in the day. As for the CO build-up, wind blowing from the south,

southwest, and west would transport air, including emissions from back-to-school vehicle traffic, from all regions of the HRM towards Lake Major, making this the most likely explanation for the morning enhancement in CO concentration on September 8th.

3.2. Comparison of Robie Street, Rice, and Lake Major OP-FTIR

Spectrometer CO Concentration Data

The locations of the three campaigns that comprise this thesis work were all chosen for different reasons. The purpose of the Robie Street campaign was to measure traffic emissions as close to vehicle sources as possible. The purpose of the Rice campaign was to measure and identify diurnal patterns of gas concentrations in an ambient city environment. Lastly, the purpose of the Lake Major campaign was to measure gas concentrations in a rural/forested environment. Figure 65 is a time series comparison plot of CO concentration from all three campaigns.

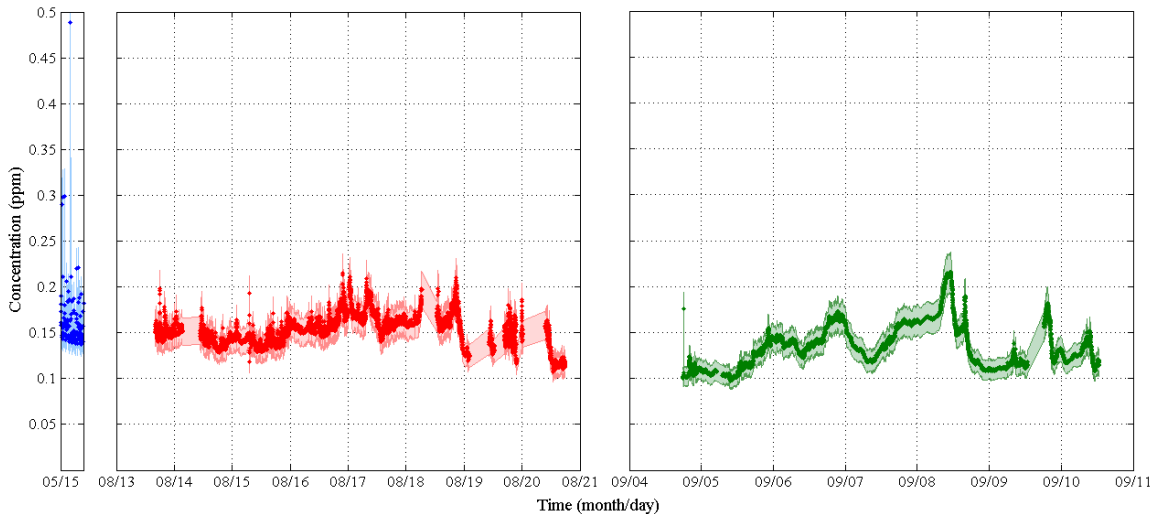


Figure 65 Time series of CO concentration from the Robie Street campaign (blue), the Rice campaign (red), and the Lake Major campaign (green) with an error of 10%.

The y-axis on all three plots and the x-axis on the Rice campaign and Lake Major campaign plots are to scale. The x-axis on the Robie Street campaign plot (representing two hours of measurement time) has been expanded in order to view the data more clearly. The baseline concentrations of CO for the Robie Street and Rice campaigns are

similar (0.15 ppm and 0.14 ppm, respectively), which is consistent because the measurement sites were in close proximity to one another. The baseline concentration of CO for the Lake Major campaign was the lowest at ~0.11 ppm, which is again consistent with the measurement location being more rural than downtown Halifax. The Rice campaign had the highest variability of CO concentrations and did not show clear diurnal patterns, however, at the start of the week on the 17th one starts to see slightly higher CO concentrations as a result of capturing the rise in activity at the start of the work week. The Lake Major campaign is the least variable of the three campaigns, but captured enhancements in CO concentration similar to and greater than levels in the city. This was unexpected as the environment at Lake Major is lighter in traffic density and more rural than downtown Halifax. An analysis of wind directions showed air being transported from the HRM to Lake Major during the morning CO enhancement on September 8th and cleaner air being transported from the north/northeast for the rest of the day. Robie Street had the highest enhancements in CO concentration of up to almost 0.5 ppm because the spectrometer detected CO emissions close to its sources (vehicles), which drove by randomly throughout the campaign. On the other hand, enhancements in CO concentration during the Rice and Lake Major campaigns only reached up to ~0.22 ppm.

4 Conclusions, Limitations, and Future Work

Carbon monoxide (CO), a toxic air pollutant emitted primarily as a result of incomplete combustion and oxidation of hydrocarbons, was measured in Halifax, Nova Scotia using an Open-Path Fourier Transform Infrared (OP-FTIR) spectrometer and compared to National Air Pollution Surveillance (NAPS) CO measurements as a verification step in the characterization of this new instrument.

Measured NAPS data was compared to OP-FTIR spectrometer results for three different measurement campaigns: the Robie Street campaign (at Inglis for 2 hours), the Rice campaign (at SMU for ~1 week), and the Lake Major campaign (in rural Dartmouth for ~1 week). For each campaign, spectra were recorded and a concentration of CO was retrieved for each spectrum by the program MALT. The retrieved CO concentrations were plotted in a time series for each campaign and compared to NAPS CO concentration measurements obtained on Barrington Street at the same time – the only local source of CO measurements in the HRM.

The first Saint Mary's University OP-FTIR spectrometer measurement results were a success in that spectral fits of CO absorption features by MALT lead to RMS values of less than 0.01 (1%) in the fit residuals for all of the measurements unaffected by fog and other systematic problems. Additionally, retrieved CO concentration values by MALT are comparable to NAPS CO concentrations. Taken together, this indicates that there are no major issues with the performance of the instrument, MALT fitting and retrievals, or the creation of time series plots of results.

As a result of this work, a quality assurance procedure was established to identify poor spectral fits based on anomalously high RMS values from spectral fit residuals.

Minor issues found in spectra that affected spectral residuals and RMS values include:

- Misfitting of the CO₂ absorption line at 2077 cm⁻¹ and the H₂O absorption line at 2107 cm⁻¹, most likely due to errors in retrieval input temperatures or spectroscopic constants.
- Interference with the IR beam by heavy fog and possibly pigeons during the Rice and Lake Major campaigns.

Although there are no major issues with the instrument or the retrieval process, analysis and interpretation of the results proved to be challenging. Time series results from all three campaigns reveal a systematic bias of up to 0.35 ppm between OP-FTIR spectrometer and NAPS measurements. Robie Street campaign measurements by the OP-FTIR spectrometer have a baseline CO concentration of ~0.15 ppm and the NAPS measurements have a baseline CO concentration of ~0.5 ppm (systematic bias of 0.35). Only once during this campaign (at 12:59pm on May 15th, 2015) did the two datasets agree within error bars. Rice campaign measurements by the OP-FTIR spectrometer have a baseline CO concentration of ~0.14 ppm and the NAPS measurements have a baseline CO concentration of ~0.4 ppm (systematic bias of 0.26). At no point during this campaign did the two datasets agree within error bars. Lake Major campaign measurements by the OP-FTIR spectrometer have a baseline CO concentration of ~0.11 ppm and the NAPS measurements have a baseline CO concentration of ~0.2 ppm (systematic bias of 0.09). At five points during this campaign (overnight/mornings) the

two datasets agreed within error bars. The reason for the majority of the OP-FTIR spectrometer measurements disagreeing with NAPS measurements is most likely the result of sampling error, however, further study is required for confirmation. Additionally, results showed unusual, and in one case, inexplicable enhancements in CO concentration at times when and where vehicle traffic is minimal. Specifically, in the morning and afternoon on September 8th, 2015 during the Lake Major campaign and overnight on August 16th and 18th during the Rice campaign, CO concentration enhancements were observed. The morning CO concentration enhancements during the Lake Major campaign were likely due to more regional first-day-of-school rush hour traffic, but the source of the shorter (~30 minutes) afternoon Lake Major enhancement, as well as the shorter (~5, ~20, and ~20 minutes) overnight CO concentration enhancements during the Rice campaign are unknown. Overall, further study is possible in order to resolve the interpretation issues discovered in this honours thesis work, including:

- Check the effect of validation on NAPS measurements.
- Track ship routes in order to include or rule out an emission source that may be causing enhancements in trace gas concentration.
- Examine the effect of wind direction and wind speed on recorded CO concentrations, especially at Lake Major and Rice, where co-located wind measurements exist.
- Consult a wildfire database in order to include or rule out wildfires in the region as a possible source.

Along with the issues noted above, this honours thesis work also faced some limitations, and they are as follows:

- Lack of truly co-located CO measurements.
- Only having approximate knowledge of winds due to extreme variability.
- The bias in pressure and temperature data, e.g., PT sensor located in room S425 during the Rice campaign and in the tent during the Lake Major campaign.
- 2015 NAPS data used for comparison with OP-FTIR spectrometer results are unvalidated and have not gone through any form of quality control.
- Blocks of data missing in the time series due to interference of the beam by fog, especially during the Rice campaign, but also during the Lake Major campaign.

While some of the above were unavoidable (e.g., fog), it is possible to mitigate lack of co-located data and bias in ancillary data (P, T, wind) in future work as follows:

- Measure CO concentrations on Barrington Street with the OP-FTIR spectrometer and compare to simultaneous NAPS measurements to provide insight into the bias observed when measuring at other locations.
- Measure CO concentrations on Barrington Street with the OP-FTIR spectrometer and also the NAPS CO Analyzer(s) in the open path and compare measurements.
- Change the location of the PT sensor from inside the tent to somewhere more representative of the conditions along the open path; include more than one sensor.
- Opt for a lighter-coloured tent (one that is less efficient at trapping heat) or a tent with a screen/screen windows, allowing for better ventilation.

- Invest in a wind sensor, or two, to setup next to the OP-FTIR spectrometer.
- Set up a camera pointing down the open path and have it record a video, or take pictures at set time intervals, to capture activity in the area surrounding the open path in order to identify potential local emission sources present at the time of measurement.
- Run tests on known gas samples in a cell with the OP-FTIR spectrometer to produce estimates of measurement errors specific to the OP-FTIR spectrometer used for this honours thesis work.

Taking some or all of the above steps will help to further quantify the accuracy and precision of the Open Path System.

5 Appendices

5.1. Sample MALT Parameter Input File

The following MALT parameter input file was one used in the simulation of a retrieved spectrum for the Robie Street campaign. The only parameters that changed with each simulation for a particular campaign were the file name, temperature, and pressure. Additionally, for each of the three campaigns, the path length parameter changed (a different path length for each campaign).

Note: The field-of-view (FOV) for Robie Street campaign retrievals was input as 21.5 mrad, which is incorrect. The FOV of the spectrometer is 21.739 mrad. For all other retrievals, the correct FOV parameter value was used.

```
!Demo MALT5 input file
!=====
!All lines beginning with ! are comments and ignored
!Comment
    Remote sensing
!Fitfile, reffile
    C:\Transporter\Students\TRSL_Julia\Julia_Thesis_Work\2015_05_15_Robie\2015_05_1
    5_17_10_02)_240_960_2_hours\MALT\CO\SPC\CO_3.spc
!Outfiles
    output_file
!Abscof file
    abs_coef.spc
!Linelist, type
    C:\malt5\hitran\hitran04.mir' 'C:\malt5\hitran\hitran.dat
!Scratch directory path
    C:\Malt5\FTS\
! #iter
    50
! low      high      ext  outspacing  SNR weight
    2050.0428 2139.9612 10. 0.0      0 0
! Ytype      #layers
    1 1
!Layer 1
!-----
```



```

! type Press unit fit Temp unit fit Path unit broad isoscale
1 1021.2 mb f 21.5 C f 343.7 m 0 0
! #malt components # library spectra
4 0
! Loop n_comp times
! comp amount unit linefile type fit display
2 400 ppm C:\malt5\hitran\hitran04.mir
C:\malt5\hitran\hitran.dat t t
5 150 ppb C:\malt5\hitran\hitran04.mir
C:\malt5\hitran\hitran.dat t t
4 300 ppb C:\malt5\hitran\hitran04.mir
C:\malt5\hitran\hitran.dat t t
1 1 % C:\malt5\hitran\hitran04.mir
C:\malt5\hitran\hitran.dat t t
!
! Instrument/ILS
!=====
! polynomial (# terms, initial values)
2 1.0 0.0 0.0 0.0
! shift resolu apod
-0.0 0.5 2
t f
! fov fap phase sym1 sym2 malign PBadj zoffset
21.5 0.0 0.0 0.0 0.0 0.0 0.0 0.0
f t t f f f f f
! Channel spectra
! period phase amplitude delay
0.0 0.0 0.0
f f f f
0.0 0.0 0.0
f f f f

```

5.2. MATLAB Code: Robie Street Campaign Individual Spectra and Time

Series

The following code was written by Dr. Li Li and outputs spectra and a concentration time series for each measurement block.

```
% run_malt_robie.m
% Li Li
% 2015-08-18
% Saint Mary's University

% =====

clc;
clear;
close all;
tic;
% for Robie 2 hours data

% *****
% raw data:
data_directory='C:\Transporter\Students\TRSL_Julia\Julia_Thesis_Work\2015_05_15_Robie\2015_05_15_17_10_02_240_960_2_hours\';

% read Pressure and temperature from PT_log file
pt_file='(2015_05_15_17_10_02_963)_240_960_progression_PT_Log.txt';
opus_result_file='(2015_05_15_17_10_02_963)_240_960_progression_ResultSeries.txt';

spec_file='(2015_05_15_17_10_02_963)_240_960_progression.prn'; % prn file, for all
spectra exported by OPUS-RS
dir_s=dir(data_directory);

molecule='CO';

malt_folder='MALT';
location_1='Robie';

mkdir(['C:\FTIR_data\Retrieved_C\' location_1 \' molecule \'Final_result\'])
% *****
% replace the PT_log file by the weather data on Weather Underground
% website
% load_weather_data(data_directory,pt_file,'C:\FTIR_data\weather\','20150813.csv');
```

```

% *****

pt_data=dlmread([data_directory pt_file],',',0,2); % p;t, 2*62

% set parameter
para=struct();

para.directory='C:\Malt5\FTS\'; % default: 'C:\malt5\demo\MaltStuff_'
para.output_file='output_file'; % name of .HKP file
para.output_folder=para.directory; % folder of retrieved results, default folder
para.filename=[para.directory 'malt_para']; % prm file

para.iter_n=50;

% target gas and interfering gases
[para.component_n,para.component_matrix]=malt_component(molecule);

para.path_length=343.70; % in meter

para.Poly_terms='2    1.0    0.0    0.0    0.0';

para.resolution=0.5; % cm-1
para.apdz=2; % 0=None, 1=Boxcar, 2=Triangle, 3=Hamming, 4=NB-wk, 5=NB-med,
6=NB-strong, 7=Blackmann Harris, 8=Cosine

para.fov=21.5;
para.fov_tf='f'; % "t" for fitting, "f" for fixed
% *****

% create folder of MALT

% find if MALT folder has existed
sss=1;
ss_name=0;
for sss=1:length(dir_s)
    if dir_s(sss).name(1)=='M' && dir_s(sss).isdir==1
        ss_name=1;
        sss=length(dir_s);
    else
        sss=sss+1;
    end;
end;

% create a new folder of MALT
if ss_name==0
    mkdir([data_directory malt_folder])
end;

```

```

% *****
% create folder for molecule

dir_m=dir([data_directory malt_folder '\']);
mmm=1;
mm_name=0;
for mmm=1:length(dir_m)
    if length(dir_m(mmm).name)==length(molecule) % except CO
        lll= dir_m(mmm).name == molecule ;
        if sum(lll)==length(molecule)
            mm_name=1;
            mmm=length(dir_m);
        else
            mmm=mmm+1;
        end;
    end;
end;
if mm_name==0
    mkdir([data_directory malt_folder '\ molecule']) % for molecule
    mkdir([data_directory malt_folder '\ molecule \SPC']) % spc files
    mkdir([data_directory malt_folder '\ molecule \OUT']) % output_file
    mkdir([data_directory malt_folder '\ molecule \FIT']) % last_fit
    mkdir([data_directory malt_folder '\ molecule \Result']) % last_result
    mkdir([data_directory malt_folder '\ molecule \Plot']) % plot of last_result
end;

molecule_folder=[data_directory malt_folder '\ molecule \SPC\'];

% *****
% load the prn file
% all spectra

all_spec=dlmread([data_directory spec_file]); % 63 x 32764

wavenumber = all_spec(1,:);

size_all=size(all_spec);

nnn=2;
s_n=size_all(1); % number of spectra

% *****

% create spc file

for nnn=2:s_n

```

```

output_spc_file=[molecule '_' num2str(nnn-1)]; % name of spc file
spec_data=[wavenumber;all_spec(nnn,:)];
output_data_spc=writespc_all(spec_data,[molecule_folder output_spc_file],molecule);

para.input_file=[molecule_folder output_spc_file]; % spc file
para.v_low=output_data_spc(1,1); % low limit of wavenumber
para.v_high=output_data_spc(end,1); % high limit of wavenumber

para.pressure=pt_data(nnn-1,1); % in mbar
para.temp=pt_data(nnn-1,2); % in degC

% *****
% create prm file
gen_prm(para);
% *****

% record the process from command window of MATLAB
diary([data_directory malt_folder '\' molecule '\MALT_Log.txt'])

% *****
% run MALT5
!malt5 c:\malt5\fts\malt_para
% *****

% copy files
copyfile([para.directory 'Last_fit.txt'],[data_directory malt_folder '\' molecule
\FIT\Fit_' output_spc_file '.txt'])
copyfile([para.directory 'Last_result.txt'],[data_directory malt_folder '\' molecule
\Result\Result_' output_spc_file '.txt'])
copyfile([para.directory 'Output_file.hkp'],[data_directory malt_folder '\' molecule
\OUT\Out_' output_spc_file '.hkp'])

% *****
% plot
output_spc_file1=strrep(output_spc_file,'_','-');
malt_plot_f([data_directory malt_folder '\' molecule '\FIT\Fit_' output_spc_file
.txt'],output_spc_file1)
% print the plot as a figure or tif
% print(gcf,'-dtiff',[data_directory malt_folder '\' molecule '\plot\' output_spc_file '.tif'])
% tif
saveas(gcf,[data_directory malt_folder '\' molecule '\plot\' output_spc_file '.fig']) %
MATLAB figure
% *****

nnn=nnn+1;
end;

```

```
% delete files after all retrievals done to avoid the wrong files copy
delete([para.directory 'Last_fit.txt'])
delete([para.directory 'Last_result.txt'])
delete([para.directory 'Output_file.hkp'])

% *****
% compare MALT5 results and OPUS-RS results
collect_malt_result(data_directory, malt_folder, molecule, opus_result_file)
% *****

% *****
% Recode complete
diary('off')
% *****

toc;
% end
```

5.3. MATLAB Code: Rice Campaign Individual Spectra and Time Series

The following code was written by Dr. Li Li and outputs spectra and a concentration time series for each measurement block.

```
% run_malt_rice_all.m
% Li Li
% 2015-09-18
% Saint Mary's University

% =====

clc;
clear;
close all;
tic;

% for data measured at Rice in August 2015

% *****
% raw data:
data_directory_all='C:\Transporter\Students\TRSL_Julia\Julia_Thesis_Work\2015_08_13
_DiurnalTest_Rice\'; % top directory
molecule='CO';
malt_folder='MALT';
% spec_file='all_spec.prn'; % prn file for all spectra, this name is only
% for data measured at Rice and Li Li's script,
% not for other person as the exported file name is
% different.
location_1='Rice'; % measurement location
mkdir(['C:\FTIR_data\Retrieved_C\' location_1 \' molecule \'Final_result\'])

% *****
path_length=681.7; % in meters
% *****

dir_top=dir(data_directory_all);

ddd=1;
for ddd=1:length(dir_top) % folders, find the right folder of data
    folder_name="";
    file_path_2="";
    general_name="";
```

```

folder_name=dir_top(ddd).name;

if length(folder_name)>11 & dir_top(ddd).isdir %folder_name(end-
9:end)==general_folder_name
    file_path_2=[folder_name '\'];
    dir_path_sub=dir([data_directory_all file_path_2]);

    general_name=dir_path_sub(2).name(1:end-4);

    data_directory=[data_directory_all file_path_2];
    dir_s=dir_path_sub;

    spec_file=[general_name '.prn']; % prn file, compact spectra, input spectrum for
MALT

% -----
    opus_result_file=[general_name '_ResultSeries.txt']; % opus result
    pt_file=[general_name '_PT_Log.txt']; % PT file
% -----

    pt_data=dlmread([data_directory pt_file],',',0,2); % p;t, 2*62

    % set parameter
    para=struct();

    para.directory='C:\Malt5\FTS\'; % default: 'C:\malt5\demo\MaltStuff_'
    para.output_file='output_file'; % name of .HKP file
    para.output_folder=para.directory; % folder of retrieved results, default folder
    para.filename=[para.directory 'malt_para']; % prm file

    para.iter_n=50;

    % target gas and interfering gases
    [para.component_n,para.component_matrix]=malt_component(molecule);

    para.path_length=path_length; % in meter

    para.Poly_terms='2    1.0  0.0  0.0  0.0'; % baseline

    para.resolution=0.5; % cm-1
    para.apdz=2; % 0=None, 1=Boxcar, 2=Triangle, 3=Hamming, 4=NB-wk, 5=NB-
med, 6=NB-strong, 7=Blackmann Harris, 8=Cosine

    para.fov=21.739;
    para.fov_tf='f'; % "t" for fitting, "f" for fixed
    % *****

```



```

% create folder of MALT

% find if MALT folder has existed
sss=1;
ss_name=0;
for sss=1:length(dir_s)
    if dir_s(sss).name(1)=='M' && dir_s(sss).isdir==1
        ss_name=1;
        sss=length(dir_s);
    else
        sss=sss+1;
    end;
end;

% create a new folder of MALT
if ss_name==0
    mkdir([data_directory malt_folder])
end;

% *****
% create folder for molecule

dir_m=dir([data_directory malt_folder '\']);
mmm=1;
mm_name=0;
for mmm=1:length(dir_m)
    if length(dir_m(mmm).name)==length(molecule) % except CO
        lll= dir_m(mmm).name == molecule ;
        if sum(lll)==length(molecule)
            mm_name=1;
            mmm=length(dir_m);
        else
            mmm=mmm+1;
        end;
    end;
end;

if mm_name==0
    mkdir([data_directory malt_folder '\ molecule]) % for molecule
    mkdir([data_directory malt_folder '\ molecule \SPC']) % spc files
    mkdir([data_directory malt_folder '\ molecule \OUT']) % output_file
    mkdir([data_directory malt_folder '\ molecule \FIT']) % last_fit
    mkdir([data_directory malt_folder '\ molecule \Result']) % last_result
    mkdir([data_directory malt_folder '\ molecule \Plot']) % plot of last_result
end;

molecule_folder=[data_directory malt_folder '\ molecule \SPC\'];

```

```

% *****
% load the prn file
% all spectra

all_spec=dlmread([data_directory spec_file]); % 63 x 32764

wavenumber = all_spec(1,:);

size_all=size(all_spec);

nnn=2;
s_n=size_all(1); % number of spectra

% *****

% create spc file

for nnn=2:s_n
    output_spc_file=[molecule '_' num2str(nnn-1)]; % name of spc file
    spec_data=[wavenumber;all_spec(nnn,:)];
    output_data_spc=writespc_all(spec_data,[molecule_folder
output_spc_file],molecule);

    para.input_file=[molecule_folder output_spc_file]; % spc file
    para.v_low=output_data_spc(1,1); % low limit of wavenumber
    para.v_high=output_data_spc(end,1); % high limit of wavenumber

    para.pressure=pt_data(nnn-1,1); % in mbar
    para.temp=pt_data(nnn-1,2); % in degC

% *****
% create prn file
gen_prm(para);
% *****

% record the process from command window of MATLAB
diary([data_directory malt_folder '\' molecule '\MALT_Log.txt'])

% *****
% run MALT5
!malt5 c:\malt5\fts\malt_para
% *****

% copy files
copyfile([para.directory 'Last_fit.txt'],[data_directory malt_folder '\' molecule
\FIT\Fit_' output_spc_file '.txt'])

```

```

        copyfile([para.directory 'Last_result.txt'],[data_directory malt_folder '\' molecule
'\Result\Result_' output_spc_file '.txt'])
        copyfile([para.directory 'Output_file.hkp'],[data_directory malt_folder '\' molecule
'\OUT\Out_' output_spc_file '.hkp'])

        % *****
        % plot
        output_spc_file1=strrep(output_spc_file,'_','_-');
        malt_plot_f([data_directory malt_folder '\' molecule '\FIT\Fit_' output_spc_file
'.txt'],output_spc_file1)
        % print the plot as a tif graph or a MATLAB figure
        % print(gcf,'-dtiff',[data_directory malt_folder '\' molecule '\plot\' output_spc_file
'.tif']) % tif file
        saveas(gcf,[data_directory malt_folder '\' molecule '\plot\' output_spc_file '.fig'])
% MATLAB figure
        % *****

        nnn=nnn+1;
end;

% delete files after all retrievals done to avoid the wrong files copy
delete([para.directory 'Last_fit.txt'])
delete([para.directory 'Last_result.txt'])
delete([para.directory 'Output_file.hkp'])

% *****
% collect MALT5 results and OPUS-RS time series
collect_malt_result(data_directory, malt_folder, molecule, opus_result_file)
molecule_file=molecule;
[molecule_real,molecule_opusrs,malt_coef]=molecule_opus(molecule_file);
% copy retrieved concentration to another folder
copyfile([data_directory malt_folder '\MALT_result_' molecule_opusrs '.txt'],...
        ['C:\FTIR_data\Retrieved_C\' location_1 '\' molecule_file '\Final_result\'
folder_name '.txt'])
        end; % end if
        ddd=ddd+1;
end; % end for loop
% *****
% Recode complete
diary('off')
% *****

toc;
% end

```

5.4. MATLAB Code: Rice Campaign Combined Time Series

The following code was written by Dr. Li Li and combines the multiple concentration time series plots, produced from the previous code, into one plot.

```
% read_rice_all.m
% by Li Li
% Saint Mary's University
% 2015.09.03
% modified on 2015-11-13

clear;
close all;
clc;
tic;

format long;

all_folder='C:\Transporter\Students\TRSL_Julia\Julia_Thesis_Work\Retrieved_C\Rice\';
% change to local directory
date_start='2015_08_13';
date_end='2015_08_20';

date_n1=datenum(date_start);
date_n2=datenum(date_end);

molecule='CO';
malt_folder='Final_result';
PT_folder='PT';

% ===== Select plot with PT or RMS here =====
% plot_selection='PT'; % remove the % to plot with PT
plot_selection='RMS'; % add a % to undo plotting with RMS
% =====

font_size=14; % can set the font size here, more means larger font
scrsz = get(0,'ScreenSize');
shift_size=50;
figure('Position',[1+shift_size scrsz(2)+shift_size scrsz(3)-2*shift_size scrsz(4)-
3*shift_size])
```

```

folder_data=[all_folder molecule '\' malt_folder '\'];
dir_all=dir(folder_data);

time_s=[];
concentration=[];
temperature=[];
pressure=[];
rms_all=[];

nnn=1;
for nnn=1:length(dir_all)
    time_1=[];
    conc_1=[];
    pressure_1=[];
    temp_1=[];
    data_1=[];
    data_2=[];
    rms_1=[];

    if length(dir_all(nnn).name)>=10 & ~dir_all(nnn).isdir

        % read MALT result for gas
        data_1=dlmread([folder_data dir_all(nnn).name],',');
        time_1=data_1(:,1);
        conc_1=data_1(:,2);
        rms_1=data_1(:,3);

        % read PT
        folder_data2=[all_folder PT_folder '\'];
        data_2=dlmread([folder_data2 dir_all(nnn).name],',');
        pressure_1=data_2(:,2);
        temp_1=data_2(:,3);

    end;

    time_s=[time_s;time_1];
    concentration=[concentration;conc_1];
    rms_all=[rms_all;rms_1];
    temperature=[temperature;temp_1];
    pressure=[pressure;pressure_1];

    nnn=nnn+1;
end;

```

```

xx_tick=linspace(date_n1,date_n2+1,date_n2+2-date_n1);

subplot(3,1,[1:2])
plot(time_s,concentration,'r.')
ylabel('Concentration (ppm)',font_size)
set(gca,'font_size',font_size)
set(gca,'XTick',xx_tick)
datetick('x','mm/dd HH:MM','kepticks')
grid;
title(['CO concentration at Rice by MALT all time'],'font_size',font_size+2)
ylim([0.1 0.3])

switch plot_selection
case 'PT'
    subplot(3,1,3)
    [AX,H1,H2]=plotyy(time_s,temperature,time_s,presure);
    set(get(AX(1),'Ylabel'),'String','T (^oC)','font_size',font_size,'color','m')
    set(get(AX(2),'Ylabel'),'String','P (hPa)','font_size',font_size,'color','c')
    set(H1,'linestyle','.', 'color','m')
    set(H2,'linestyle','.', 'color','c')
    set(AX(1),'font_size',font_size,'Ycolor','m')
    set(AX(2),'font_size',font_size,'Ycolor','c')
    set(AX(1),'XTick',xx_tick)
    set(AX(2),'XTick',xx_tick)
    datetick(AX(1),'x','mm/dd HH:MM','kepticks')
    datetick(AX(2),'x','mm/dd HH:MM','kepticks')
    xlabel('Time series (month/day hour:min)','font_size',font_size)
    grid;
case 'RMS'
    subplot(3,1,3)
    plot(time_s,rms_all,'b.')
    ylabel('RMS','font_size',font_size)
    xlabel('Time series (month/day hour:min)','font_size',font_size)
    set(gca,'font_size',font_size)
    set(gca,'XTick',xx_tick)
    datetick('x','mm/dd HH:MM','kepticks')
    grid;
end;

saveas(gcf,['C:\FTIR_data\Retrieved_C\Rice\' molecule '\ molecule '_Rice_all_'
plot_selection '.fig'])

toc;

```

5.5. MATLAB Code: Lake Major Campaign Individual Spectra and Time

Series

The following code was written by Dr. Li Li and outputs spectra and a concentration time series for each measurement block.

```
% run_malt_lake_major.m
% Li Li
% 2015-09-18
% Saint Mary's University

% =====

clc;
clear;
close all;
tic;

% *****
% raw data:
data_directory_all='C:\Transporter\Students\TRSL_Julia\Julia_Thesis_Work\2015_09_La
ke_Major\'; % top directory
molecule='CO';
malt_folder='MALT';
general_folder_name='Lake_Major';

location_1='Lake_Major'; % measurement location
mkdir(['C:\FTIR_data\Retrieved_C\' location_1 \' \' molecule \'Final_result\'])
% *****
path_length=317.7; % in meters
% *****

dir_top=dir(data_directory_all);

ddd=1;
for ddd=1:length(dir_top) % folders, find the right folder of data
    folder_name='';
    file_path_2='';
    general_name='';
```

```

folder_name=dir_top(ddd).name;

if length(folder_name)>11 & folder_name(end-9:end)==general_folder_name
    file_path_2=[folder_name '\'];
    dir_path_sub=dir([data_directory_all file_path_2]);

    general_name=dir_path_sub(2).name(1:end-4);

    data_directory=[data_directory_all file_path_2];
    dir_s=dir_path_sub;

    spec_file=[general_name '.prn']; % prn file
    opus_result_file=[general_name '_ResultSeries.txt']; % opus result
    pt_file=[general_name '_PT_Log.txt']; % PT file

    pt_data=dlmread([data_directory pt_file],',',0,2); % p;t, 2*62

    % set parameter
    para=struct();

    para.directory='C:\Malt5\FTS\'; % default: 'C:\malt5\demo\MaltStuff_'
    para.output_file='output_file'; % name of .HKP file
    para.output_folder=para.directory; % folder of retrieved results, default folder
    para.filename=[para.directory 'malt_para']; % prm file

    para.iter_n=50;

    % target gas and interfering gases
    [para.component_n,para.component_matrix]=malt_component(molecule);

    para.path_length=path_length; % in meter

    para.Poly_terms='2    1.0  0.0  0.0  0.0'; % baseline

    para.resolution=0.5; % cm-1
    para.apdz=2; % 0=None, 1=Boxcar, 2=Triangle, 3=Hamming, 4=NB-wk, 5=NB-med,
6=NB-strong, 7=Blackmann Harris, 8=Cosine

    para.fov=21.739;
    para.fov_tf='f'; % "t" for fitting, "f" for fixed
    % *****

    % create folder of MALT

```



```

% find if MALT folder has existed
sss=1;
ss_name=0;
for sss=1:length(dir_s)
    if dir_s(sss).name(1)=='M' && dir_s(sss).isdir==1
        ss_name=1;
        sss=length(dir_s);
    else
        sss=sss+1;
    end;
end;

% create a new folder of MALT
if ss_name==0
    mkdir([data_directory malt_folder])
end;

% *****
% create folder for molecule

dir_m=dir([data_directory malt_folder '\']);
mmm=1;
mm_name=0;
for mmm=1:length(dir_m)
    if length(dir_m(mmm).name)==length(molecule) % except CO
        lll= dir_m(mmm).name == molecule ;
        if sum(lll)==length(molecule)
            mm_name=1;
            mmm=length(dir_m);
        else
            mmm=mmm+1;
        end;
    end;
end;
if mm_name==0
    mkdir([data_directory malt_folder '\ molecule]) % for molecule
    mkdir([data_directory malt_folder '\ molecule '\SPC']) % spc files
    mkdir([data_directory malt_folder '\ molecule '\OUT']) % output_file
    mkdir([data_directory malt_folder '\ molecule '\FIT']) % last_fit
    mkdir([data_directory malt_folder '\ molecule '\Result']) % last_result
    mkdir([data_directory malt_folder '\ molecule '\Plot']) % plot of last_result
end;

molecule_folder=[data_directory malt_folder '\ molecule '\SPC\'];

```

```

% *****
% load the prn file
% all spectra

all_spec=dlmread([data_directory spec_file]); % 63 x 32764

wavenumber = all_spec(1,:);

size_all=size(all_spec);

nnn=2;
s_n=size_all(1); % number of spectra

% *****

% create spc file

for nnn=2:s_n
    output_spc_file=[molecule '_' num2str(nnn-1)]; % name of spc file
    spec_data=[wavenumber;all_spec(nnn,:)];
    output_data_spc=writespc_all(spec_data,[molecule_folder
output_spc_file],molecule);

    para.input_file=[molecule_folder output_spc_file]; % spc file
    para.v_low=output_data_spc(1,1); % low limit of wavenumber
    para.v_high=output_data_spc(end,1); % high limit of wavenumber

    para.pressure=pt_data(nnn-1,1); % in mbar
    para.temp=pt_data(nnn-1,2); % in degC

% *****
% create prm file
gen_prm(para);
% *****

% record the process from command window of MATLAB
diary([data_directory malt_folder '\' molecule '\MALT_Log.txt'])

% *****
% run MALT5
!malt5 c:\malt5\fts\malt_para
% *****

```

```

% copy files
copyfile([para.directory 'Last_fit.txt'],[data_directory malt_folder '\ molecule
\FIT\Fit_' output_spc_file '.txt'])
copyfile([para.directory 'Last_result.txt'],[data_directory malt_folder '\ molecule
\Result\Result_' output_spc_file '.txt'])
copyfile([para.directory 'Output_file.hkp'],[data_directory malt_folder '\
molecule \OUT\Out_' output_spc_file '.hkp'])
% *****
% plot
output_spc_file1=strrep(output_spc_file,'_','_-');
malt_plot_f([data_directory malt_folder '\ molecule \FIT\Fit_' output_spc_file
.txt'],output_spc_file1)
% print the plot
% print(gcf,'-dtiff',[data_directory malt_folder '\ molecule \plot\' output_spc_file
.tif']) % tif
saveas(gcf,[data_directory malt_folder '\ molecule \plot\' output_spc_file '.fig'])
% MATLAB figure
% *****
nnn=nnn+1;
end;

% delete files after all retrievals done to avoid the wrong files copy
delete([para.directory 'Last_fit.txt'])
delete([para.directory 'Last_result.txt'])
delete([para.directory 'Output_file.hkp'])
% *****
% compare MALT5 results and OPUS-RS results
collect_malt_result(data_directory, malt_folder, molecule, opus_result_file)
molecule_file=molecule;
[molecule_real,molecule_opusrs,malt_coef]=molecule_opus(molecule_file);
% copy retrieved concentration to another folder
copyfile([data_directory malt_folder '\MALT_result_' molecule_opusrs '.txt'],...
[C:\FTIR_data\Retrieved_C\Lake_Major\' molecule_file '\Final_result\'
folder_name '.txt'])
end; % end if
ddd=ddd+1;
end; % end for loop
% *****
% Recode complete
diary('off')
% *****

toc;
% end

```

5.6. MATLAB Code: Lake Major Campaign Combined Time Series

The following code was written by Dr. Li Li and combines the multiple concentration time series plots, produced from the previous code, into one plot.

```
% read_lake_major_all.m
% by Li Li
% Saint Mary's University
% 2015.09.23
% modified on 2015-11-13

clear;
close all;
clc;
tic;

format long;

molecule_all={'CO'}; % can add other gas here
malt_folder='Malt';
font_size=10;
mmm=1;
for mmm=1:length(molecule_all)
    molecule=molecule_all{mmm};

    [molecule_real,molecule_opusrs,malt_coef]=molecule_opus(molecule);
    malt_result_file=['MALT_result_' molecule_opusrs '.txt'];
    molecule_opusrs1=strrep(molecule_opusrs,' ','-');
% =====

all_folder='C:\Transporter\Students\TRSL_Julia\Julia_Thesis_Work\2015_09_Lake_Major\'; % change your measurement folder here
% =====
    folder_name='Lake_Major';
    dir_all=dir(all_folder);

    time_s=[];
    concentration=[];
    concentration_opus=[];
    temperature=[];
    pressure=[];
```

```

conc_humi_water=[];

nnn=1;
for nnn=1:length(dir_all)
    file_folder="";
    time_1=[];
    conc_1=[];
    mole_conc_rs=[];
    temp_1=[];
    pressure_1=[];
    conc_humi_1=[];

    if length(dir_all(nnn).name)>=10 & dir_all(nnn).isdir & dir_all(nnn).name(end-
9:end)==folder_name % not '.' and '..'
        file_folder=[all_folder dir_all(nnn).name '\'];

        dir_path_sub=dir(file_folder);
        general_name=dir_path_sub(2).name(1:end-4);

        rs_result_file=[general_name '_ResultSeries.txt']; % opus result
        pt_file=[general_name '_PT_Log.txt']; % PT file

        % read MALT result
        data_1=dlmread([file_folder malt_folder '\' malt_result_file],',');
        time_1=data_1(:,1);
        conc_1=data_1(:,2);
        l_c(nnn)=length(conc_1);

        % read PT data
        pt_data=dlmread([file_folder pt_file],',',0,2);
        temp_1=pt_data(:,2);
        pressure_1=pt_data(:,1);
        l_t(nnn)=length(temp_1);

    end;
    time_s=[time_s;time_1];
    concentration=[concentration;conc_1];

    temperature=[temperature;temp_1];
    pressure=[pressure;pressure_1];

    nnn=nnn+1;
end;

```

```

concentration_final=concentration;
molecule_display=molecule_opusrs;

subplot(3,1,[1:2])
plot(time_s,concentration_final,'r.','linewidth',2)
ylabel('Concentration (ppm)','fontsize',font_size)
title([strrep(molecule_display,' ','-') ' Lake Major by MALT'],'fontsize',font_size+2)
set(gca,'fontsize',font_size)
datetick('x','mm/dd HH:MM','kepticks')
grid;

subplot(3,1,3)
[AX,H1,H2]=plotyy(time_s,temperature,time_s,pressure);
set(get(AX(1),'Ylabel'),'String','T(^oC)','fontsize',font_size)
set(get(AX(2),'Ylabel'),'String','P(hPa)','fontsize',font_size)
set(H1,'Marker','.','linestyle','none')
set(H2,'Marker','.','linestyle','none')
set(AX(1),'fontsize',font_size)
set(AX(2),'fontsize',font_size)
datetick(AX(1),'x','mm/dd HH:MM','kepticks')
datetick(AX(2),'x','mm/dd HH:MM','kepticks')
xlabel('Time series (month/day hour:min)','fontsize',font_size)
grid;

% print(gcf,'-dtiff',['C:\FTIR_data\Retrieved_C\Lake_Major\' molecule \' molecule_real
'_MALT_Lake_Major.tif'])
saveas(gcf,['C:\FTIR_data\Retrieved_C\Lake_Major\' molecule \' molecule_real
'_MALT_Lake_Major_all.fig'])

mmm=mmm+1;
end; % end for
toc;

```

5.7. MATLAB Code: Generation of Maximum Residual Time Series

The following code was written by Dr. Li Li and identifies and retrieves the maximum residual value from each generated spectrum in a campaign. This code includes all residuals in the full CO spectral window.

```
% malt_residual_plot_for_Julia
% 2016/03/08
% by Li Li
% TRSL, SMU

% this program plots the output data of MALT 5.5.8
% format of the fit file of MALT:
% line 1: description of every column
% column 1: wavenumber
% column 2: measured spectrum
% column 3: fitted spectrum
% column 4: residual spectrum
% column 5-end: spectral of selected gas
%

clear;
close all;
clc;
tic;

file_name_head='Fit_CO_';
length_head=length(file_name_head);
molecule='CO';

% ===== Robie Street =====
top_folder='C:\Users\s5938780\Transporter\TRSL_Julia\Julia_Thesis_Work\2015_05_15
_Robie\2015_05_15_17_10_02_240_960_2_hours\MALT\';
sub_folder='CO\FIT\';
location_1='Robie Street';
folder_name=[top_folder sub_folder];
dir_all=dir(folder_name);
rrr=1;
mmm=1;
max_res=[];
```

```

% max residual
for rrr=1:length(dir_all)
    file_name="";
    data_out=[];
    residual_data=[];

    if ~dir_all(rrr).isdir
        file_name=dir_all(rrr).name;
        data_out=dlmread([folder_name file_name],",",1,0);
        residual_data=data_out(:,4);
        [max_v,max_i]=max(abs(residual_data));
        max_res(mmm)=residual_data(max_i);
        mmm=mmm+1;
        rrr=rrr+1;
    else
        rrr=rrr+1;
    end;
end;
% time series
data_directory=top_folder;
result_file='MALT_result_CO.txt';
result_all=dlmread([data_directory result_file]);
time_num=result_all(:,1);
% *****
% plot
xx_tick=linspace(time_num(1),time_num(end),7);
day_1=datestr(time_num(1),'yyyy/mm/dd');
plot(time_num,max_res,'b-o','linewidth',2,'markerface','b');
ylabel('Max residual','fontsize',14)
set(gca,'XTick',xx_tick)
datetick('x',15,'kepticks')
xlabel('Time series','fontsize',14)
xlim([time_num(1) time_num(end)])
set(gca,'fontsize',14)
title([molecule ' ' location_1 ' ' day_1],'fontsize',14)
grid;
saveas(gcf,['C:\Users\s5938780\Transporter\TRSL_Share\To Julia\' molecule
'_max_residual_' strrep(location_1,' ','_') '.fig'])

% ===== Rice =====
top_folder='C:\Users\s5938780\Transporter\TRSL_Julia\Julia_Thesis_Work\2015_08_13
_DiurnalTest_Rice\';
malt_folder='MALT\';
sub_folder='CO\FIT\';

```



```

location_1='Rice';
dir_all_folder=[];
dir_all_folder=dir(top_folder);
ddd=1;
rrr=1;
mmm=1;
time_num_all=[];
max_res_all=[];
for ddd=1:length(dir_all_folder);
    if length(dir_all_folder(ddd).name)>10
        measurement_folder=dir_all_folder(ddd).name;
        folder_name=[top_folder measurement_folder '\' malt_folder sub_folder];
        dir_all=[];
        dir_all=dir(folder_name);
        rrr=1;
        mmm=1;
        max_res=[];
        time_num=[];
        % max residual
        for rrr=1:length(dir_all)
            file_name="";
            data_out=[];
            residual_data=[];

            if ~dir_all(rrr).isdir
                file_name=dir_all(rrr).name;
                data_out=dlmread([folder_name file_name],",",1,0);
                residual_data=data_out(:,4);
                [max_v,max_i]=max(abs(residual_data));
                max_res(mmm,1)=residual_data(max_i);
                mmm=mmm+1;
                rrr=rrr+1;
            else
                rrr=rrr+1;
            end;
        end;
    end;
    % time series
    data_directory=[top_folder measurement_folder '\' malt_folder];
    result_file='MALT_result_CO.txt';
    result_all=dlmread([data_directory result_file]);
    time_num=result_all(:,1);

    max_res_all=[max_res_all;max_res];
    time_num_all=[time_num_all;time_num];

```

```

end;
ddd=ddd+1;
end;

% *****
% plot
xx_tick=linspace(floor(time_num_all(1)),ceil(time_num_all(end)),9);
day_1=datestr(time_num_all(1),'yyy/mm');
plot(time_num_all,max_res_all,'b.')
ylabel('Max residual','fontsize',14)
set(gca,'XTick',xx_tick)
datetick('x','mm/dd','keepticks')
xlabel('Time series','fontsize',14)
xlim([floor(time_num_all(1)) ceil(time_num_all(end))])
set(gca,'fontsize',14)
title([molecule ' ' location_1 ' ' day_1],'fontsize',14)
grid;
saveas(gcf,['C:\Users\s5938780\Transporter\TRSL_Share\To Julia\' molecule
'_max_residual_' location_1 '.fig'])

% ===== Lake Major =====
top_folder='C:\Users\s5938780\Transporter\TRSL_Julia\Julia_Thesis_Work\2015_09_La
ke_Major\';
malt_folder='MALT\';
sub_folder='CO\FIT\';
location_1='Lake Major';
dir_all_folder=[];
dir_all_folder=dir(top_folder);
ddd=1;
rrr=1;
mmm=1;
time_num_all=[];
max_res_all=[];
for ddd=1:length(dir_all_folder);
    if length(dir_all_folder(ddd).name)>10
        measurement_folder=dir_all_folder(ddd).name;
        folder_name=[top_folder measurement_folder '\ ' malt_folder sub_folder];
        dir_all=[];
        dir_all=dir(folder_name);
        rrr=1;
        mmm=1;
        max_res=[];
        time_num=[];
        % max residual

```

```

for rrr=1:length(dir_all)
    file_name="";
    data_out=[];
    residual_data=[];

    if ~dir_all(rrr).isdir
        file_name=dir_all(rrr).name;
        data_out=dlmread([folder_name file_name],",",1,0);
        residual_data=data_out(:,4);
        [max_v,max_i]=max(abs(residual_data));
        max_res(mmm,1)=residual_data(max_i);
        mmm=mmm+1;
        rrr=rrr+1;
    else
        rrr=rrr+1;
    end;
end;
% time series
data_directory=[top_folder measurement_folder '\ malt_folder];
result_file='MALT_result_CO.txt';
result_all=dlmread([data_directory result_file]);
time_num=result_all(:,1);
max_res_all=[max_res_all;max_res];
time_num_all=[time_num_all;time_num];
end;
ddd=ddd+1;
end;
% *****
% plot
xx_tick=linspace(floor(time_num_all(1)),ceil(time_num_all(end)),8);
day_1=datestr(time_num_all(1),'yyyy/mm');
plot(time_num_all,max_res_all,'b.')
ylabel('Max residual','fontsize',14)
set(gca,'XTick',xx_tick)
datetick('x','mm/dd','kepticks')
xlabel('Time series','fontsize',14)
xlim([floor(time_num_all(1)) ceil(time_num_all(end))])
set(gca,'fontsize',14)
title([molecule ' ' location_1 ' ' day_1],'fontsize',14)
grid;
saveas(gcf,['C:\Users\s5938780\Transporter\TRSL_Share\To Julia\' molecule
'_max_residual_' strrep(location_1,' ','_') '.fig'])

toc;

```

The following code was written by Dr. Li Li and identifies and retrieves the maximum residual value from each generated spectrum in a campaign. This code includes residuals only from the CO spectral window of 2075-2080 cm^{-1} .

```
% malt_residual_narrow_plot_for_Julia
% 2016/03/08
% by Li Li
% TRSL, SMU

% this program plots the output data of MALT 5.5.8
% format of the fit file of MALT:
% line 1: description of every column
% column 1: wavenumber
% column 2: measured spectrum
% column 3: fitted spectrum
% column 4: residual spectrum
% column 5-end: spectral of selected gas
%

clear;
close all;
clc;
tic;

file_name_head='Fit_CO_';
length_head=length(file_name_head);
molecule='CO';
narrow_window=[2075 2080];
folder1='C:\Users\s5938780\Transporter\TRSL_Julia\Julia_Thesis_Work\2015_05_15_R
obie\2015_05_15_17_10_02_240_960_2_hours\MALT\CO\FIT\';
example_file='Fit_CO_1.txt';
example_data=dlmread([folder1 example_file],',',1,0);
wavenumber=example_data(:,1);
[low1 low_i]=min(abs(wavenumber-narrow_window(1)));
[up1 up_i]=min(abs(wavenumber-narrow_window(2)));

% ===== Robie Street =====
top_folder='C:\Users\s5938780\Transporter\TRSL_Julia\Julia_Thesis_Work\2015_05_15
_Robie\2015_05_15_17_10_02_240_960_2_hours\MALT\';
sub_folder='CO\FIT\';
location_1='Robie Street';
```

```

folder_name=[top_folder sub_folder];
dir_all=dir(folder_name);
rrr=1;
mmm=1;
max_res=[];
% max residual
for rrr=1:length(dir_all)
    file_name="";
    data_out=[];
    residual_data=[];

    if ~dir_all(rrr).isdir
        file_name=dir_all(rrr).name;
        data_out=dlmread([folder_name file_name],",",1,0);
        residual_data=data_out(:,4);
        [max_v,max_i]=max(abs(residual_data(low_i:up_i)));
        max_res(mmm)=residual_data(max_i+low_i-1);
        mmm=mmm+1;
        rrr=rrr+1;
    else
        rrr=rrr+1;
    end;
end;
% time series
data_directory=top_folder;
result_file='MALT_result_CO.txt';
result_all=dlmread([data_directory result_file]);
time_num=result_all(:,1);
% *****
% plot
xx_tick=linspace(time_num(1),time_num(end),7);
day_1=datestr(time_num(1),'yyyy/mm/dd');

plot(time_num,max_res,'b-o','linewidth',2,'markerface','b');
ylabel('Max residual','fontsize',14)
set(gca,'XTick',xx_tick)
datetick('x',15,'kepticks')
xlabel('Time series','fontsize',14)
xlim([time_num(1) time_num(end)])
set(gca,'fontsize',14)
title([molecule ' ' location_1 ' ' day_1],'fontsize',14)
grid;
saveas(gcf,['C:\Users\s5938780\Transporter\TRSL_Share\To Julia\' molecule
'_max_residual_' strrep(location_1,' ','_') '_narrow.fig'])

```

```

% ===== Rice =====
top_folder='C:\Users\s5938780\Transporter\TRSL_Julia\Julia_Thesis_Work\2015_08_13
_DiurnalTest_Rice\';
malt_folder='MALT\';
sub_folder='CO\FIT\';
location_1='Rice';
dir_all_folder=[];
dir_all_folder=dir(top_folder);
ddd=1;
rrr=1;
mmm=1;
time_num_all=[];
max_res_all=[];
for ddd=1:length(dir_all_folder);
    if length(dir_all_folder(ddd).name)>10
        measurement_folder=dir_all_folder(ddd).name;
        folder_name=[top_folder measurement_folder '\ ' malt_folder sub_folder];
        dir_all=[];
        dir_all=dir(folder_name);
        rrr=1;
        mmm=1;
        max_res=[];
        time_num=[];
        % max residual
        for rrr=1:length(dir_all)
            file_name='';
            data_out=[];
            residual_data=[];

            if ~dir_all(rrr).isdir
                file_name=dir_all(rrr).name;
                data_out=dlmread([folder_name file_name],",",1,0);
                residual_data=data_out(:,4);
                [max_v,max_i]=max(abs(residual_data(low_i:up_i)));
                max_res(mmm,1)=residual_data(max_i+low_i-1);
                mmm=mmm+1;
                rrr=rrr+1;
            else
                rrr=rrr+1;
            end;
        end;
    end;
end;
% time series

```

```

data_directory=[top_folder measurement_folder '\' malt_folder];
result_file='MALT_result_CO.txt';
result_all=dlmread([data_directory result_file]);
time_num=result_all(:,1);

max_res_all=[max_res_all;max_res];
time_num_all=[time_num_all;time_num];
end;
ddd=ddd+1;
end;

% *****
% plot
xx_tick=linspace(floor(time_num_all(1)),ceil(time_num_all(end)),9);
day_1=datestr(time_num_all(1),'yyyy/mm');
plot(time_num_all,max_res_all,'b.')
ylabel('Max residual','fontsize',14)
set(gca,'XTick',xx_tick)
datetick('x','mm/dd','keepticks')
xlabel('Time series','fontsize',14)
xlim([floor(time_num_all(1)) ceil(time_num_all(end))])
set(gca,'fontsize',14)
title([molecule ' ' location_1 ' ' day_1],'fontsize',14)
grid;
saveas(gcf,['C:\Users\s5938780\Transporter\TRSL_Share\To Julia\' molecule
'_max_residual_' location_1 '_narrow.fig'])

% ===== Lake Major =====
top_folder='C:\Users\s5938780\Transporter\TRSL_Julia\Julia_Thesis_Work\2015_09_La
ke_Major\';
malt_folder='MALT\';
sub_folder='CO\FIT\';
location_1='Lake Major';
dir_all_folder=[];
dir_all_folder=dir(top_folder);
ddd=1;
rrr=1;
mmm=1;
time_num_all=[];
max_res_all=[];
for ddd=1:length(dir_all_folder);
    if length(dir_all_folder(ddd).name)>10
        measurement_folder=dir_all_folder(ddd).name;

```

```

folder_name=[top_folder measurement_folder '\' malt_folder sub_folder];
dir_all=[];
dir_all=dir(folder_name);
rrr=1;
mmm=1;
max_res=[];
time_num=[];
% max residual
for rrr=1:length(dir_all)
    file_name='';
    data_out=[];
    residual_data=[];

    if ~dir_all(rrr).isdir
        file_name=dir_all(rrr).name;
        data_out=dlmread([folder_name file_name],",",1,0);
        residual_data=data_out(:,4);
        [max_v,max_i]=max(abs(residual_data(low_i:up_i)));
        max_res(mmm,1)=residual_data(max_i+low_i-1);
        mmm=mmm+1;
        rrr=rrr+1;
    else
        rrr=rrr+1;
    end;
end;
% time series
data_directory=[top_folder measurement_folder '\' malt_folder];
result_file='MALT_result_CO.txt';
result_all=dlmread([data_directory result_file]);
time_num=result_all(:,1);

max_res_all=[max_res_all;max_res];
time_num_all=[time_num_all;time_num];
end;
ddd=ddd+1;
end;

% *****
% plot
xx_tick=linspace(floor(time_num_all(1)),ceil(time_num_all(end)),8);
day_1=datestr(time_num_all(1),'yyyy/mm');
plot(time_num_all,max_res_all,'b.')
ylabel('Max residual','fontsize',14)
set(gca,'XTick',xx_tick)

```



```
datetick('x','mm/dd','keepticks')
xlabel('Time series','fontsize',14)
xlim([floor(time_num_all(1)) ceil(time_num_all(end))])
set(gca,'fontsize',14)
title([molecule ' ' location_1 ' ' day_1],'fontsize',14)
grid;
saveas(gcf,['C:\Users\s5938780\Transporter\TRSL_Share\To Julia\' molecule
'_max_residual_' strrep(location_1,',' '_') '_narrow.fig'])

toc;
```

6 Bibliography

[Untitled image of the electromagnetic spectrum]. Retrieved from <https://experiment.com/u/1whA>

[Untitled image of the troposphere and its planetary boundary layer]. Retrieved from <https://www.shodor.org/os411/courses/411c/module06/unit01/page01.html>

Banwell, C. N., & McCash, E. M. (1994). *Fundamentals of molecular spectroscopy* (4th ed.). Berkshire, England: McGraw-Hill International (UK) Limited.

Bruker Corporation. (2015). *Open path air monitoring system: Operating manual*.

Canadian Council of Ministers of the Environment. (2012). *Guidance document on achievement determination Canadian ambient air quality standards for fine particulate matter and ozone*. Retrieved from http://www.ccme.ca/files/Resources/air/aqms/pn_1483_gdad_eng.pdf

Dentener, F., Kinne, S., Bond, T., Boucher, O., Cofala, J., Generoso, S., ... Wilson, J. (2006). Emissions of primary aerosol and precursor gases in the years 2000 and 1750 prescribed data-sets for AeroCom. *Atmospheric Chemistry and Physics*, 6, 4321-4344. doi:10.5194/acp-6-4321-2006

Environment and Climate Change Canada. (2013). *National Air Pollution Surveillance Program (NAPS)*. Retrieved from <http://www.ec.gc.ca/rnspa-naps/>

Finlayson-Pitts, B. J., & Pitts, J. N., Jr. (2000). *Chemistry of the upper and lower atmosphere*. San Diego, CA: Academic Press.

Gibson, M. D., Guernsey, J. R., Beauchamp, S., Waugh, D., Heal, M. R., Brook, J. R., ...

- Terashima, M. (2009). Quantifying the spatial and temporal variation of ground-level ozone in the rural Annapolis Valley, Nova Scotia, Canada using nitrite-impregnated passive samplers. *Journal of the Air & Waste Management Association*, 59(3), 310-320. doi:10.3155/1047-3289.59.3.310
- Gibson, M. D., Kundu, S., & Satish, M. (2013). Dispersion model evaluation of PM_{2.5}, NO_x and SO₂ from point and major line sources in Nova Scotia, Canada using AERMOD Gaussian plume air dispersion model. *Atmospheric Pollution Research*, 4, 157-167. doi:10.5094/APR.2013.016
- Griffith, D. W. T. (1996). Synthetic calibration and quantitative analysis of gas phase infrared spectra. *Applied Spectroscopy*, 50(1), 59-70.
- Griffith, D. W. T. (2010). *Computational retrieval of trace gas concentrations from FTIR spectra*. Manuscript in preparation.
- Griffiths, P. R., & de Haseth, J. A. (2007). *Fourier transform infrared spectrometry* (2nd ed.). Hoboken, NJ: John Wiley & Sons.
- Harvard-Smithsonian Center for Astrophysics. (2015). The HITRAN database. Retrieved from <https://www.cfa.harvard.edu/hitran/>
- Holloway, A. M., & Wayne, R. P. (2010). *Atmospheric chemistry*. Cambridge, England: The Royal Society of Chemistry.
- Houtman, A., Karr, S., & Interlandi, J. (2013). *Environmental science for a changing world*. New York, NY: W. H. Freeman and Company.
- Jacob, D. J. (1999). *Introduction to atmospheric chemistry*. Princeton, NJ: Princeton University Press.

- Jacobson, M. Z. (2012). *Air pollution and global warming: History, science, and solutions* (2nd ed.). New York, NY: Cambridge University Press.
- Kellogg, W. W., Cadle, R. D., Allen, E. R., Lazrus, A. L., & Martell, E. A. (1972). The sulfur cycle. *Science*, *175*(4022), 587–596. Retrieved from <http://www.jstor.org/stable/1732918>
- Martin, W., Weber, T. P., Meyer, J., von Kegler, S., Van Aken, H., & Booke, M. (2002). Affinity of carbon monoxide to hemoglobin increases at low oxygen fractions. *Biochemical and Biophysical Research Communications*, *295*(4), 975-977. doi:10.1016/S0006-291X(02)00781-7
- Miller, G. T., & Hackett, D. (2014). *Living in the environment* (3rd Canadian ed.). Toronto, Canada: Nelson Education Ltd.
- Millet, D. B., Goldstein, A. H., Holzinger, R., Williams, B. J., Allan, J. D., Jimenez, J. L., ... Stohl, A. (2006). Chemical characteristics of North American surface layer outflow: Insights from Chebogue Point, Nova Scotia. *Journal of Geophysical Research*, *111*(D23). doi:10.1029/2006JD007287
- Nova Scotia Environment, Air Quality Branch. (2009). *The Air We Breathe: Nova Scotia's Air Quality Report, 2000-2007*. Retrieved from <http://www.novascotia.ca/nse/air/docs/TheAirWeBreathe-NS-Air-Quality2000-2007.pdf>
- Nova Scotia Environment, Air Quality Branch. (2010). *Nova Scotia Ambient Air Quality Monitoring Network*. Retrieved from <https://www.novascotia.ca/nse/air/docs/AirMonitoringNetworkMap.pdf>
- Nova Scotia Environment, Air Quality Branch. (2015). *Nova Scotia Air Zone Report:*

Nova Scotia Air Quality Unit, 2014. Retrieved from <https://novascotia.ca/nse/air/docs/15-43405%20AirZone%20V3.pdf>

Patil, M. N., Patil, S. D., Waghmare, R. T., & Dharmaraj, T. (2013). Planetary boundary layer height over the Indian subcontinent during extreme monsoon years. *Journal of Atmospheric and Solar-Terrestrial Physics, 92*, 94-99. doi:10.1016/j.jastp.2012.10.011

PLX Innovative Optical Systems. (n.d.). *Hollow Retroreflector Arrays for modern FTIR long-path spectroscopy.* Retrieved from <http://www.plxinc.com/products/hollow-retroreflector-arrays-hra>

Reyes, M., Díaz, J., Tobias, A., Montero, J. C., & Linares, C. (2014). Impact of Saharan dust particles on hospital admissions in Madrid (Spain). *International Journal of Environmental Health Research, 24*(1), 63-72. doi:10.1080/09603123.2013.782604

Rothman, L. S., Gordon, I. E., Babikov, Y., Barbe, A., Benner, D. C., Bernath, P. F., ... Birk, M. (2013). The HITRAN2012 molecular spectroscopic database. *Journal of Quantitative Spectroscopy & Radiative Transfer, 130*, 4-50. doi:10.1016/j.jqsrt.2013.07.002

Russwurm, G. M. & Childers, J. W. (2002). Open-path Fourier transform infrared spectroscopy. In J. M. Chalmers & P. R. Griffiths (Eds.), *Handbook of vibrational spectroscopy (1750-1773)*. Chichester, England: John Wiley & Sons.

Sharpe, S. W., Johnson, T. J., Sams, R. L., Chu, P. M., Rhoderick, G. C., & Johnson, P. A. (2004). Gas-phase databases for quantitative infrared spectroscopy. *Society*

for Applied Spectroscopy, 58(12), 1452-1461. Retrieved from [https://secure2.pnl.gov/nsd/NSD.nsf/aef8f6faed1a17a6882569970003bbcb/60fb69425bc73ddb8825705100744d85/\\$FILE/DataBase%20Paper.pdf](https://secure2.pnl.gov/nsd/NSD.nsf/aef8f6faed1a17a6882569970003bbcb/60fb69425bc73ddb8825705100744d85/$FILE/DataBase%20Paper.pdf)

Smith, B. C. (1996). *Fundamentals of Fourier transform infrared spectroscopy*. Boca Raton, FL: CRC Press, Inc.

Smith, T. E. L., Wooster, M. J., Tattaris, M., & Griffith, D. W. T. (2011). Absolute accuracy and sensitivity analysis of OP-FTIR retrievals of CO₂, CH₄ and CO over concentrations representative of “clean air” and “polluted plumes”. *Atmospheric Measurement Techniques*, 4, 97-116. doi:10.5194/amt-4-97-2011

Teledyne API. (2006). *Model 300 carbon monoxide analyzer: Operating manual*.

Townsend, C. L., & Maynard, R. L. (2002). Effects on health of prolonged exposure to low concentrations of carbon monoxide. *Occupational and Environmental Medicine*, 59, 708-711. doi:10.1136/oem.59.10.708

Weather Underground. (2015). *Wind speed/gust and wind direction in Halifax, Nova Scotia* [Data file]. Retrieved from <https://www.wunderground.com/>

Whalley, L. K., Furneaux, K. L., Goddard, A., Lee, J. D., Mahajan, A., Oetjen, H., ...

Heard, D. E. (2010). The chemistry of OH and HO₂ radicals in the boundary layer over the tropical Atlantic Ocean. *Atmospheric Chemistry and Physics*, 10, 1555-1576. doi:10.5194/acp-10-1555-2010, 2010